The Influence of Alkyl Nitrates from Anthropogenic and Biogenic Precursors on Regional Air Quality in Eastern Texas

AQRP Project 16-019

Prepared for:

David Sullivan
Texas Air Quality Research Program
The University of Texas at Austin

and

Jim Smith
Texas Commission on Environmental Quality

Prepared by:

Principal Investigators: Elena McDonald-Buller[1], Greg Yarwood[2], Lea Hildebrandt-Ruiz[2]
Research Team: Bonyoung Koo[2], Yosuke Kimura[1], Uarporn Nopmongcol[2]

[1]Center for Energy and Environmental Resources, The University of Texas at Austin
[2]Ramboll Environ

QA Requirements: Audits of Data Quality: 10% Required

August 30, 2017

CONTENTS

APPENDICES

TABLES

FIGURES

Acknowledgment

The preparation of this report is based on work supported by the State of Texas through the Air Quality Research Program administered by The University of Texas at Austin by means of a Grant from the Texas Commission on Environmental Quality.

Executive Summary

Alkyl nitrates have the potential to influence tropospheric ozone and secondary organic aerosol formation over regional to global spatial scales. Advances in analytical techniques and their applications in laboratory studies and major field campaigns have led to new insights on the atmospheric chemistry and fate of alkyl nitrates. The objectives of this study were to integrate these findings into the Comprehensive Air quality Model with extensions (CAMx) and investigate the effects on predicted regional ozone and fine particulate mass and composition in eastern Texas. Updates to the CB6 chemical mechanism in CAMx (from a starting point of CB6r4) focused on alkyl nitrates formed from biogenic monoterpene precursors and anthropogenic alkane precursors relevant to Texas emission inventories as well as characterization of the loss of alkyl nitrates due to hydrolysis. This new mechanism version is CB6r6d4.

The most recent release of CAMx, v.6.40, with meteorological fields from the Weather Research and Forecast (WRF) model v.3.6.1 and the CB6r4 gas-phase mechanism, was applied for the time period of August 18-September 30, 2013 that spanned the Deriving Information on Surface Conditions from Column and Vertically Resolved Observations Relevant to Air Quality (DISCOVER-AQ) campaign in southeastern Texas. Model performance was assessed using observations from CAMs surface sites in eastern Texas and observations at the surface and aloft made during DISCOVER-AQ. Three schemes for organic gas-aerosol partitioning and oxidation in CAMx were evaluated: 1.5-D Volatility Basis Set (VBS), Secondary Organic Aerosol Partitioning (SOAP2), and a new scheme developed in this work, SOAP2r3, that included secondary organic aerosol (SOA) loss by photolysis. The SOAP2r3 and 1.5-D VBS schemes provided generally comparable model performance for trace gases and $PM_{2.5}$ total mass and component concentrations. The SOAP2r3 scheme is expected to be more easily applied for modeling efforts that support air quality planning and management and was selected for the base case.

Sensitivity studies were conducted that considered the individual and net effects of modifications to the CB6r4 gas-phase mechanism and SOA yields of the base case:

Hydrolysis of Multifunctional Organic Nitrates

Hydrolysis of multifunctional organic nitrates (i.e., the CB6 NTR2 species) was represented in the base case CB6r4 mechanism as a pseudo gas-phase reaction producing nitric acid (HNO_3) with lifetime of 6-hours. The lifetime against hydrolysis was reduced to 1-hour consistent with recent findings that very short lifetimes are appropriate for acidic aerosols. Regional ozone concentrations were insensitive to more rapid hydrolysis. Hourly total $PM_{2.5}$ mass concentrations increased by as much as 0.5 $\mu g/m^3$ on average due to an increase in particulate NO_3. Maximum increases in total $PM_{2.5}$ mass concentrations were approximately 6 $\mu g/m^3$ and occurred in areas where the sensitivity of multifunctional organic nitrates to biogenic volatile organic compound (BVOC) emissions dominated anthropogenic emissions.

Monoterpene Chemistry

Recent studies have indicated the importance of nitrate radical (NO_3)-monoteprene chemistry to SOA formation, but that SOA yields are variable, with α-pinene consistently lower than for other monoterpenes. The CB6r4 mechanism was modified to split terpenes to α-pinene (APIN) and other terpenes (TERP). Revisions were made to the gas-phase reactions of TERP and APIN with hydroxyl radical (OH), ozone (O_3), and NO_3 and to SOA yields for TERP and APIN reactions with NO_3. The impacts of these modifications primarily occurred in terpene-rich areas of the modeling domain including northeastern Texas, western Louisiana, southwestern Arkansas, and southern Mississippi. Average decreases in hourly ozone concentrations were 0.5 ppb with a maximum of 1 to 2 ppb. Differences in hourly total $PM_{2.5}$ mass and organic aerosol were within ±0.5 μg/m^3 on average with maximum differences of -2 to +5 μg/m^3.

Alkane Chemistry

Long-chain alkanes are precursors to alkyl nitrates that contribute to SOA formation and serve as a potential NO_x sink via hydrolysis. Alkanes were split into PAR and PARH, which has a high AN yield, according to chain length. Revisions were made to the gas-phase reactions for PAR and PARH as well as ketones. PAR and PARH fractions were applied by emissions source sector with, for example, lower PARH fractions applied for the oil and gas sector (10%) than mobile sources (20%). Total $PM_{2.5}$ mass concentrations were relatively insensitive to the modifications in AN yields using the PARH scheme. Widespread increases in ozone were 1-2 ppb. Application of the PARH scheme decreased the total alkyl nitrate burden and increased ozone sensitivity to VOC emissions from the oil and gas sector and other anthropogenic sources.

The following recommendations resulted from the study:

- Faster hydrolysis of organic nitrates is recommended for use in CAMx as being more consistent with recent field study data.
- The updated SOA scheme for CAMx, SOAP2r3, is recommended for use as the primary SOA scheme in CAMx. The 1.5D VBS SOA scheme continues to provide a useful alternative but requires greater computational resources and is not compatible with PM source apportionment (PSAT).
- Additional testing and evaluation is recommended for the updated terpene and alkane chemistry developed for CB6r6d4. These mechanism changes are improvements, but their impact was not large in the testing conducted here. Because these mechanism changes add reactions and species they slow down model simulations to a minor extent.
- Additional study of how terpenes are represented in emission inventories, such as MEGAN version 3, and regional models, such as CAMx with the CB6r6d4 is recommended. Evaluation should exploit recent field study data from the southeastern United States to evaluate concentrations of terpenes, nitrate radical, and their reaction products including ANs.
- The ability of photochemical grid models to represent interactions between biogenic VOC and anthropogenic NOx in rural environments with heterogeneous land cover

should be investigated as sub-grid scale interactions that have the potential to alter sensitivity of O_3 and PM to emissions and atmospheric chemistry schemes.

1. Introduction

1.1 Background

Major metropolitan areas in eastern Texas have experienced significant declines in ozone design values over the past decade while annual average $PM_{2.5}$ design values have remained below the National Ambient Air Quality Standard (NAAQS). Continued progress in future air quality planning and management efforts requires an understanding of anthropogenic and biogenic emissions sources and chemical and physical processes that influence regional air quality. Mono and multifunctional alkyl nitrates (ANs) are formed from the oxidation of biogenic or anthropogenic volatile organic compound (VOC) precursors and serve as a reservoir or sink of nitrogen oxides (NO_x). Alkyl nitrates have sufficiently long atmospheric chemical lifetimes (hours to days), such that they can influence tropospheric ozone and secondary organic aerosol (SOA) formation over regional to global spatial scales affecting air quality, climate, and ecosystem nutrient cycling (Perring et al., 2013; Fisher et al., 2016).

Advances in analytical techniques and their applications in laboratory studies and major field campaigns in recent years have provided new insights on the atmospheric chemistry and fate of ANs. Primary pathways for the formation of ANs are OH-initiated oxidation of anthropogenic or biogenic VOC precursors in the presence of NO_x during the daytime and O_3 or NO_3-initiated oxidation of VOC precursors primarily at nighttime (Perring et al., 2013; Hildebrandt Ruiz and Yarwood, 2013). VOC precursors to alkyl nitrates, including alkanes, alkenes, and aromatics, vary by location with anthropogenic or biogenic emission source regions (Day et al, 2010; Perring et al., 2013). Alkyl nitrates form in the presence of NO_x or NO_3, which are primarily of anthropogenic origin. Thus the formation of ANs from biogenic hydrocarbon precursors is a main mechanism through which biogenic and anthropogenic emissions interact and affect air quality (Boyd et al., 2015).

AN functionalities, yields, and fates are known to depend upon the size and structure of the organic backbone (R), as well as the location of the organic nitrate functional group on the backbone. Depending on their structure, ANs can be transported, chemically processed, removed by deposition to vegetation and other surfaces, or undergo partitioning into the aerosol phase where hydrolysis may serve as a loss mechanism (Bean and Hildebrandt Ruiz, 2016; Boyd et al., 2015; Liu et al., 2012). Chemical processing of ANs can result in loss of the nitrate group and release of nitrogen dioxide (NO_2) or retention of the nitrate group but changes in the level of functionality and vapor pressure of the product that influence its fate (Perring et al., 2013). Retention or release of the nitrate functional group appears to be dependent on the structure of the initial AN, with a higher rate of nitrate retention if the nitrate group is separated from reactive hydrogen atoms or double bonds as in longer, linear ANs (Perring et al., 2013). While photolysis of larger ANs is not a dominant process, photolysis of small ANs (C1-C4) has been shown to liberate NO_2, such that NO_x is “recycled” (i.e., sequestered and released) and is available to participate in ozone production. Alkyl nitrates from large

precursors (aromatics, terpenes, large alkanes) or chemically aged ANs from smaller precursors (anthropogenic alkenes, isoprene, and smaller alkanes) that have acquired additional functionalization and have lower vapor pressures are expected to partition into the aerosol phase and be subject to loss by hydrolysis or alternatively removed by deposition. Hydrolysis and deposition are processes that act as NO_x sinks. For water-soluble multifunctional organic nitrates, such as isoprene hydroxy nitrates, gas-phase dry deposition can be a significant loss process (Nguyen et al., 2015).

Ambient observations of ANs in the gas and aerosol-phases have been made in urban and rural or remote locations within the United States (Fry et al., 2013; Day et al., 2003; Day et al., 2010; and elsewhere (Browne et al., 2013). In southeastern Texas, airborne and stationary and mobile surface measurements during the TexAQS 2000, TexAQS 2006, and the TRAMP, SEAC4RS, and DISCOVER-AQ campaigns in 2013 have identified the fractional contributions of ANs to the total reactive nitrogen (NO_y) budget (Day et al., 2003; Ryerson et al, 2003), biogenic and urban and industrial anthropogenic VOC precursors and their source regions (Rosen et al., 2004; Stutz et al., 2010; Teng et al, 2015) and spatial and diurnal variations in the contribution of ANs to organic aerosol mass loadings (Leong et al., 2017; Bean et al., 2016). Field campaigns in the southeastern United States, including the Southern Oxidant and Aerosol Study (SOAS) and Studies of Emissions, Atmospheric Composition, Clouds and Climate Coupling by Regional Surveys (SEAC^{4}RS) that occurred in 2013 provided an unprecedented scale of surface and airborne observations and coordinated laboratory chamber experiments aimed at understanding the chemical processing of biogenic VOCs in low and high NO_x environments during the day and night and the implications for regional air quality (Mao et al., 2016). Findings included identification of the contributions of biogenic VOC precursors to AN formation, the molecular speciation of ANs in the gas and particle phases, and the influence of ANs on NO_x budgets and SOA production (Fisher et al., 2015; Fisher et al., 2016; Lee et al., 2016). Coordinated laboratory chamber studies have led to new insights on SOA formation from monoterpene and nitrate radical chemistry (Boyd et al., 2015; Xu et al., 2015; Nah et al., 2016; Ng et al., 2017).

Regional and global chemical transport models are essential for the development and assessment of air quality policies and should be representative of the current scientific understanding of key atmospheric processes. The SAS studies have provided new observational constraints for the simulation of ANs derived from biogenic VOC precursors. Fisher et al. (2016) and Pye et al. (2015), for example, developed new mechanisms for organic nitrate formation from isoprene and monoterpene oxidation and treatments of gas-particle partitioning and particle phase hydrolysis in the GEOS-Chem and CMAQ models, respectively, for evaluation of model predictions using SOAS or SEAC^{4}RS observations.

The Texas Commission on Environmental Quality (TCEQ) uses the Comprehensive Air quality Model with extensions (CAMx) for air quality planning and management and

State Implementation Plan (SIP) development efforts. Two previous AQRP projects, 10-042 and 12-012, updated the treatment of ANs in the Carbon Bond 6 (CB6) gas-phase chemical mechanism to reflect the state of the science at the time. Project 10-042 evaluated NO_x source and sink reactions in environmental chamber studies with updates to CB6 (identified as CB6r1) that included NO_x recycling from the degradation of alkyl nitrates by photolysis and reaction with OH (Yarwood et al., 2012). Project 12-012 modified the CB6 chemical mechanism (CB6r2) to differentiate between simple alkyl nitrates that remain in the gas-phase and multi-functional ANs that can partition into OA and undergo hydrolysis to nitric acid (Hildebrandt Ruiz and Yarwood, 2013). Since that time the CB6 mechanism in CAMx has undergone two additional revisions. CB6r3 implemented temperature and pressure dependent yields of organic nitrates for alkanes larger than ethane (Emery et al., 2015). CB6r4 included the revisions of CB6r3 with a more computationally efficient, condensed set of reactions involving ocean-borne inorganic iodine that maintained the reactions of the three important catalytic cycles of ozone destruction by iodine as well as the dominant iodine removal reactions. CB6r4 also added the pseudo-heterogeneous hydrolysis of isoprene-derived organic nitrate (INTR) and a new heterogeneous SO_2 oxidation pathway for primary crustal fine particulate matter. No changes were made to the gas-phase reactions of organic nitrates for CB6r4 (Emery et al., 2016). The most recent public release of CAMx, v.6.40, includes the CB6r4 mechanism (Ramboll Environ, 2016).

1.2 Project Objectives

The objectives of this project were to apply the findings from recent environmental chamber experiments and field campaigns to refine the CB6r4 chemical mechanism in CAMx v.6.40 in order to examine the implications for regional air quality in eastern Texas and neighboring states. The updates had three major areas of focus: (1) AN yields and gas-particle partitioning from CB6r4 surrogate species for alkanes (primarily PAR); (2) the formation and fate of ANs derived from the oxidation of monoterpenes; and (3) loss of ANs due to hydrolysis in the particle phase. CAMx model predictions were evaluated against airborne and surface observations during the DISCOVER-AQ campaign in southeastern Texas. Sensitivity tests with CAMx evaluated the effects of updates to the CB6r4 mechanism on regional ozone and organic aerosol concentrations.

1.3 Report Overview

Section 2 of the report describes the CAMx configuration and base case model performance relative to surface and aircraft observations. Sections 3 describe the updates to the chemical mechanism, and Section 4 evaluates their effects on regional ozone and particulate matter total mass and component concentrations. Audits of data quality are described in Section 5. Section 6 provides a summary of findings from the project and recommendations for future work. Section 7 includes references.

2. CAMx Configuration and Base Case Model Performance

The most recent release of CAMx,v.6.40 (Ramboll Environ, 2016), was applied for an episode spanning the DISCOVER-AQ time period of August 18-September 30, 2013. The CAMx configuration used in this work leveraged meteorological and air quality model development and application efforts from Nopmongcol et al. (2015; TCEQ Work Order 582-15-54264-010).

Several updates, described in this section, were made to reflect more recent versions of the CAMx model and CB6 chemical mechanism and to improve model performance. This section describes the CAMx base case configuration and model performance evaluation using surface and aircraft observations specific to the time period.

2.1 CAMx Modeling Domain

The CAMx modeling domain is shown in Figure 2-1 along with the grid structure in Table 2-1. The nested horizontal domain consists of 36-km outer continental United States, 12-km Texas regional, and 4-km eastern Texas grids. The 4-km domain was expanded from that used by Nopmongcol et al. (2015), which covered only the Houston-Galveston-Brazoria-Beaumont-Port Arthur areas, to include all major metropolitan areas in eastern Texas. This nested horizontal grid structure has been widely used in recent years by the TCEQ for modeling to support air quality planning and management efforts. The vertical layer structure is shown in Figure 2-2 and included 28 layers from the surface to 15 km and a surface layer depth of 34m.

Source: https://www.tceq.texas.gov/airquality/airmod/data/domain

Figure 2-1. Nested 36-km/12-km/4-km horizontal grid domains for WRF (red/dark blue/dark green) and CAMx (black/light blue/light green).

Table 2-1. CAMx horizontal grid structure.

Domain	Range		Number of Cells		Cell Size (km)	
	Easting	Northing	Easting	Northing	Easting	Northing
WRF						
36-km	(-2916, 2916)	(-2304, 2304)	163	129	36	36
12-km	(-1188, 900)	(-1800, -144)	175	139	12	12
4-km	(-396, 468)	(-1620, -468)	217	289	4	4
CAMx						
36-km	(-2736, 2592)	(-2088, 1944)	148	112	36	36
12-km	(-984, 804)	(-1632, -312)	149	110	12	12
4-km	(-328, 436)	(-1516, -644)	191	218	4	4

Source: https://www.tceq.texas.gov/airquality/airmod/data/domain

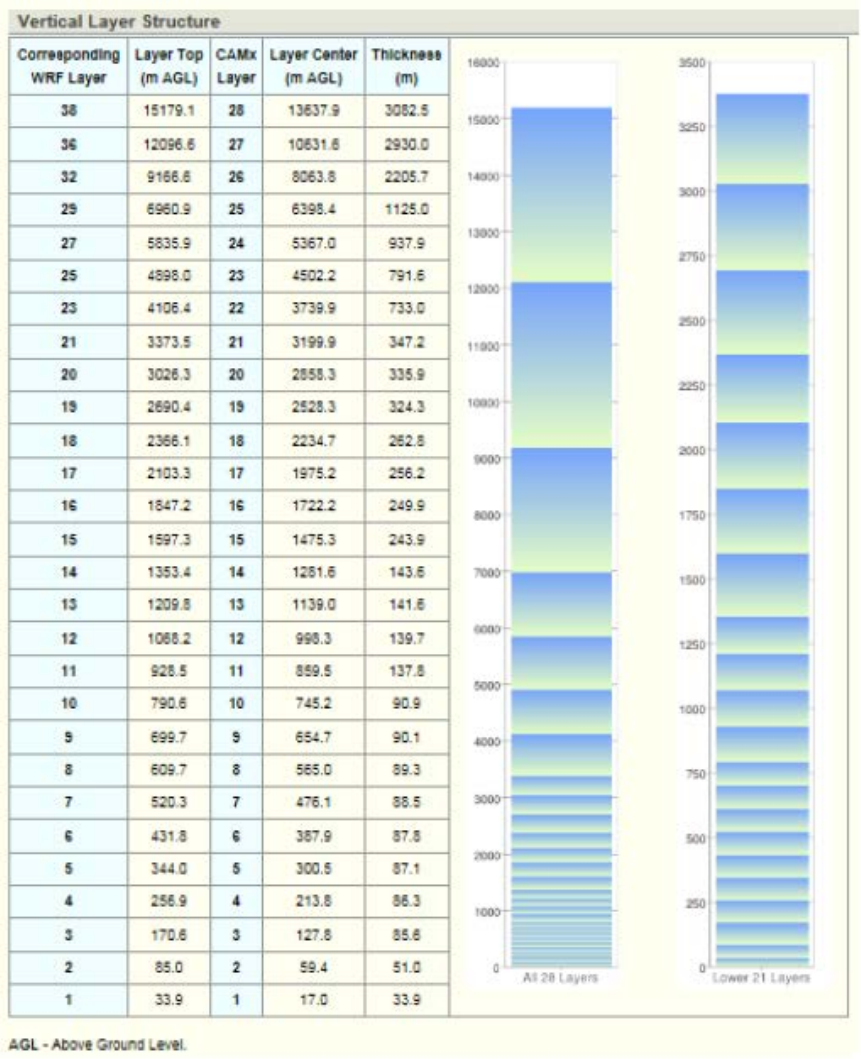

Vertical Layer Structure

Corresponding WRF Layer	Layer Top (m AGL)	CAMx Layer	Layer Center (m AGL)	Thickness (m)
38	15179.1	28	13637.9	3082.5
36	12096.6	27	10631.6	2930.0
32	9166.6	26	8063.8	2205.7
29	6960.9	25	6398.4	1125.0
27	5835.9	24	5367.0	937.9
25	4898.0	23	4502.2	791.6
23	4106.4	22	3739.9	733.0
21	3373.5	21	3199.9	347.2
20	3026.3	20	2858.3	335.9
19	2690.4	19	2528.3	324.3
18	2366.1	18	2234.7	262.8
17	2103.3	17	1975.2	256.2
16	1847.2	16	1722.2	249.9
15	1597.3	15	1475.3	243.9
14	1353.4	14	1281.6	143.6
13	1209.8	13	1139.0	141.6
12	1068.2	12	998.3	139.7
11	928.5	11	859.5	137.8
10	790.6	10	745.2	90.9
9	699.7	9	654.7	90.1
8	609.7	8	565.0	89.3
7	520.3	7	476.1	88.5
6	431.8	6	387.9	87.8
5	344.0	5	300.5	87.1
4	256.9	4	213.8	86.3
3	170.6	3	127.8	85.6
2	85.0	2	59.4	51.0
1	33.9	1	17.0	33.9

AGL - Above Ground Level.

Source: Nopmongcol et al. (2015)

Figure 2-2. CAMx vertical layer structure.

2.2 Meteorological Model Configuration and Performance

The Weather Research and Forecast (WRF) model version 3.6.1 was used to provide meteorological data fields for the CAMx simulations. The horizontal modeling domain and grid structure for the WRF simulation are shown in Figure 2-1 and Table 2-1, respectively; the vertical grid structure is shown in Figure 2-2. The WRF configuration is summarized in Table 2-2. Raw meteorological fields were prepared for CAMx using the preprocessor program WRFCAMx. The Yonsei University (YSU) planetary boundary layer parameterization scheme was applied within WRFCAMx for closer consistency between the WRF and CAMx models. Other modifications to the raw data fields applied by Nopmongcol et al. (2015) included enhancing sub-grid cloudiness for all domains using a diagnosis of thermodynamic properties similar to that for the Community Multi-scale Air Quality (CMAQ) Modeling System and applying patches to the vertical diffusivity fields to enhance nighttime mixing in urban areas ("Kv100") and mixing below convective clouds ("Kv cloud patch").

Table 2-2. Summary of the WRF configuration.

WRF version	3.6.1
Horizontal Resolution	36/12/4/1.333 km (The 1.333 km domain covered the Houston-Galveston area only and was considered only in reference to the evaluation of WRF model performance by Nopmongcol et al. (2015). It was otherwise not included in this project.)
Microphysics	WRF Single-Moment 6-Class Microphysics Scheme (WSM6)
Longwave Radiation	Rapid Radiative Transfer Model for GCMs (RRTMG)
Shortwave Radiation	RRTMG as above but for shortwave radiation
Surface Layer Physics	Revised 5th generation Pennsylvania State University /National Center for Atmospheric Research Mesoscale Model (MM5) similarity
Land Surface Model (LSM)	Noah
PBL scheme	Yonsei University (YSU)
Cumulus parameterization	Kain-Fritsch (4km/1.33km: off)
Boundary and Initial Conditions Data Source	12-km North American Model (NAM) analysis
Analysis Nudging Coefficients (s^{-1})	36/12 km: 3-D 4 km: None
Winds	$3x10^{-4}$
Temperature	$3x10^{-4}$ (above boundary layer only)
Mixing Ratio	$3x10^{-4}$ (above boundary layer only)
Observation Nudging Coefficients (s^{-1})	36/12/4 km: None
Winds	None
Temperature	None
Mixing Ratio	None
Miscellaneous Notes	12-h spin-up, 5-day integration

Nopmongcol et al. (2015) evaluated WRF predictions of wind speed, wind direction, solar radiation, and 2-meter temperature at Continuous Ambient Monitoring Station (CAMS) sites within the portion of the WRF 4-km horizontal domain that overlapped the 1.33-km domain shown in Figure 2-3. The 1.33-km domain encompassed the aircraft flight paths conducted during the DISCOVER-AQ campaign, as comparisons of WRF and CAMx predictions with observations during the campaign were a primary focus of the study by Nopmongcol et al. (2015). The 1.33-km domain was not otherwise considered in this project. Statistical performance metrics (i.e., normalized mean bias, normalized mean error, root mean squared error) for the meteorological parameters, except solar radiation, were evaluated using data from the National Center for Atmospheric Research's (NCAR's) ds427.0 sites (commercial and municipal airports) located within the 1.33-km domain.

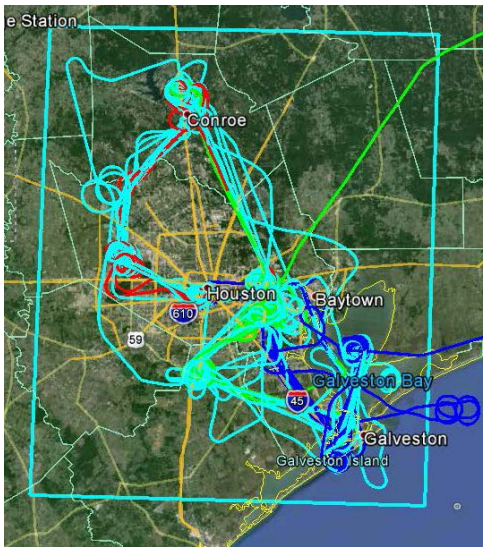

Source: Nopmongcol et al. (2015)

Figure 2-3. 1.33-km horizontal domain and aircraft flight paths during the DISCOVER-AQ campaign. Nopmongcol et al. (2015) evaluated WRF performance for the portion of the WRF 4-km domain that overlapped this area.

Overall Nopmongcol et al. (2015) determined that WRF model performance was suitable for photochemical modeling in the region. Performance statistics for 2-m temperature, wind speed, and wind direction collectively across CAMS and ds472.0 sites, respectively, are summarized in Table 2-3. Differences in performance between CAMs and ds472.0 sites could be attributable to differences in network siting, spatial distribution, and/or density. Nopmongcol et al. (2015) developed soccer plots of daily or monthly average error versus daily or monthly average bias for each meteorological parameter measured at the ds472.0 sites as shown in Figure 2-4 and evaluated performance in the context of benchmarks for simple (Emery et al., 2001) and complex (Kemball-Cook et al., 2005) conditions. The application of simple or complex condition benchmarks, shown in Table 2-4, was determined on a site-by-site basis depending on

terrain or local circulation patterns. All meteorological parameters exhibited daily variability in performance across the time period. Similar to other meteorological modeling efforts for the Houston-Galveston area, characterization of land-sea breeze circulations patterns, daytime and nocturnal winds, convective activity and the timing and location of clouds contributed to variability in WRF model performance. The soccer plots indicated relatively good performance for temperature and wind speed. Predictions of humidity may be affected by poor performance in the characterization of clouds and/or convection on some days. Wind direction performance may be affected by the characterization of the timing of land-sea breeze circulations on some days.

Table 2-3. WRF performance statistics for the 4-km grid across all CAMS and ds472.0 airport sites within the Houston-Galveston 1.33-km domain shown in Figure 2-3.

Site	Temperature			Wind Speed (cutoff 1mph)			Wind Direction			Solar Radiation		
	NMB (%)	NME (%)	RMSE (°F)	NMB (%)	NME (%)	RMSE mph)	NMB (%)	NME (%)	RMSE (°)	NMB (%)	NME (%)	RMSE (W/m^2)
CAMS	1.2	3.2	3.3	31.2	57.1	4.1	-0.2	33.6	53.2	7.22	50.2	163.5
ds472.0	0.9	3.1	3.3	2.4	39.7	3.9	-0.9	28.4	47.3	*	*	*

*Solar radiation is not measured at ds472.0 sites
Source: Nopmongcol et al. (2015)

Table 2-4. WRF performance benchmark for simple and complex conditions.

Parameter	Simple Conditions (Emery et al., 2001)	Complex Conditions (Kemball-Cook et al., 2005)
Temperature Bias	≤ ±0.5 K	≤±2.0 K
Temperature Error	≤2.0 K	≤3.5 K
Humidity Bias	≤ ±1.0 g/kg	≤ ±0.8 g/kg
Humidity Error	≤2.0 g/kg	≤2.0 g/kg
Wind Speed Bias	≤±0.5 m/s	≤±1.5 m/s
Wind Speed RMSE	≤2.0 m/s	≤2.5 m/s
Wind Direction Bias	≤± 10 degrees	(not addressed)
Wind Direction Error	≤ 30 degrees	≤ 55 degrees

2.3 Anthropogenic and Biogenic Emission Inventories

Nopmongcol et al. (2015) obtained anthropogenic emissions inventories for the 36/12/4 km domains in CAMx-ready format and compatible with the CB6 gas-phase chemical mechanism from the TCEQ (2015). Elevated point source emissions included day-specific continuous emissions monitoring system (CEMS) data made available by the Acid Rain Program for the September 2013 modeling period. Surface emissions, including area, mobile, and low-level point sources, were from the TCEQ's 2012 day-of-week specific emissions inventory. The TCEQ's anthropogenic emissions included PM precursors and primary fine PM emissions. Emissions of coarse PM were not included. Day-specific biogenic emissions estimates for the 36/12/4 km domains were generated by Nopmongcol et al. (2015) using the Model of Emissions of Gases and Aerosols from

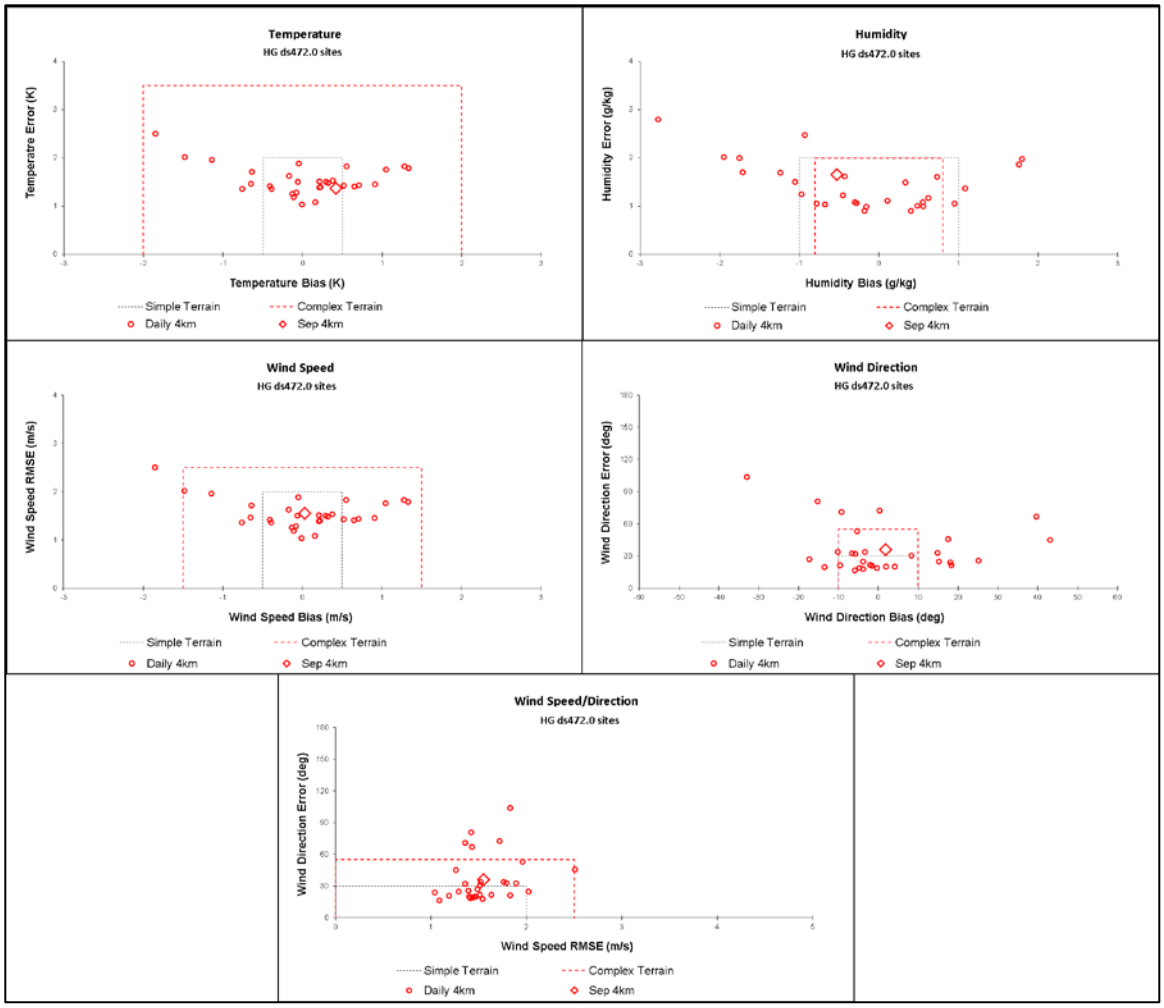

Figure 2-4. Soccer plots across all HG ds472.0 airports (13 sites) for temperature (top left), humidity (top right), wind speed (middle left), wind direction (middle right) and wind speed/wind direction (bottom) for the WRF 4 km results. Daily statistics are shown as circles and monthly statistics are shown as diamonds. Simple terrain benchmarks are marked with a black dashed line and complex terrain benchmarks are marked with a red dashed line (Nopmongcol et al., 2015).

Nature (MEGAN) version 2.1 (Guenther et al., 2012) with data for leaf area index (LAI) obtained from the TCEQ and daily meteorology (temperature and solar radiation) from the WRF model simulation. Isoprene emissions were reduced by a factor of two based on previous studies that suggested MEGAN exhibited an overprediction bias (ENVIRON and ERG, 2013; Johnson et al., 2013).

Fire emission estimates were based on the Fire Inventory from NCAR version 1 (FINNv1) dataset (http://bai.acom.ucar.edu/Data/fire/; accessed June 1, 2014) and processed for CAMx using the Emissions Processing System version 3.20 that incorporated the Western Regional Air Partnership (WRAP) methodology to temporally and vertically allocate the emissions.

Emissions of sea-salt particles including sodium, chloride, and sulfate were estimated from the WRF model. Sea salt aerosol fluxes from both open oceans (Smith and Harrison 1998; Gong, 2003) and breaking waves in the surf zone (de Leeuw et al., 2000) were a function of wind speed at 10-m height.

Nopmongcol et al. (2015) merged anthropogenic and natural emissions (i.e., biogenic, fire, sea salt) to obtain day-specific emissions for input to CAMx. Because CAMx treats anthropogenic toluene, xylene, and benzene as secondary organic aerosol precursors and requires that the emissions of these species be provided separately for gas-phase and aerosol-phase chemistry, TCEQ anthropogenic emissions were updated with secondary aerosol precursor emissions before merging. Anthropogenic emissions of TOL, XYL and BENZ model species for gas-phase chemistry were replicated and renamed to TOLA, XYLA, and BNZA, respectively, for the aerosol-phase chemistry. Similarly, biogenic emissions of ISOP and TERP model species for gas-phase chemistry were replicated and renamed as ISP and TRP, respectively, for the aerosol-phase chemistry prior to merging. Sesquiterpene emissions were included only for the aerosol-phase chemistry and denoted as SQT. Surface anthropogenic and natural emissions were then merged for each simulation day for the 36/12/4km domain using Ramboll Environ's EPS3 MRGUAM program. For elevated sources, anthropogenic emissions were merged with FINN fire emissions using the PTSMERGE program.

Typical weekday emissions of NO_x, carbon monoxide (CO), VOC, sulfur dioxide (SO_2), ammonia (NH_3), and total fine particulate mass ($PM_{2.5}$) by source category for the CAMx 4 km-grid (Figure 2-1) are summarized in Table 2-5. Spatial distributions of anthropogenic and natural emissions are shown in Figure 2-5 and Figure 2-6, respectively.

Table 2-5. Typical weekday (Wednesday) emissions (short tons per day) by source category from Nopmongcol et al. (2015).

Category	NO_x	CO	VOC	SO_2	NH_3	$PM_{2.5}$
Anthropogenic						
Area	605	900	3,130	63	627	695
Nonroad	432	2,573	274	1	2	36
Offroad	180	137	15	10	0	7
Low-point	987	4,338	378	6	23	27
Elevated point	1,053	1,053	136	1,659	10	122
Mexico	69	63	285	9	3	19
Natural						
Biogenic	258	1,865	18,100	-	-	-
Sea-salt	-	-	-	-	-	702
Fire	9	141	11	1	2	20
Total	3,593	11,069	22,328	1,749	666	1,628

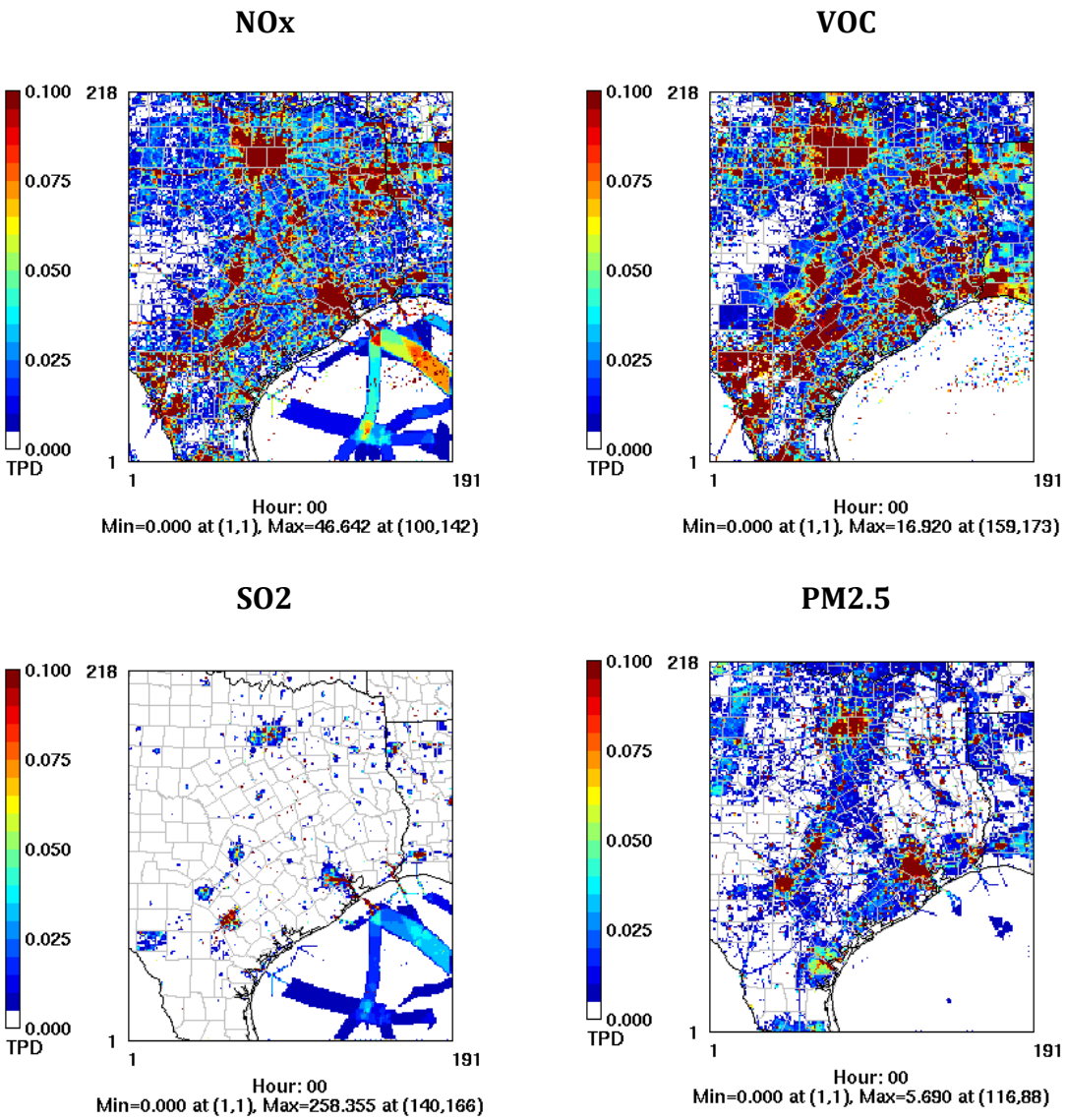

Figure 2-5. Typical weekday (September 18) anthropogenic NO_x, VOC, SO_2, and $PM_{2.5}$ emissions (short tons per day) (Nopmongcol et al., 2015).

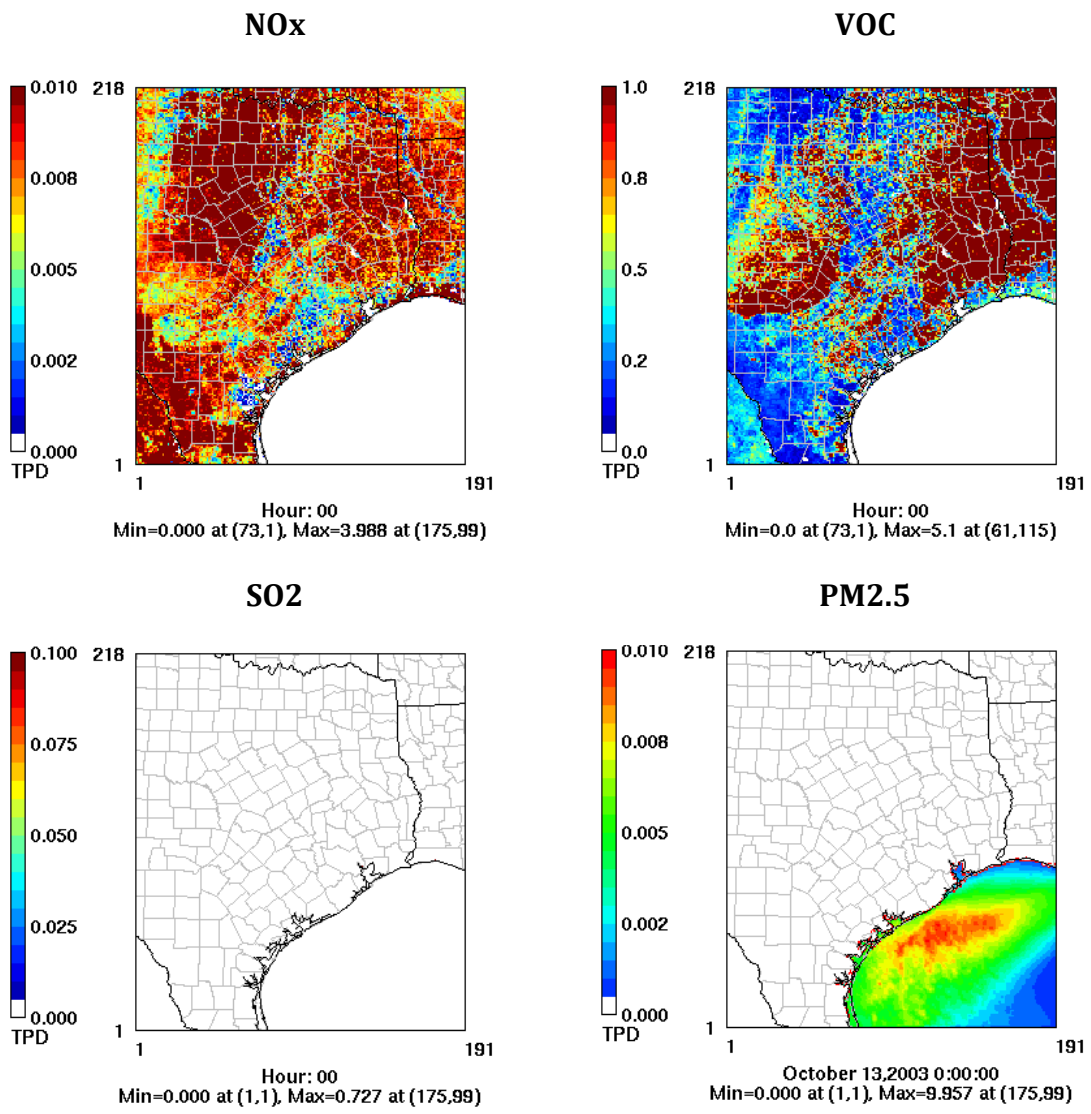

Figure 2-6. Typical weekday (September 18) natural NO_x, VOC, SO_2, and $PM_{2.5}$ emissions (short tons per day) (Nopmongcol et al., 2015).

2.4 CAMx Boundary Conditions and Other Inputs

Nopmongcol et al. (2015) extracted initial and boundary conditions (IC/BCs) for the 36-km domain from MOZART global model output for the year 2013 using the Mozart2CAMx version 3.0 software. MOZART outputs are for every 6-hour interval and are at 1.9x2.5 degree resolution with 56 vertical layers. A constant 15 ppb ozone reduction was applied over the Gulf of Mexico and Atlantic Ocean in order to deplete the ozone coming onshore. A constant 5 ppb ozone reduction was applied elsewhere.

The ozone column input file was prepared using 2013 day-specific values from 1 degree Total Ozone Mapping Spectrometer (TOMS) satellite ozone column data and used to

generate photolysis rates. Land use/land cover inputs were generated using a U.S. Geological Survey (USGS) 24-category dataset. Monthly LAI data were generated from the MODIS satellite product. Both the land use/land cover and monthly LAI were updated based on 2012 data for this project.

2.5 CAMx Configuration

The CAMx configuration is summarized in Table 2-6. Nopmongcol et al. (2015) used CAMx version 6.2 with the CB6r2 gas-phase chemical mechanism. The CB6 mechanism has undergone revisions since that study. CB6r3 implemented temperature and pressure dependent yields of organic nitrates for alkanes larger than ethane (Emery et al., 2015). CB6r4 included the revisions of CB6r3 with a more computationally efficient, condensed set of reactions involving ocean-borne inorganic iodine that maintained the reactions of the three important catalytic cycles of ozone destruction by iodine as well as the dominant iodine removal reactions. CB6r4 also added the pseudo-heterogeneous hydrolysis of isoprene-derived organic nitrate (INTR) and a new heterogeneous SO_2 oxidation pathway for primary crustal fine particulate matter. For this project, CAMx version 6.40 with the CB6r4 mechanism was used in the base case, reflecting the most recent, publicly released versions of the air quality model and CB6 mechanism. The WATERMASK program was applied to distinguish between ocean and fresh water bodies, which is required to use in-line oceanic inorganic emissions for the new halogen chemistry mechanism in CB6r4.

Two-way grid nesting was implemented across the domains in this project. In contrast, Nopmongcol et al. (2015) first ran CAMx using two-way nested grids for the 36-km and 12-km domains with a 15-day spin up period and then ran the 4-km domain using one-way nested grid for consistency with CMAQ.

Table 2-6. CAMx base case configuration options.

Model Option	Configuration
Version	6.40
Horizontal Grid Mesh	36/12/4 km
Vertical Grid Mesh	28 layers
Initial Conditions	15 days full spin-up for the 36/12-km grids; 5 days for the 4-km grid
Boundary Conditions	Ref. Sections 2.4 and 2.5
Emissions Processing	Ref. Section 2.3
Gas-Phase Chemistry	CB6r4
Aerosol Chemistry	ISORROPIA equilibrium and SOAP2r3*; CF scheme.
Meteorological Processor	WRFCAMx3.4
Horizontal Transport	Piecewise Parabolic Method (PPM) scheme
Horizontal Diffusion	K-theory
Vertical Advection Scheme	WRF
Vertical Eddy Diffusivity Scheme	K-theory
Vertical Diffusivity Corrections	Kv-patch depending on land use category up to 100 m and to cloud tops
Deposition Scheme	Zhang

* CAMx simulations, described in Section 2.6, evaluated and compared the VBS, SOAP2 and a revised version of SOAP2 developed in this project, SOAP2r3. The SOAP2r3 scheme was used in the final base case that served as the reference for evaluating chemical mechanism updates.

2.5.1 Organic Aerosol-Gas Partitioning and Oxidation Scheme

Aerosol chemistry was implemented with gas-phase chemistry for the project. As noted in Table 2-6, the CF scheme was selected to model aerosol size distribution. The CF scheme divides the size distribution into two static modes (coarse and fine). Primary species are modeled as fine and/or coarse particles, while all secondary species are modeled as fine particles only. Partitioning of inorganic aerosol constituents (i.e., sulfate, nitrate, ammonium, sodium, chloride) between the gas and aerosol phases was modeled using the ISORROPIA inorganic aerosol thermodynamic equilibrium model (Nenes et al., 1998, 1999).

CAMx 6.40 includes two algorithms for organic gas-aerosol partitioning and oxidation: the hybrid 1.5-dimensional (1.5-D) Volatility Basis Set (VBS) or Secondary Organic Aerosol Partitioning (SOAP) schemes. The VBS approach (refer to Ramboll Environ, 2016; Donahue et al., 2006; Robinson et al., 2007; Donahue et al., 2011; Koo et al., 2014) provides a unified framework for gas-aerosol partitioning and chemical aging of primary organic aerosol (POA) and SOA. It uses a set of semi-volatile OA species, the basis set, whose volatility is equally spaced in a logarithmic scale. Member species of the basis set are allowed to react further in the atmosphere (chemical aging) to describe volatility changes (i.e., shifting between volatility bins). The first generation VBS (Donahue et al.,

2006) used one-dimensional basis sets (1-D VBS) where organic compounds were grouped only by volatility. Donahue et al. (2011; 2012) later developed a two-dimensional VBS approach (2-D VBS) where organic compounds were grouped by oxidation state as well as volatility in order to describe the varying degree of oxidation observed in atmospheric OA of similar volatility. A hybrid VBS approach (1.5-D VBS; described by Koo et al. 2014; Ramboll Environ, 2016) is implemented in CAMx that combines the 1-D VBS with the ability to describe evolution of OA in the 2-D space of oxidation state and volatility. The 1.5-D uses five basis sets (refer to Table 5-2 in Ramboll Environ, 2016) to describe varying degrees of oxidation in ambient OA: two basis sets for chemically aged oxygenated OA (OOA; anthropogenic and biogenic) and three for freshly emitted OA (hydrocarbon-like OA [HOA] from meat-cooking and other anthropogenic sources and biomass burning OA [BBOA]). Each basis set has five volatility bins ranging from 10^{-1} to 10^{3} μg m^{-3} in saturation concentration (C*) (refer to Table 5-7 in Ramboll Environ, 2016). Total OA is the sum of all model OA species in the five volatility bins from primary formation from anthropogenic sources, cooking or biomass burning or secondary formation from anthropogenic or biogenic sources. The 1.5-D VBS approach was applied previously in AQRP project 14-024 to improve the understanding of organic aerosol formation, including the contribution of organic nitrates, in southeastern Texas during the 2013 DISCOVER-AQ campaign.

Nopcomgcol et al. (2015) applied the SOAP semi-volatile equilibrium scheme (Strader et al., 1999) in CAMx to describe organic aerosol-gas partitioning and oxidation chemistry (Ramboll Environ, 2016). Primary organic aerosol in SOAP is a single non-volatile species that does not chemically evolve. SOA species exist in equilibrium with condensable gases (CG) that can be produced by VOC oxidation. The CAMx SOA module consists of two parts: gas-phase oxidation chemistry that forms CGs and equilibrium partitioning between gas and aerosol phases for each CG/SOA pair. Each anthropogenic (benzene, toluene, xylene or intermediate volatile organic compound IVOC) or biogenic precursor (isoprene, monoterpene, sesquiterpene) produces three CG species: more-volatile, less-volatile and non-volatile products. More- and less-volatile CG products from all anthropogenic precursors are lumped to CG1 and CG2 that yield corresponding SOA species SOA1 and SOA2, respectively. The CG products from all biogenic precursors are similarly lumped to CG3 and CG4 yielding SOA species SOA3 and SOA4, respectively. Non-volatile products are instantly condensed to form SOA (SOPA and SOPB from anthropogenic and biogenic precursors, respectively). SOAP assumes that semi-volatile SOAs are polymerized to form non-volatile SOAs (SOPA and SOPB) with a half-life of 20 hours (Kalberer et al., 2004). In-cloud SOA formation obtained in CAMx using the Regional Acid Deposition Model (RADM) scheme (Ramboll Environ, 2016) is added to SOPB.

SOAP has been recently updated for the latest information on SOA yields, saturation concentrations, and water solubility (Zhang et al., 2014; Hodzic et al., 2016; Hodzic et al., 2014; Knote et al., 2015). Polymerization of biogenic SOA is disabled assuming that it is accounted for in the new yield data. The latest version of SOAP is known as SOAP2

and is available in CAMx 6.40. Physical properties of SOAP2 species can be found in Table 5-6 of Ramboll Environ (2016). Total SOA is the sum of SOA1-4 plus SOPA and SOPB. Total organic aerosol is the sum of total SOA and the single POA species.

At the outset of the project, it was planned that the 1.5-D VBS scheme in CAMx 6.40 would be used in the base case that would serve as a reference for evaluating the effects of the chemical mechanism updates. However, the SOAP scheme is more widely used for air quality planning and management because of its lower computational burden and less extensive emission inventory processing requirements. Consequently both schemes were considered during the project. As described in the next section, the SOAP2 algorithm was updated in this project with the objectives of improving model performance based on surface and aircraft observations during the DISCOVER-AQ campaign and improving consistency with CAMx predictions based on the 1.5-D VBS algorithm.

2.5.2 Revisions to the SOAP2 Scheme: SOAP2r3

Initial CAMx v.6.40 base case simulations with the CB6r4 mechanism were completed at the Texas Advanced Computing Center (TACC) at the University of Texas at Austin using the 1.5-D VBS or SOAP2 schemes. Model performance was evaluated using surface and aircraft observations for the DISCOVER-AQ time period in southeastern Texas. Both simulations exhibited a high bias in hourly average $PM_{2.5}$, organic aerosol, and organic carbon (OC) concentrations relative to surface observations, in particular with the SOAP2 scheme. Sodium and nitrate, indicative of sea salt emissions, also exhibited a high bias. Predictions of contemporary carbon contributions were biased low relative to radiocarbon source apportionment analysis at Conroe. The Particulate Source Apportionment Technology (PSAT) tool was enabled in a simulation with SOAP2 for diagnostic purposes, and the results were used to guide refinements.

The SOAP2 scheme in CAMx v.6.40 implicitly accounted for functionalization (and fragmentation) by chemical aging of SOA components in the gas phase based on a parameterization that describes multiple generations of oxidation of SOA precursors (Hodzic et al., 2016). However, it did not include SOA loss by photolysis, which can be competitive with other aging mechanisms of atmospheric SOA (Henry and Donahue, 2012; Hodzic et al., 2016). To account for this removal process in the particle phase, the photolytic loss of SOA, as a first-order decay reaction with a photolysis rate derived by scaling the NO_2 photolysis rate, was implemented in a new version of SOAP identified as SOAP2r3:

$$\frac{d[SOA]}{dt} = -J_{SOA}\,[SOA] = -s\,J_{NO_2}\,[SOA]$$

Significant uncertainties in the SOA photolysis rate remain with estimates varying by orders of magnitudes (Henry and Donahue, 2012; Hodzic et al., 2016). For this work, the rate was estimated as 0.4% of J_{NO_2} assuming a photolysis lifetime of approximately one

day as suggested by Henry and Donahue (2012).

The performance of CAMx v.6.40 with the SOAP2, 1.5-D VBS, and SOAP2r3 schemes was evaluated against observations at CAMS sites throughout eastern Texas and surface and aircraft observations in southeastern Texas, with an additional focus on aerosol measurements at the Conroe surface site. CAMx v6.40 with the SOAP2r3 scheme was eventually selected as the base case for simulations that evaluated updates to the CB6r4 mechanism, and its performance is described in detail in Section 2.6 below. Comparisons with CAMx simulations using the SOAP2 and 1.5-D VBS schemes are shown in Section 2.6 and Appendices A and C. CAMx predictions with SOAP2r3 were generally comparable to those using the hybrid 1.5-D VBS scheme. The rationale for selection of the SOAP2r3 scheme for the base case is described in further detail in Section 2.6.4.

2.5.3 Processing of SOA Precursor Emissions

Emissions of anthropogenic and biogenic SOA precursors, shown in Table 2-7, were processed for use with the 1.5-D VBS and SOAP2/SOAP2r3 schemes. Emission estimates for IVOCs by specific source category were prepared for the VBS scheme and then summed to obtain the IVOA species of SOAP2 and SOAP2r3.

IVOC emissions were based on source-specific 2012 emissions inventory data for the 8-county Houston-Galveston-Brazoria area from the TCEQ and unspeciated fractions of total NMOG emissions estimated by Jathar et al. (2014). Table 2-8 shows NMOG mass fractions of three combustion source types by emission source sector and estimated mass fractions of NMOG emissions that were mapped to IVOC species for the VBS scheme. Speciation profiles were normalized to the sum of speciated compounds rather than total NMOG emissions. Unspeciated NMOG emissions were assumed to be IVOC emissions. As this accounted for all the original unspeciated fraction of NMOG emissions, speciated emissions were reduced by renormalization (Jathar 2014).

Similar to the approach used to develop IVOC emissions estimates, mass fractions of five VBS POA species (gasoline vehicles, diesel vehicles, meat cooking, other anthropogenic sources and biomass burning) were estimated by emission source sector, as shown in Table 2-9. This approach was not required for SOAP2/SOAP2r3 as it had only one POA species.

Table 2-7. Mapping of anthropogenic and biogenic SOA precursors to 1.5-D VBS and SOAP2/SOAP2r3 species.

Species	Present in TCEQ (anthropgenic) or MEGAN (biogenic) Inventories	SOAP2/ SOAP2r3 Species	1.5-D VBS Species	Description
Benzene	Yes	BNZA	BNZA	-
Toluene	Yes	TOLA	TOLA	-
Xylene	Yes	XYLA	XYLA	-
Isoprene	Yes	ISP	ISP	-
Monoterpenes	Yes	TRP	TRP	-
Sesquiterpenes	Yes	SQT	SQT	-
Intermediate Volatility Organic Compounds	No	IVOA	IVOG	Gasoline engines
			IVOD	Diesel engines
			IVOB	Biomass burning
			IVOA	Other anthropogenic sources
Primary Organic Aerosol	Yes	POA	POA_GV	Gasoline vehicles
			POA_DV	Diesel vehicles
			POA_MC	Meat cooking
			POA_OP	Other anthropogenic sources
			POA_BB	Biomass burning

Table 2-8. NMOG mass contribution by combustion source type and emission source sector and mapping of estimated mass fractions of NMOG emissions to IVOC species for the VBS scheme.

Emission Source Sector	Mass contribution by combustion source type to total NMOG emissions *			VBS IVOC species and other VOCs as mass fractions of NMOG emissions			
	Gasoline	Diesel	Biomass Burning	IVOG	IVOD	IVOB	VOC excluding IVOC
On-road	88.6%	11.4%	0%	0.2215	0.0228	0	0.7557
Non-road	80.9%	10.1%	0%	0.2023	0.0202	0	0.7776
Off-road	5.5%	94.2%	0%	0.0138	0.1884	0	0.7979
Area	0%	0%	1.9%	0	0	0.0038	0.9962
Oil & Gas	0%	0%	0%	0	0	0	1
Fires	0%	0%	100%	0	0	0.2000	0.8000

* Based on TCEQ source-specific 2012 emission inventory data for the 8-county HGB area. Unspeciated fractions of NMOG emissions from gasoline engines, diesel engines, and biomass burning were 25%, 20%, and 20%, respectively (Jathar et al., 2014) and were assumed to be IVOC emissions.

Table 2-9. Mass fractions of five VBS POA species by emission source sector.

Emission Source Sector	VBS POA Species				
	POA_GV	POA_DV	POA_MC	POA_OP	POA_BB
On-road	0.2735	0.7265	0	0	0
Non-road	0.3227	0.6468	0	0.0255	0
Off-road	0.1116	0.8743	0	0.0094	0
Area	0	0	0.2624	0.3571	0.3805
Oil & Gas	0	0.6443	0	0.3557	0
Point	0	0	0	1	0
Mexico & Canada	0	0	0	1	0
Fire	0	0	0	0	1

2.6 Model Performance Evaluation

2.6.1 Evaluation of Model Performance at CAMS Surface Sites

CAMx predictions with the SOAP2r3 scheme were evaluated against surface observations at TCEQ CAMS sites in major metropolitan areas within the 4-km eastern Texas domain and against surface and aircraft observations in the Houston area collected during the DISCOVER-AQ campaign. Statistical performance metrics used for the evaluation of CAMx performance are shown in Table 2-10. The selected metrics are recommended by the U.S. Environmental Protection Agency's Draft Modeling Guidance for Demonstrating Attainment of Air Quality Goals for Ozone, $PM_{2.5}$, and Regional Haze (U.S. EPA, 2014) and Simon et al. (2012). Figure 2-7 shows TCEQ CAMS monitoring sites and the number of observations available at each for the evaluation of CAMx performance for ozone, NO, NO_2, and $PM_{2.5}$. Comparisons between CAMx predictions of ozone, NO, NO_2, and $PM_{2.5}$concentrations with SOAP2r3 and the SOAP2 and 1.5-D VBS schemes are shown in Appendix A.

Table 2-10. Statistical metrics used for the evaluation of CAMx performance.

Metric	Definition[1]
Mean Bias (MB)	$\frac{1}{N}\sum_{i=1}^{N}(P_i - O_i)$
Mean Error (ME)	$\frac{1}{N}\sum_{i=1}^{N}\lvert P_i - O_i\rvert$
Normalized Mean Bias (NMB) (-100% to +∞)	$\frac{\sum_{i=1}^{N}(P_i - O_i)}{\sum_{i=1}^{N} O_i}$
Normalized Mean Error (NME) (0% to +∞)	$\frac{\sum_{i=1}^{N}\lvert P_i - O_i\rvert}{\sum_{i=1}^{N} O_i}$
Fractional Bias (FB) (-200% to +200%)	$\frac{2}{N}\sum_{i=1}^{N}\left(\frac{P_i - O_i}{P_i + O_i}\right)$
Fractional Error (FE) (0% to +200%)	$\frac{2}{N}\sum_{i=1}^{N}\left\lvert\frac{P_i - O_i}{P_i + O_i}\right\rvert$
Coefficient of Determination (r^2) (0 to 1)	$\left(\frac{\sum_{i=1}^{N}(P_i - \overline{P})(O_i - \overline{O})}{\sqrt{\sum_{i=1}^{N}(P_i - \overline{P})^2 \sum_{i=1}^{N}(O_i - \overline{O})^2}}\right)^2$
Root Mean Squared Error (RMSE)	$\sqrt{\frac{\sum_{i=1}^{N}(P_i - O_i)^2}{N}}$

[1] P_i and O_i are prediction and observation at the *i*-th site, respectively; $\overline{P}$ and $\overline{O}$ are mean prediction and observation, respectively.

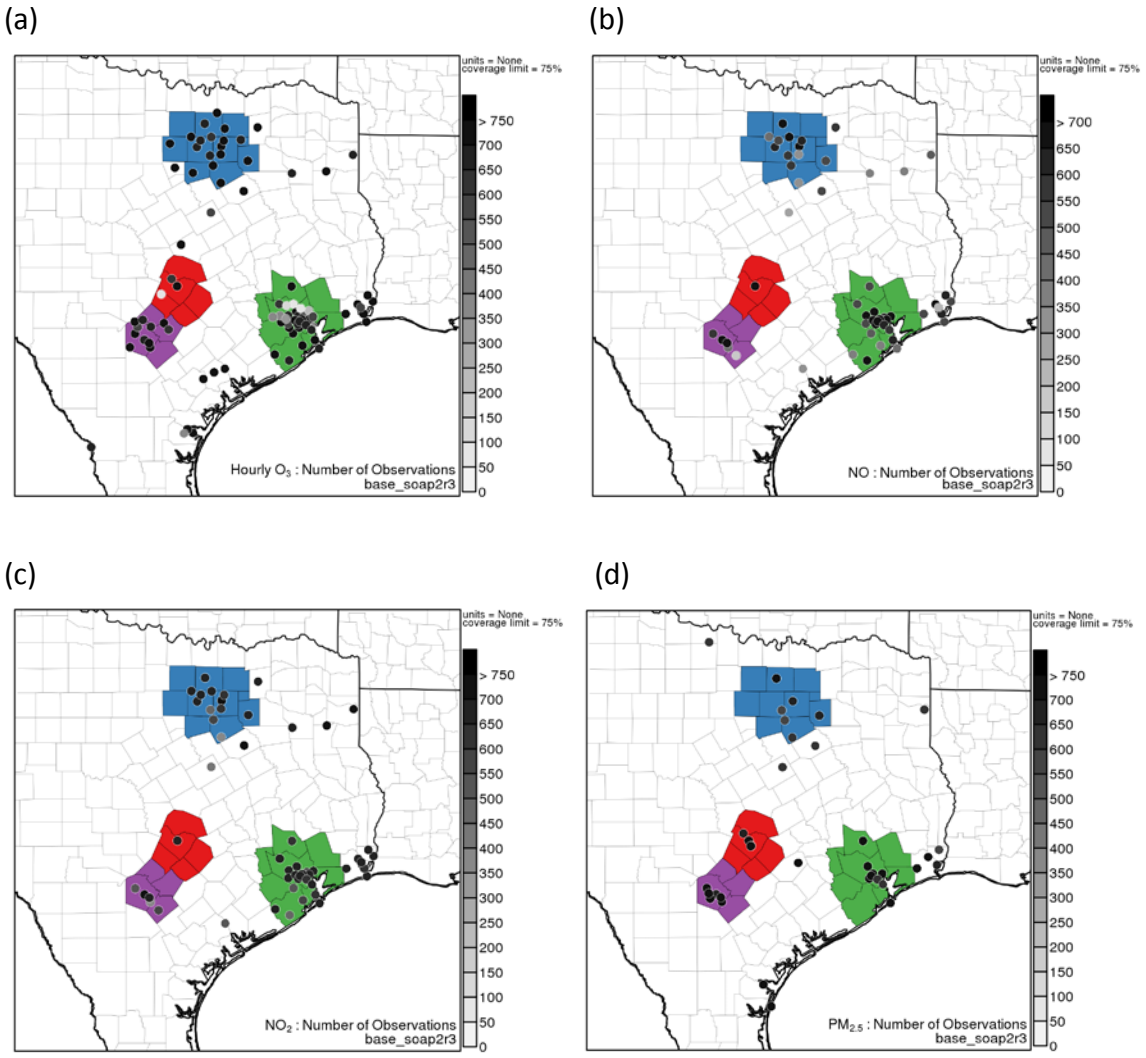

Figure 2-7. CAMS monitoring sites and number of observations available for used in the evaluation of CAMx performance for (a) ozone, (b) NO, (c) NO_2, and (d) $PM_{2.5}$. The Dallas/Fort Worth (blue), Austin (red), San Antonio (purple), and Houston-Galveston (green) metropolitan areas are shown.

2.6.1.1 Ozone

Figure 2-8 shows scatter plots of modeled and observed hourly ozone and maximum daily average 8-hour (MDA8) ozone concentrations at CAMS sites within the 4-km eastern Texas domain. Modeled and observed concentrations are paired in space and time. Compilations of operational performance statistics for hourly and MDA8 ozone concentrations reported by Simon et al. (2012) are shown in Figure 2-9. Figures 2-10 and 2-11 show statistical performance metrics for predictions relative to observed hourly ozone and MDA8 ozone concentrations, respectively, at individual CAMS sites during the episode time period.

Averaged over all days of the episode, the model exhibited a tendency toward overestimation of observed hourly and MDA8 ozone concentrations throughout the 4-km domain. Overestimation of observed hourly and MDA8 ozone was most pronounced in the Houston-Galveston and coastal areas and to some extent for hourly ozone concentrations measured in the San Antonio area. Nopmongcol et al. (2015) noted that September 1 through 10 were cloudy days resulting in low ozone concentrations. Heavy rain occurred before a frontal passage on September 21 that lowered ozone levels across the Houston-Galveston and Beaumont-Port Arthur areas. A second frontal boundary passed through Houston on September 25 with ozone exceedances at several sites on that day and on September 26.

The overprediction bias exhibited by regional photochemical models during periods with low ozone concentrations in coastal areas along the Gulf of Mexico occurs commonly and has been noted in previous studies (e.g., McGaughey et al., 2017; Simon et al., 2011; Yarwood et al., 2012; Smith et al., 2013; Kemball-Cook et al., 2015). Nopmongcol et al. (2015) suggested that poor ozone performance could be related to insufficient clouds simulated by the meteorological model, but a sensitivity study that increased non-boundary layer cloudiness did not yield significant responses in ozone predictions. Revisions to the CB6 mechanisms aimed at improving the representation of halogen chemistry in CAMx (Emery et al., 2016; Ramboll Environ et al., 2016) have resulted in improvements in model performance in coastal areas but future work should continue to pursue investigation of the persistence of the overprediction bias.

Model performance was evaluated when measured ambient ozone concentrations were above a minimum threshold in order to separate low and high ozone days. Appendix B shows daily performance metrics for hourly and MDA8 ozone averaged over all episode days and for time periods when observed ozone concentrations were at or above a threshold of 60 ppb in the Dallas-Fort Worth, Houston-Galveston, Austin, and San Antonio areas. Differences in model performance were evident for high ozone days, during which underestimation of observed ozone concentrations was more frequent. In a compilation of hourly and MDA8 ozone performance metrics from modeling studies, Simon et al. (2012) describe that without consideration of a threshold ambient concentration, modeled ozone generally exhibits a tendency toward overestimation because metrics are averaged over high and low ozone hours and days, for which performance during low ozone periods dominates. In contrast, modeled MDA8 ozone concentrations above cutoff values of 60 ppb or 75 ppb were underestimated indicating that model performance varied with ozone concentration. Comparisons between predicted ozone concentrations using the SOAP2r3, SOAP2, or 1.5-D VBS schemes with observations at CAMS sites, shown in Appendix A, indicated that differences in model performance due to the three organic gas-aerosol partitioning and oxidation schemes were minimal.

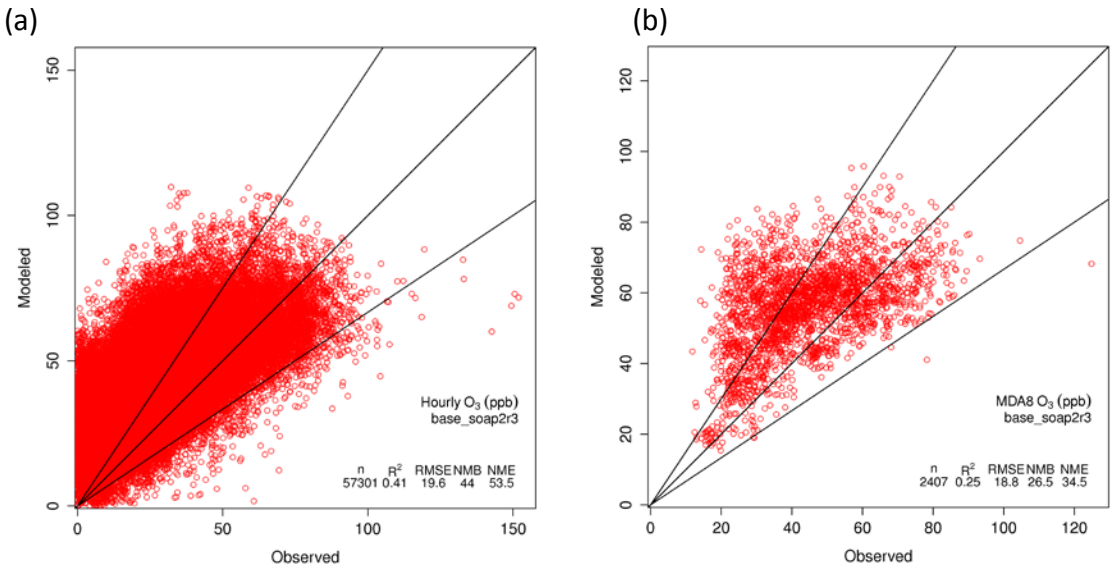

Figure 2-8. Scatter plots of modeled and observed (a) hourly ozone and (b) maximum daily average 8-hour (MDA8) ozone concentrations, paired in space and time, at CAMS monitoring sites within the 4-km eastern Texas domain.

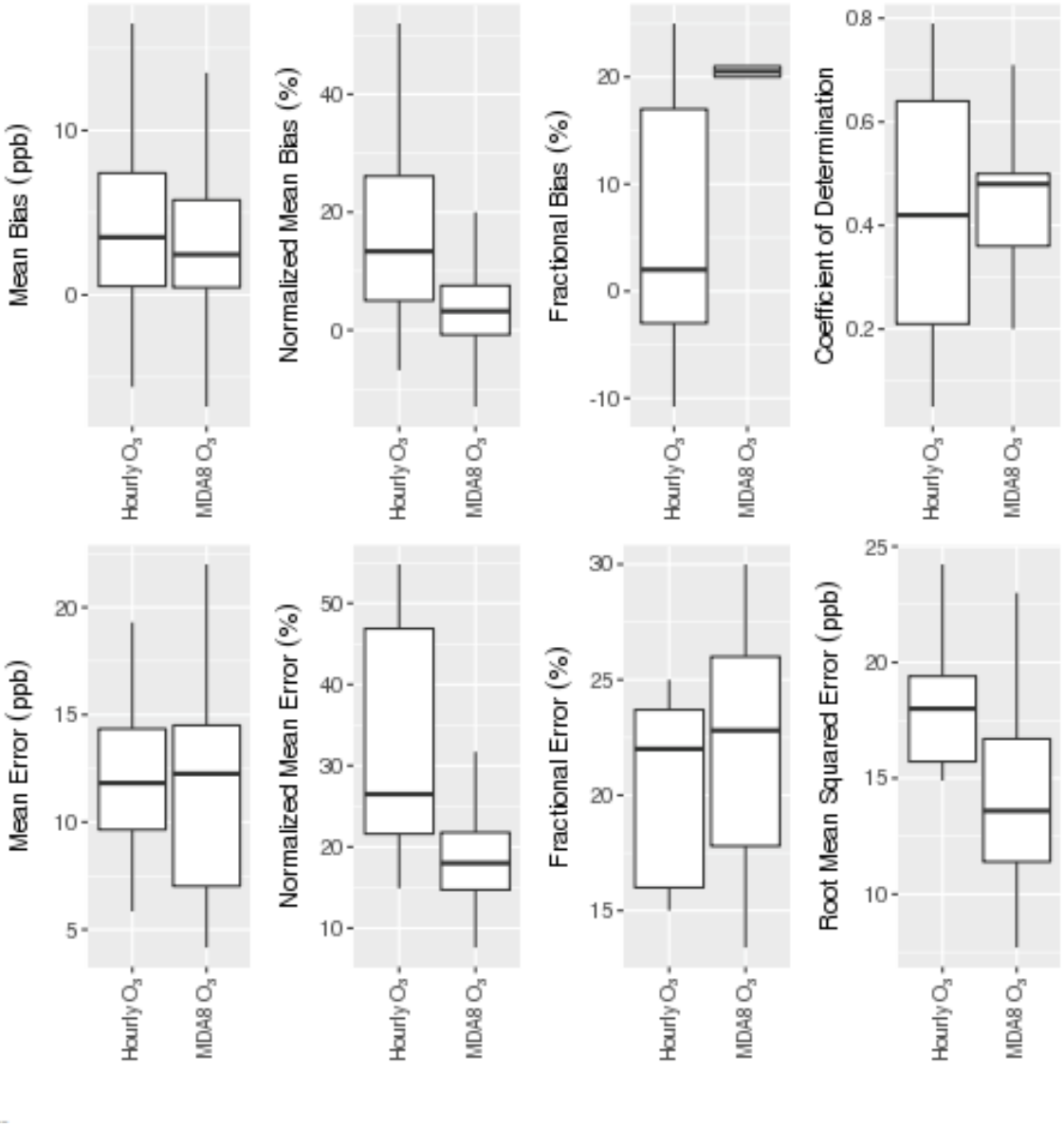

Figure 2-9. Compilation of hourly and MDA8 ozone performance metrics from Simon et al. (2012; ref. Fig 4). Centerlines show median values, boxes outline the 25th and 75th percentile values and whiskers extend to 1.5 times the interquartile range.

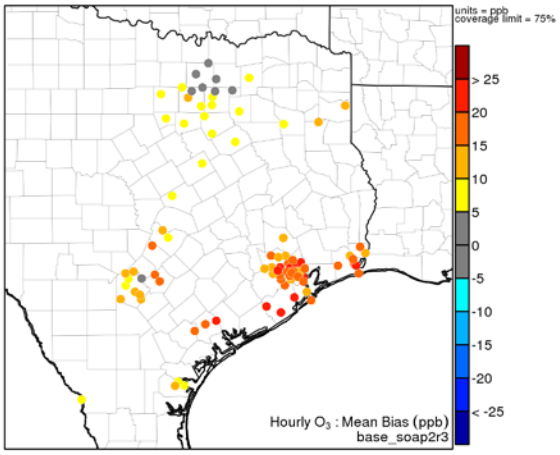
units = ppb
coverage limit = 75%
> 25
20
15
10
5
0
-5
-10
-15
-20
< -25
Hourly O3 : Mean Bias (ppb)
base_soap2r3

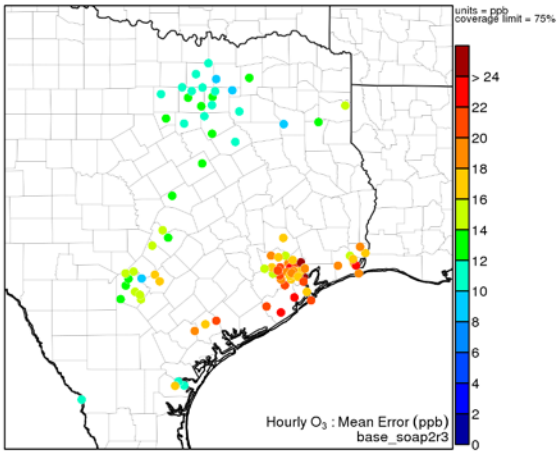
units = ppb
coverage limit = 75%
> 24
22
20
18
16
14
12
10
8
6
4
2
0
Hourly O3 : Mean Error (ppb)
base_soap2r3

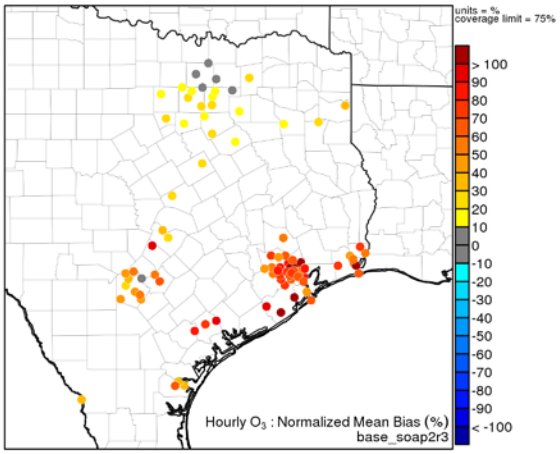
units = %
coverage limit = 75%
> 100
90
80
70
60
50
40
30
20
10
0
-10
-20
-30
-40
-50
-60
-70
-80
-90
< -100
Hourly O3 : Normalized Mean Bias (%)
base_soap2r3

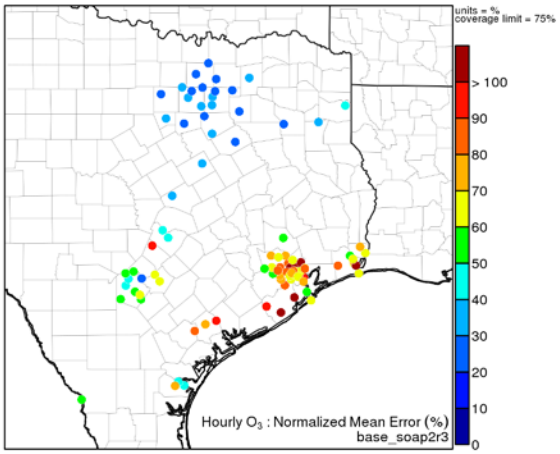
units = %
coverage limit = 75%
> 100
90
80
70
60
50
40
30
20
10
0
Hourly O3 : Normalized Mean Error (%)
base_soap2r3

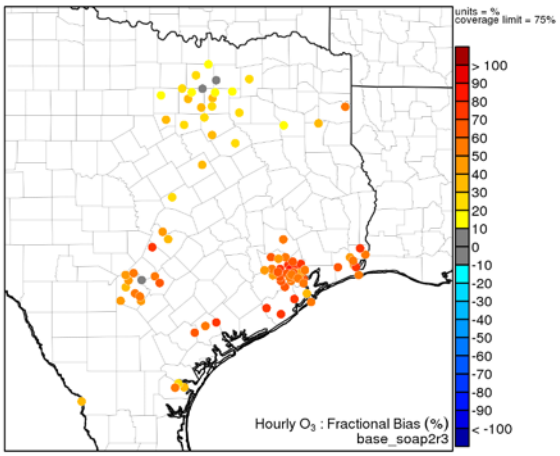
units = %
coverage limit = 75%
> 100
90
80
70
60
50
40
30
20
10
0
-10
-20
-30
-40
-50
-60
-70
-80
-90
< -100
Hourly O3 : Fractional Bias (%)
base_soap2r3

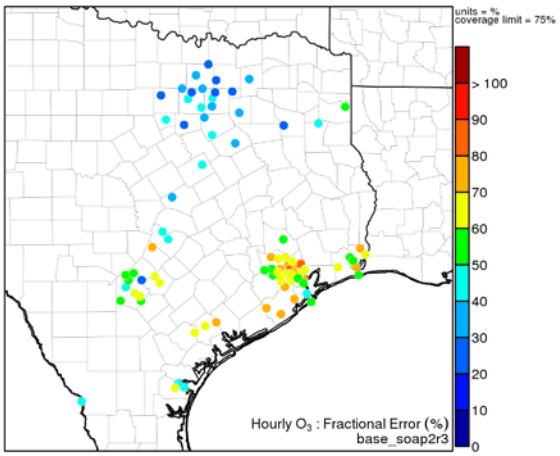
units = %
coverage limit = 75%
> 100
90
80
70
60
50
40
30
20
10
0
Hourly O3 : Fractional Error (%)
base_soap2r3

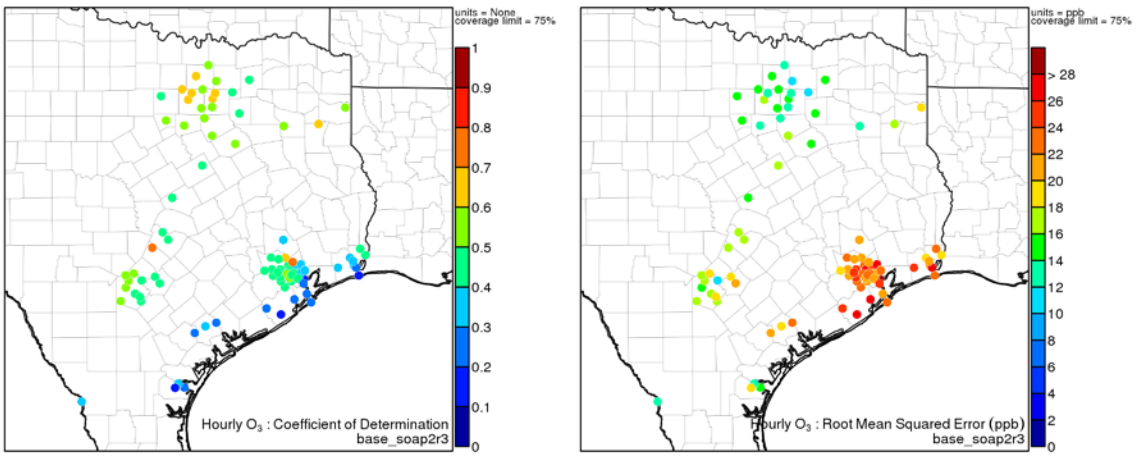

Figure 2-10. Performance metrics for modeled hourly ozone concentrations at CAMS monitoring sites in eastern Texas during the episode time period.

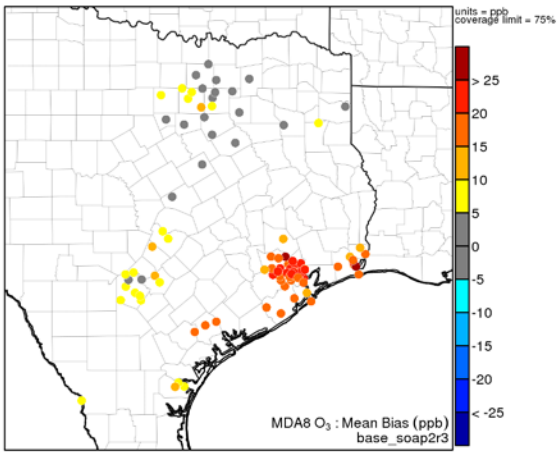
units = ppb
coverage limit = 75%
> 25
20
15
10
5
0
-5
-10
-15
-20
< -25
MDA8 O3 : Mean Bias (ppb)
base_soap2r3

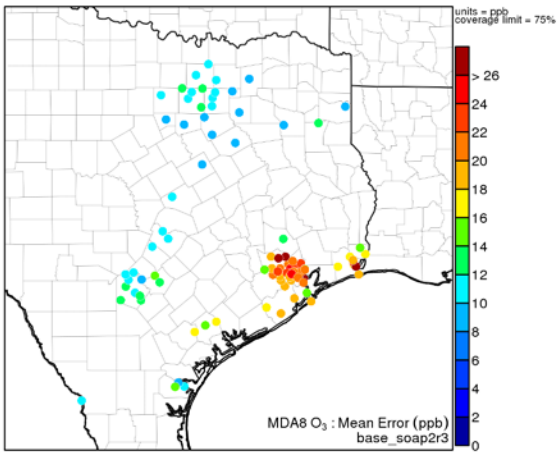
units = ppb
coverage limit = 75%
> 26
24
22
20
18
16
14
12
10
8
6
4
2
0
MDA8 O3 : Mean Error (ppb)
base_soap2r3

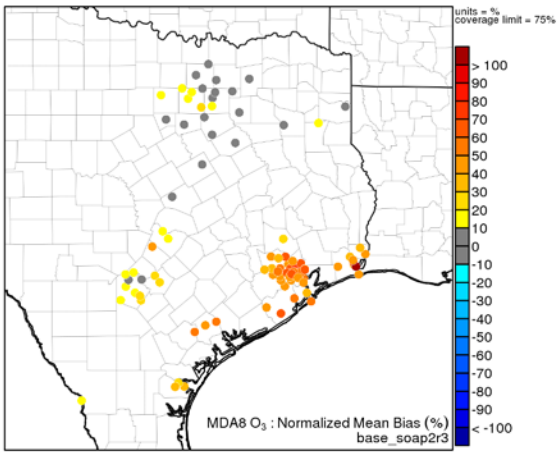
units = %
coverage limit = 75%
> 100
90
80
70
60
50
40
30
20
10
0
-10
-20
-30
-40
-50
-60
-70
-80
-90
< -100
MDA8 O3 : Normalized Mean Bias (%)
base_soap2r3

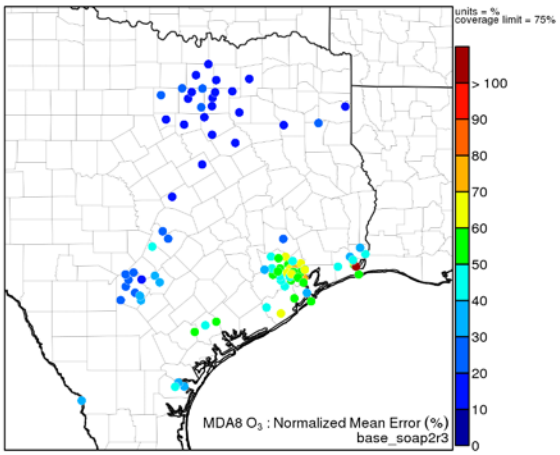
units = %
coverage limit = 75%
> 100
90
80
70
60
50
40
30
20
10
0
MDA8 O3 : Normalized Mean Error (%)
base_soap2r3

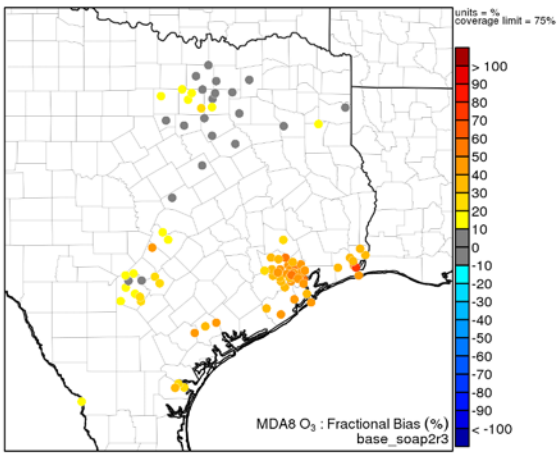
units = %
coverage limit = 75%
> 100
90
80
70
60
50
40
30
20
10
0
-10
-20
-30
-40
-50
-60
-70
-80
-90
< -100
MDA8 O3 : Fractional Bias (%)
base_soap2r3

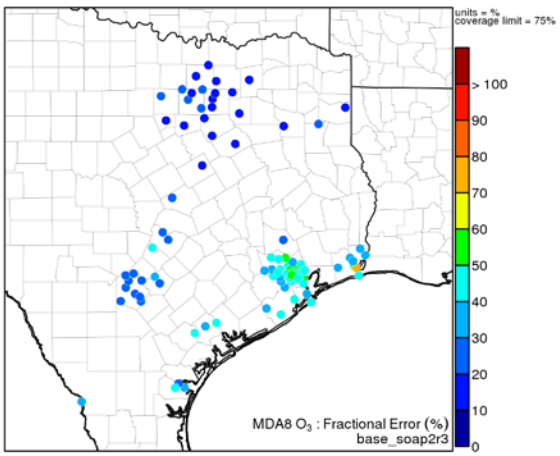
units = %
coverage limit = 75%
> 100
90
80
70
60
50
40
30
20
10
0
MDA8 O3 : Fractional Error (%)
base_soap2r3

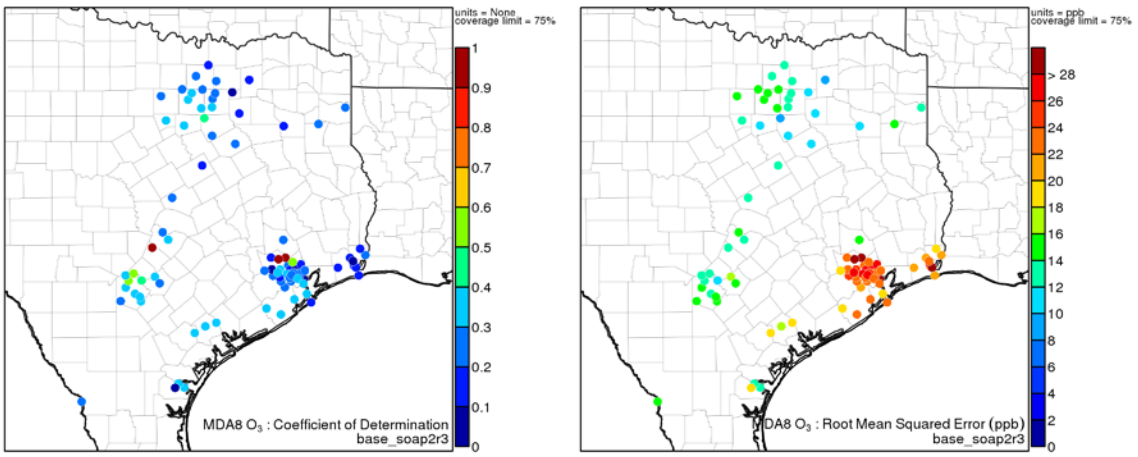

Figure 2-11. Performance metrics for modeled MDA8 ozone concentrations at CAMS monitoring sites in eastern Texas during the episode time period.

2.6.1.2 Nitric Oxide (NO) and Nitrogen Dioxide (NO_2)

Figure 2-12 shows scatter plots of modeled and observed hourly NO and NO_2 concentrations, paired in space and time, at CAMS sites within the 4-km eastern Texas domain. Figures 2-13 and 2-14 show statistical performance metrics for predictions relative to observed hourly NO and NO_2 concentrations, respectively, at individual CAMS sites during the episode time period. Appendix B shows daily performance metrics for hourly NO and NO_2 concentrations averaged over all episode days separately for the Dallas-Fort Worth, Houston-Galveston, Austin, and San Antonio areas.

Predicted NO concentrations underestimated observed NO at most CAMS sites within the eastern Texas 4-km domain over the episode. Nopmongcol et al. (2015) found that CAMx and CMAQ underestimated observed NO concentrations in the Houston-Galveston area during the DISCOVER-AQ time period. They noted that a lack of temporal resolution in the emissions inventory for anthropogenic sources without CEMS could contribute to underestimation of observed NO concentrations. In addition, CAMx and other photochemical grid models instantaneously disperse pollutants within a grid cell, which may not adequately capture narrow episodic plumes of primary emitted pollutants, such as NO, that may affect observations at CAMS sites. The CAMx plume-in-grid modeling capability (specifically the Greatly Reduced Execution and Simplified Dynamics Plume-in-Grid approach, referred to as "GREASD-PiG) was invoked for all simulations in this work but only to large elevated point sources. Other sources of NO_x may benefit from similar treatments (Karamchandani et al., 2011).

Model performance for NO_2 exhibited more spatial variability within the 4-km eastern Texas domain. Predicted NO_2 concentrations across most CAMS site in Houston and at the single measurement site in Austin overestimated observed concentrations relatively consistently throughout the episode. In the San Antonio area, model predictions overestimated observed concentrations at the CAMs site northwest of the city but underestimated observed NO_2 concentrations at sites to the southeast of the city across the episode. Model predictions of NO_2 concentrations tended to overestimate observations within or near the Dallas-Fort Worth metroplex, in contrast to performance at outlying sites. Comparisons between predicted NO and NO_2 concentrations using the SOAP2r3, SOAP2, or 1.5-D VBS schemes with observations at CAMS sites, shown in Appendix A, indicated that differences in model performance due to the three organic gas-aerosol partitioning and oxidation schemes were minimal.

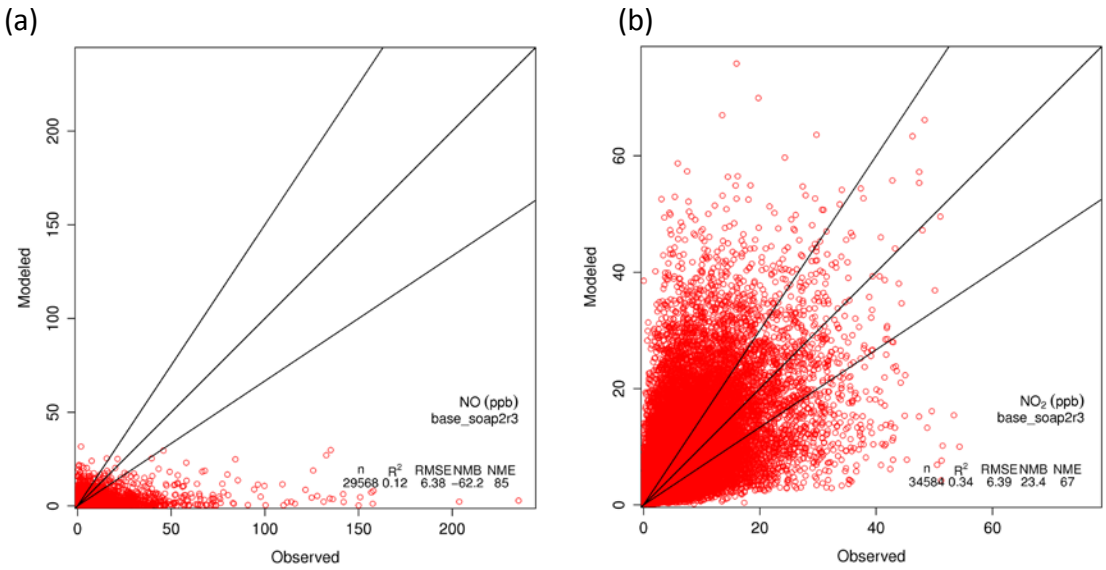

Figure 2-12. Scatter plots of modeled and observed (a) hourly NO and (b) hourly NO_2 concentrations, paired in space and time, at CAMS monitoring sites within the 4-km eastern Texas domain.

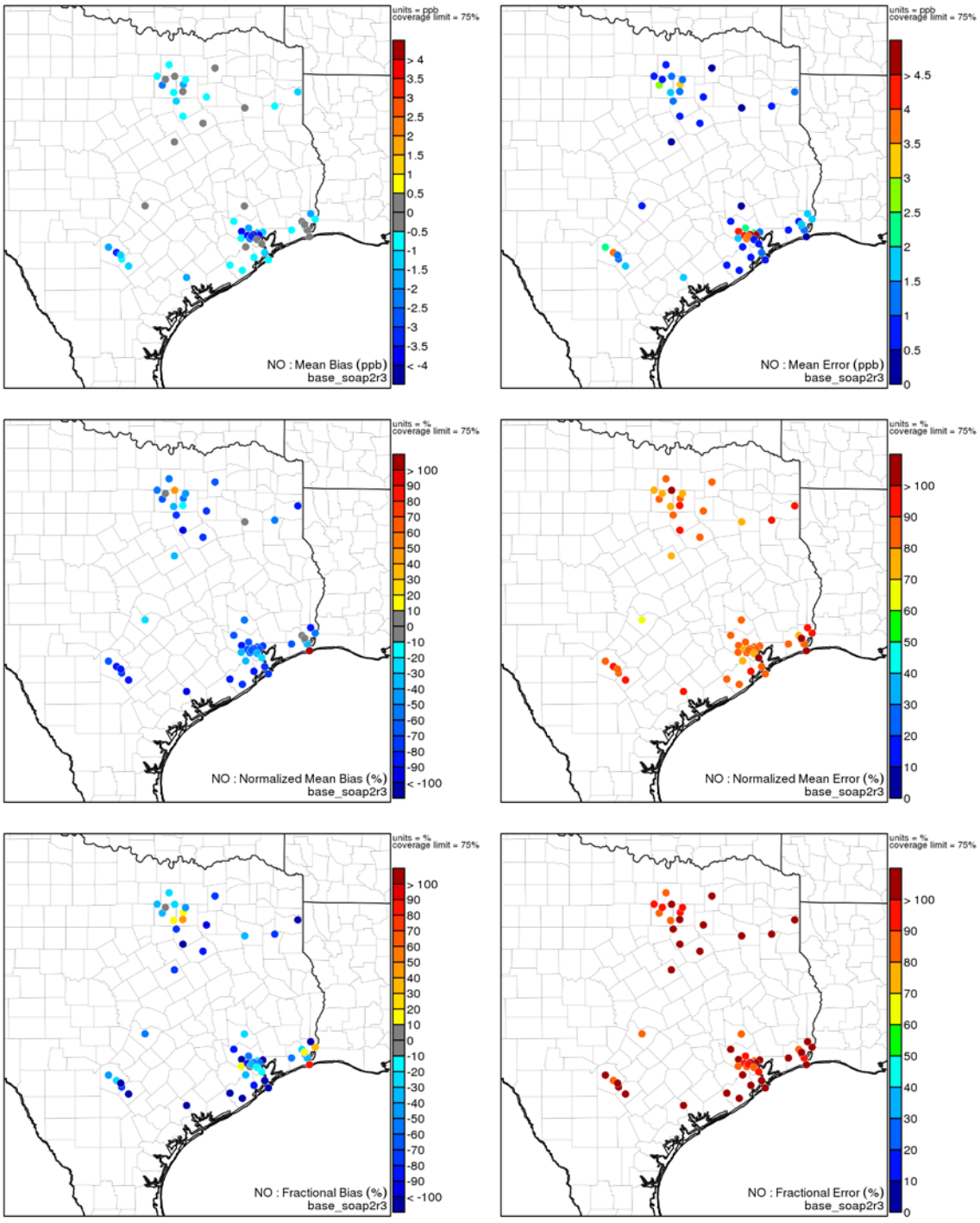
units = ppb
coverage limit = 75%
> 4
3.5
3
2.5
2
1.5
1
0.5
0
-0.5
-1
-1.5
-2
-2.5
-3
-3.5
< -4
NO : Mean Bias (ppb)
base_soap2r3
units = ppb
coverage limit = 75%
> 4.5
4
3.5
3
2.5
2
1.5
1
0.5
0
NO : Mean Error (ppb)
base_soap2r3
units = %
coverage limit = 75%
> 100
90
80
70
60
50
40
30
20
10
0
-10
-20
-30
-40
-50
-60
-70
-80
-90
< -100
NO : Normalized Mean Bias (%)
base_soap2r3
units = %
coverage limit = 75%
> 100
90
80
70
60
50
40
30
20
10
0
NO : Normalized Mean Error (%)
base_soap2r3
units = %
coverage limit = 75%
> 100
90
80
70
60
50
40
30
20
10
0
-10
-20
-30
-40
-50
-60
-70
-80
-90
< -100
NO : Fractional Bias (%)
base_soap2r3
units = %
coverage limit = 75%
> 100
90
80
70
60
50
40
30
20
10
0
NO : Fractional Error (%)
base_soap2r3

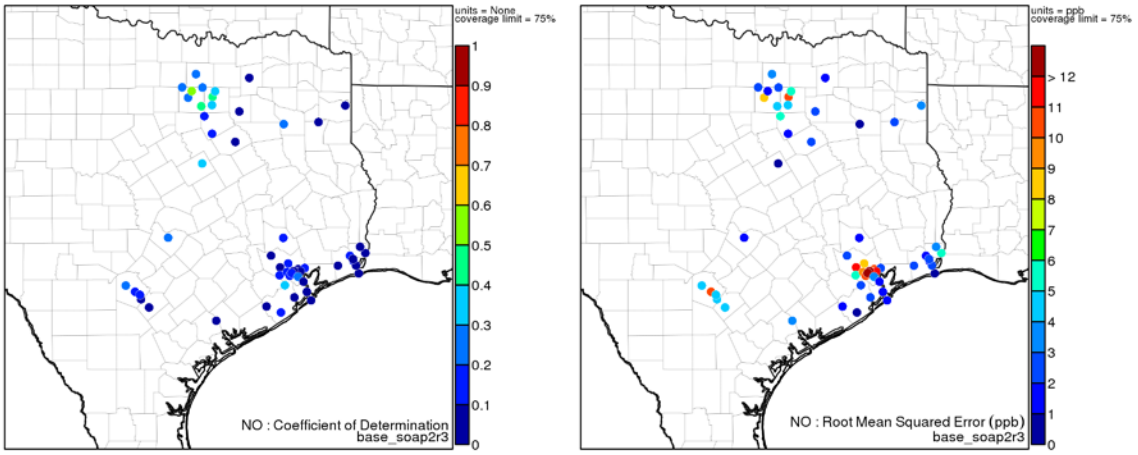

Figure 2-13. Performance metrics for modeled hourly NO concentrations at CAMS monitoring sites in eastern Texas during the episode time period.

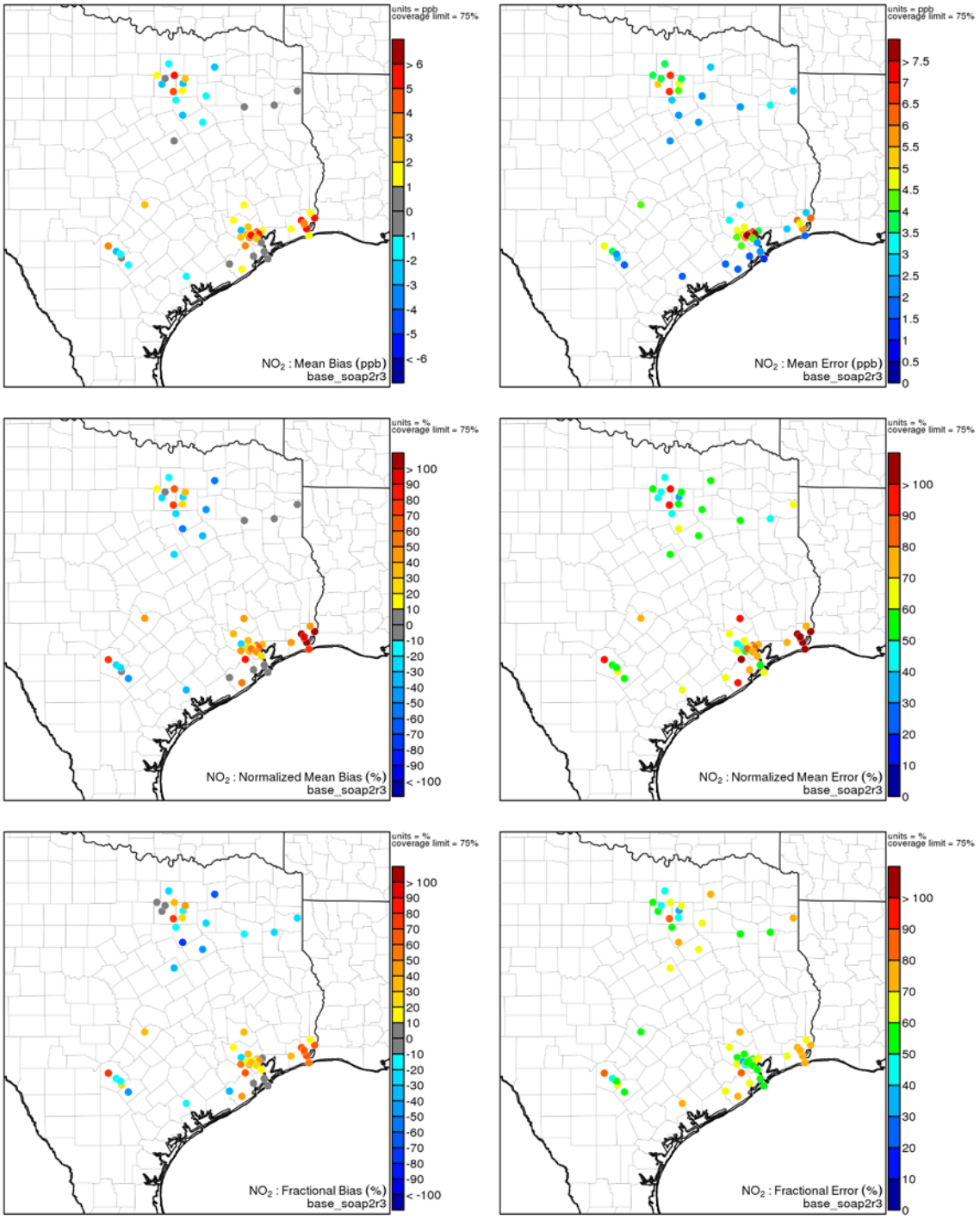
units = ppb
coverage limit = 75%
> 6
5
4
3
2
1
0
-1
-2
-3
-4
-5
< -6
NO2 : Mean Bias (ppb)
base_soap2r3
units = ppb
coverage limit = 75%
> 7.5
7
6.5
6
5.5
5
4.5
4
3.5
3
2.5
2
1.5
1
0.5
0
NO2 : Mean Error (ppb)
base_soap2r3
units = %
coverage limit = 75%
> 100
90
80
70
60
50
40
30
20
10
0
-10
-20
-30
-40
-50
-60
-70
-80
-90
< -100
NO2 : Normalized Mean Bias (%)
base_soap2r3
units = %
coverage limit = 75%
> 100
90
80
70
60
50
40
30
20
10
0
NO2 : Normalized Mean Error (%)
base_soap2r3
units = %
coverage limit = 75%
> 100
90
80
70
60
50
40
30
20
10
0
-10
-20
-30
-40
-50
-60
-70
-80
-90
< -100
NO2 : Fractional Bias (%)
base_soap2r3
units = %
coverage limit = 75%
> 100
90
80
70
60
50
40
30
20
10
0
NO2 : Fractional Error (%)
base_soap2r3

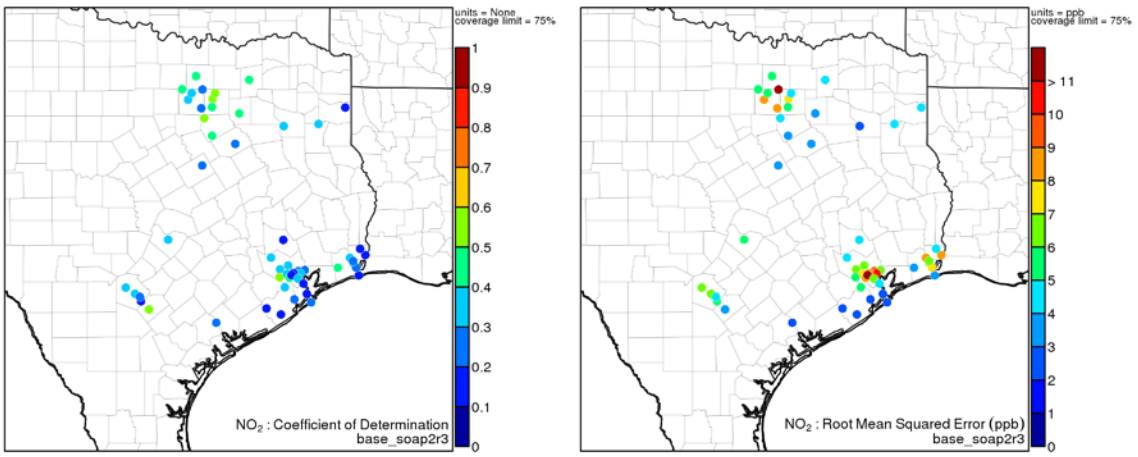

Figure 2-14. Performance metrics for modeled hourly NO_2 concentrations at CAMS monitoring sites in eastern Texas during the episode time period.

2.6.1.3 Fine particulate Matter ($PM_{2.5}$)

A scatter plot of modeled and observed hourly $PM_{2.5}$ mass concentrations at CAMS sites within the 4-km eastern Texas domain is shown in Figure 2-15. Compilations of operational performance statistics for total $PM_{2.5}$ mass concentrations reported by Simon et al. (2012) are shown in Figure 2-16. Their analysis is based on a compilation of measurements made over different time periods and across different urban and rural networks throughout the United States. Figures 2-17 show statistical performance metrics for predictions relative to observed hourly $PM_{2.5}$ mass concentrations, respectively, at individual CAMS sites during the episode time period. Appendix B shows daily performance metrics for hourly $PM_{2.5}$ averaged over all episode days separately for the Dallas-Fort Worth, Houston-Galveston, Austin, and San Antonio areas.

Modeled $PM_{2.5}$ mass concentrations overestimated observed concentrations at CAMS sites within the 4-km domain, notably in the Houston-Galveston and Austin areas. Model performance with the SOAP2r3 scheme was markedly better than with SOAP2 and comparable to that with the 1.5-D VBS scheme at eastern Texas CAMs sites (Appendix A). Investigation of 10-day back trajectories during September 2013 indicated a low probability that substantial Saharan dust was impacting Texas on most days during the month. Analysis of predicted sea-salt sodium (Na) and particulate nitrate (PNO_3) concentrations indicated overestimation biases that may have contributed to the overestimation of $PM_{2.5}$ observations along the Gulf Coast (Figure 2-18). The results suggested that nitrate displacement of chloride in sea salt could be overestimated. The characterization of fires may have affected modeled particulate matter concentrations within Texas during September 2013. Agricultural burning in the Mississippi River Valley and wildfires in Texas, the Plains States, and Mississippi River Valley was associated with increased aerosol optical depth (AOD) in the region during the month. The fire emissions model, FINN v.1, was used in this work, but the model underwent revisions in previous AQRP projects (12-018 and 14-011). FINN v.2 was made available to the TCEQ as a result of AQRP Project 14-011, but completion of the full global model for public release is still pending. Although beyond the scope of this current project, future work should evaluate the effects of more recent versions of FINN on $PM_{2.5}$ model performance.

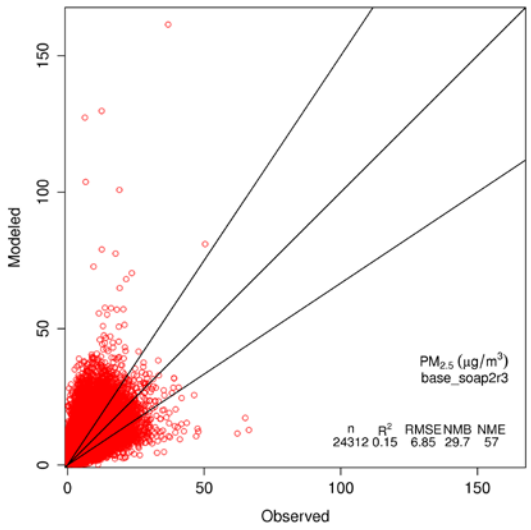

Figure 2-15. Scatter plot of modeled and observed hourly $PM_{2.5}$ concentrations, paired in space and time, at CAMS monitoring sites within the 4-km eastern Texas domain.

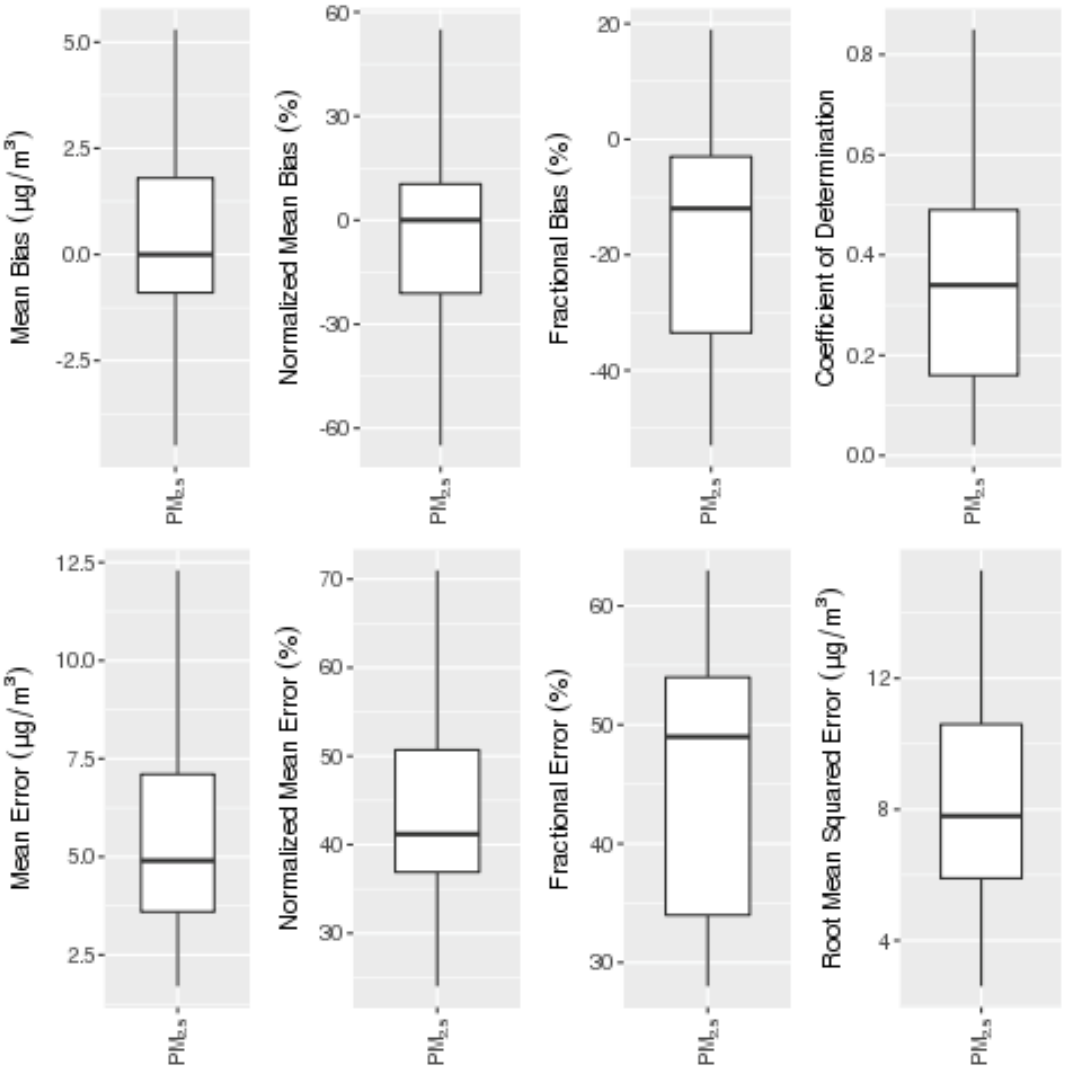

Figure 2-16. Compilation of $PM_{2.5}$ performance metrics from Simon et al. (2012; ref. Fig 4). Centerlines show median values, boxes outline the 25th and 75th percentile values and whiskers extend to 1.5 times the interquartile range.

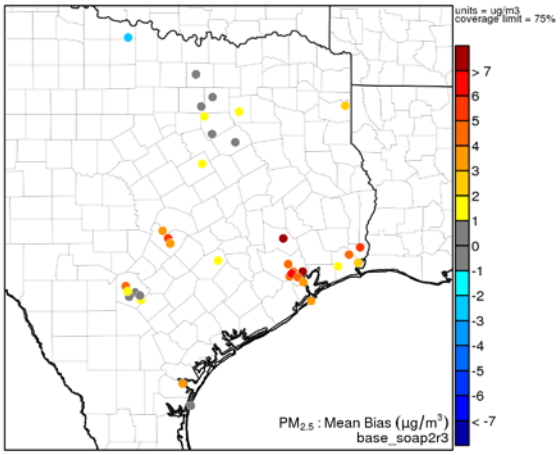
units = ug/m3
coverage limit = 75%
> 7
6
5
4
3
2
1
0
-1
-2
-3
-4
-5
-6
< -7
PM2.5 : Mean Bias (µg/m3)
base_soap2r3

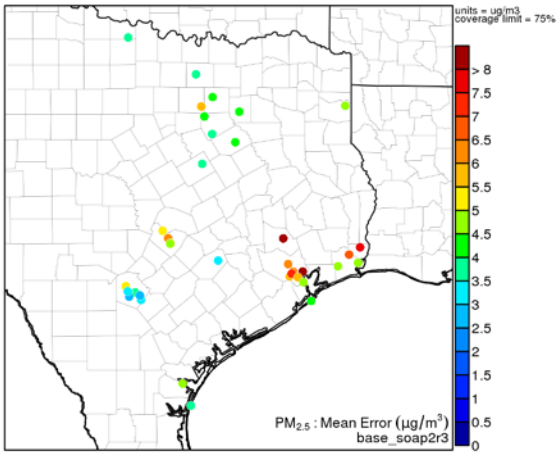
units = ug/m3
coverage limit = 75%
> 8
7.5
7
6.5
6
5.5
5
4.5
4
3.5
3
2.5
2
1.5
1
0.5
0
PM2.5 : Mean Error (µg/m3)
base_soap2r3

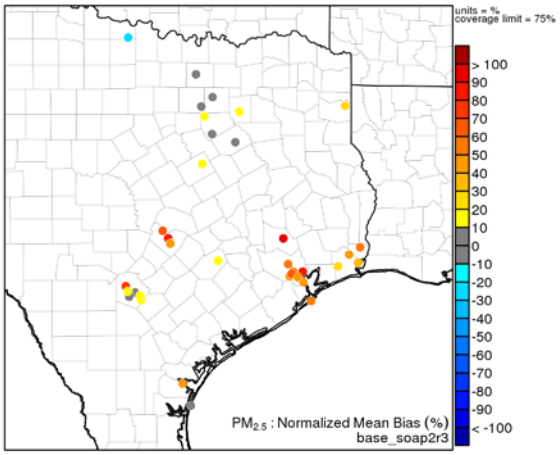
units = %
coverage limit = 75%
> 100
90
80
70
60
50
40
30
20
10
0
-10
-20
-30
-40
-50
-60
-70
-80
-90
< -100
PM2.5 : Normalized Mean Bias (%)
base_soap2r3

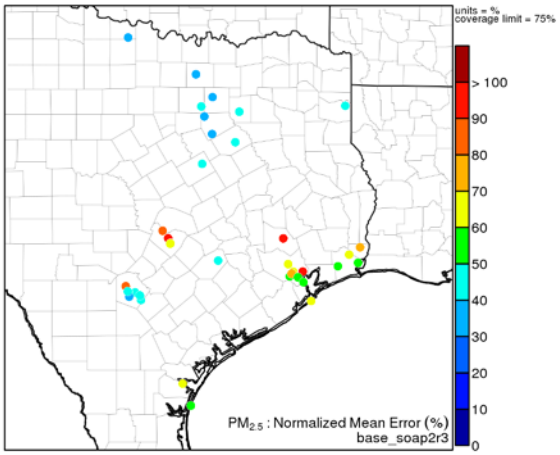
units = %
coverage limit = 75%
> 100
90
80
70
60
50
40
30
20
10
0
PM2.5 : Normalized Mean Error (%)
base_soap2r3

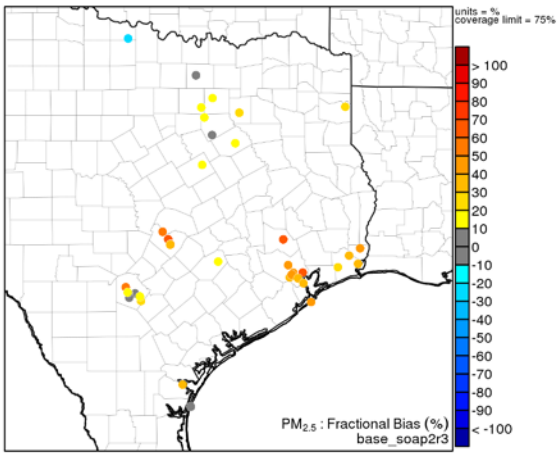
units = %
coverage limit = 75%
> 100
90
80
70
60
50
40
30
20
10
0
-10
-20
-30
-40
-50
-60
-70
-80
-90
< -100
PM2.5 : Fractional Bias (%)
base_soap2r3

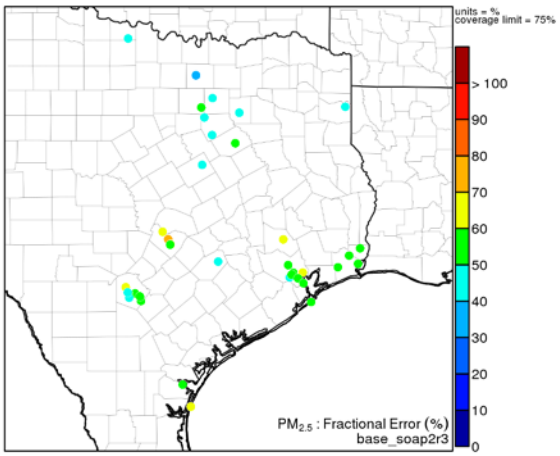
units = %
coverage limit = 75%
> 100
90
80
70
60
50
40
30
20
10
0
PM2.5 : Fractional Error (%)
base_soap2r3

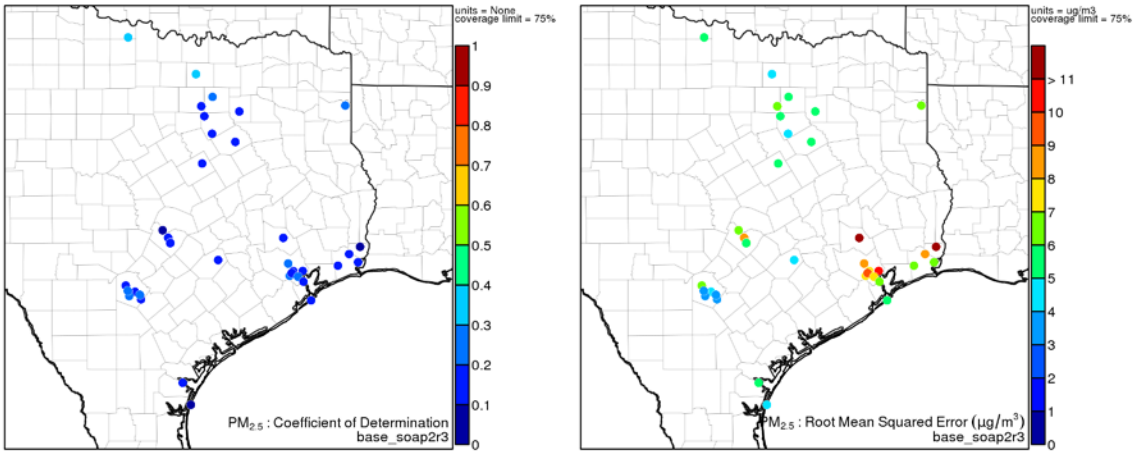

Figure 2-17. Performance metrics for modeled hourly $PM_{2.5}$ concentrations at CAMS monitoring sites in eastern Texas during the episode time period.

(a)

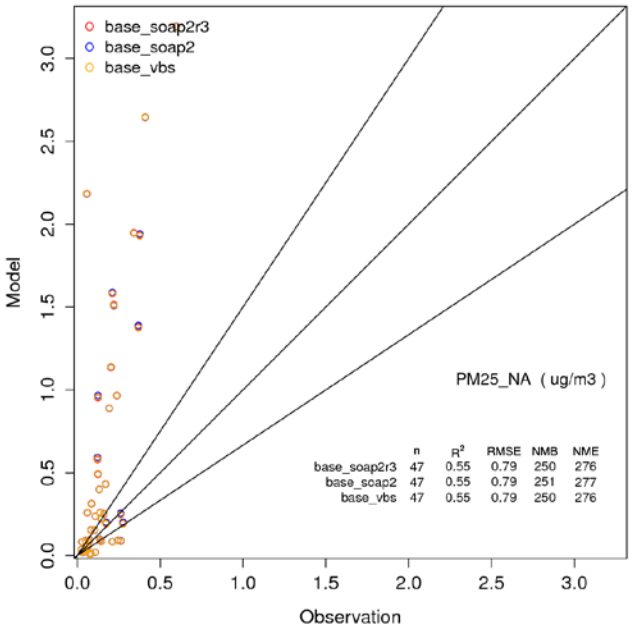

(b)

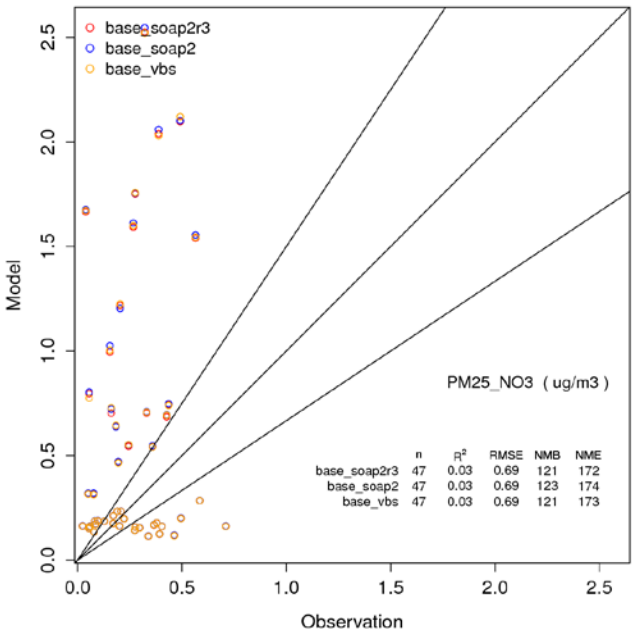

Figure 2-18. CAMx model predictions of (a) predicted sea-salt sodium (Na) and (b) particulate nitrate (PNO_3) concentrations with three organic aerosol-gas partitioning and oxidation schemes: 1.5-D VBS, SOAP2, and SOAP2r3 versus observed concentrations.

2.6.2 PM Speciation at DISCOVER-AQ Surface Sites

PM speciation measurements were made at several surface sites in the Houston-Galveston area during the DISCOVER-AQ time period and provided insights on organic aerosol concentrations. Comparisons were made between observations and CAMx predictions with three different organic aerosol-gas partitioning and oxidation schemes, 1.5-D VBS, SOAP2, and SOAP2r3. These analyses helped to guide refinements to the SOAP2 mechanism that led to the development of SOAP2r3.

Filter-based $PM_{2.5}$ measurements at the Conroe (CAMS 78), Moody Tower, and Manvel Croix (CAMS 84) monitoring stations were conducted by Baylor University during the 2013 DISCOVER-AQ campaign (AQRP Project 14-029). $PM_{2.5}$ samples were collected using the TISCH Environmental high volume sampler (HV2.5) and the URG Corporation medium volume sampler (MV2.5) at Moody Tower and Manvel Croix. Only high volume sampler data was available at Conroe. Two common measurements techniques were used to quantify OC and EC: thermal optical reflectance (TOR) and thermal optical transmittance (TOT). OC and EC concentrations at the Conroe, Moody Tower, and Manvel Croix sites were analyzed using TOT. Hildebrandt Ruiz et al. (2015) estimated TOR OC and EC using relationships derived from data collected at the TCEQ Clinton Drive site (CAMS 403) in Houston, which were also applied in this work:

$$OC_{TOR} = 0.91\ OC_{TOT} + 0.0067$$
$$EC_{TOR} = 1.34\ EC_{TOT} - 0.0079$$

Time series of modeled and observed OC and EC concentrations are compared in Figures 2-19 and 2-20, respectively. Differences between TOT and TOR data for both OC and EC were small. CAMx consistently overpredicted observed EC concentrations at the three sites with no differences between aerosol schemes. CAMx predictions of OC concentrations with SOAP2 were consistently greater than with SOAP2r3 or 1.5-D VBS at all three sites. OC predictions with SOAP2 overestimated observed OC concentrations at Conroe during most of September and at Manvel Croix during approximately the first half of the month, while predictions using the 1.5-D VBS or SOAP2r3 schemes were in better agreement with observations. The peak in observed OC concentrations on September 26 at Conroe was replicated well by CAMx using the 1.5-D VBS scheme but overestimated by SOAP2r3 and to a greater extent by SOAP2. Between September 21-26 at Manvel Croix and Moody Tower, CAMx predictions tended to underestimate daily and episode peak OC concentrations regardless of the aerosol scheme.

Figure 2-21 compares CAMx predictions of hourly $PM_{2.5}$ OA concentrations using the 1.5-D VBS, SOAP2, or SOAP2r3 schemes with PM_1 organic aerosol data obtained from an aerosol chemical speciation monitor (ACSM) located at the Conroe site using the approach of Hildebrandt Ruiz et al. (2015). High time resolution ACSM data were aggregated into hourly averages for consistency with the model output interval. CAMx predictions demonstrated capability in simulating daily variability in OA concentrations for many but not all episode days. Predictions based on the 1.5-D VBS scheme were less

than observed concentrations throughout most of the modeling period, in contrast to those based on the SOAP2r3 scheme that were in better agreement with observations. Predictions with the SOAP2 scheme exhibited a stronger overestimation tendency. Figure 2-22 compares the diurnal profiles of OA concentrations modeled by CAMx versus the ACSM measurements. The three modeled OA profiles replicated diurnal trends in the observational data with lower concentrations during the daytime than through the evening and early morning hours; modeled hourly average OA concentrations with SOAP2 were greater than those based on the 1.5-D VBS or the SOAP2r3 schemes and the observed OA profiles.

Figure 2-23 provides insights on OA composition showing diurnal profiles of organic aerosol composition from Positive Matrix Factorization (PMF) analysis of aerosol mass spectrometer (AMS) data collected during the DISCOVER-AQ campaign with CAMx model predictions based on the three different three organic aerosol-gas partitioning and oxidation schemes. The average oxygenated organic aerosol (OOA) fraction from the PMF analysis (LO-OOA + MO-OOA) was higher than that predicted by CAMx with the three different aerosol schemes. Diurnal profiles of OA composition between the PMF analysis and CAMx predictions also differed. CAMx profiles show distinct decreases in the HOA and BBOA fractions during the early morning hours and increases during the morning rush hour that are not reflected in the PMF data. CAMx 1.5-D VBS and SOAP2r3 profiles are relatively flat throughout much of the day, with the BBOA fraction of the 1.5-D VBS scheme increasing in the evening. The total OOA from the PMF analysis is relatively flat during the day but the transformation of LO-OOA to MO-OOA (aging) is evident in the afternoon; HOA and LO-OOA fractions increase during the evening hours. Analysis of O:C ratios by Hildebrandt Ruiz et al. (2015) indicated that modeled OA with the 1.5-D VBS scheme was less oxidized than observed during the DISCOVER-AQ time period.

Figure 2-24 shows the source apportionment of contemporary carbon in atmospheric organic aerosol from radiocarbon analysis at the Conroe, Moody Tower and Manvel Croix sites performed by Baylor University (AQRP Project 14-029) during the last week of September 2013. The contemporary carbon fraction of the measured organic carbon was estimated based on the $^{14}C/^{12}C$ ratio for the filter sample. The CAMX prediction of the contemporary fraction of the modeled organic carbon from the 1.5-D VBS scheme was determined as the sum of biogenic SOA (PBS) and BBOA (PFP). Contemporary carbon fractions of the modeled organic carbon from SOAP2 and SOAP2r3 were determined using the CAMx particulate source apportionment technology (PSAT) tool. The PSAT estimate was based on the contributions of biogenic emissions from MEGAN, biomass burning emissions estimates from FINN v.1, TRP species from area sources, the portion of IVOA that corresponded to IVOB in the VBS scheme, and the portion of POA that corresponded to POA_MC. For most days, CAMx predictions using SOAP2r3 were in reasonable agreement with observed contemporary carbon fractions at the three sites. In general, predictions based on SOAP2r3 were slightly less than those using SOAP2 and

greater than with the 1.5-D VBS scheme, which tended to underestimate observed values.

(a)

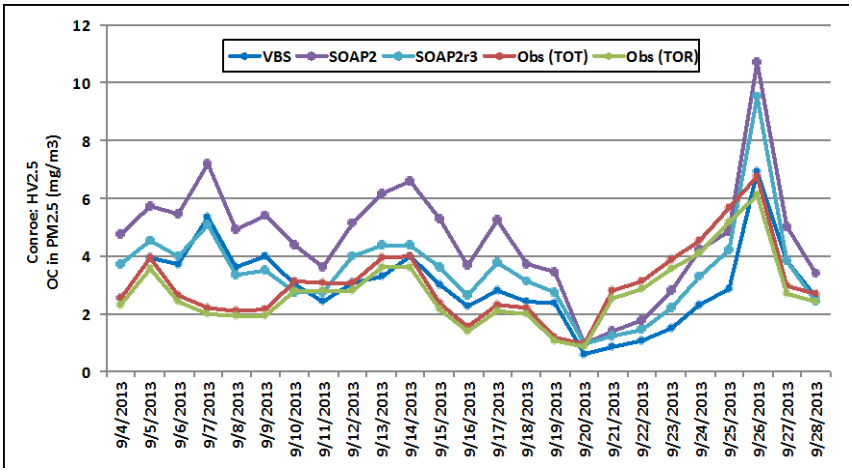
VBS
SOAP2
SOAP2r3
Obs (TOT)
Obs (TOR)
Conroe: HV2.5
OC in PM2.5 (mg/m3)
0
2
4
6
8
10
12
9/4/2013
9/5/2013
9/6/2013
9/7/2013
9/8/2013
9/9/2013
9/10/2013
9/11/2013
9/12/2013
9/13/2013
9/14/2013
9/15/2013
9/16/2013
9/17/2013
9/18/2013
9/19/2013
9/20/2013
9/21/2013
9/22/2013
9/23/2013
9/24/2013
9/25/2013
9/26/2013
9/27/2013
9/28/2013

(b)

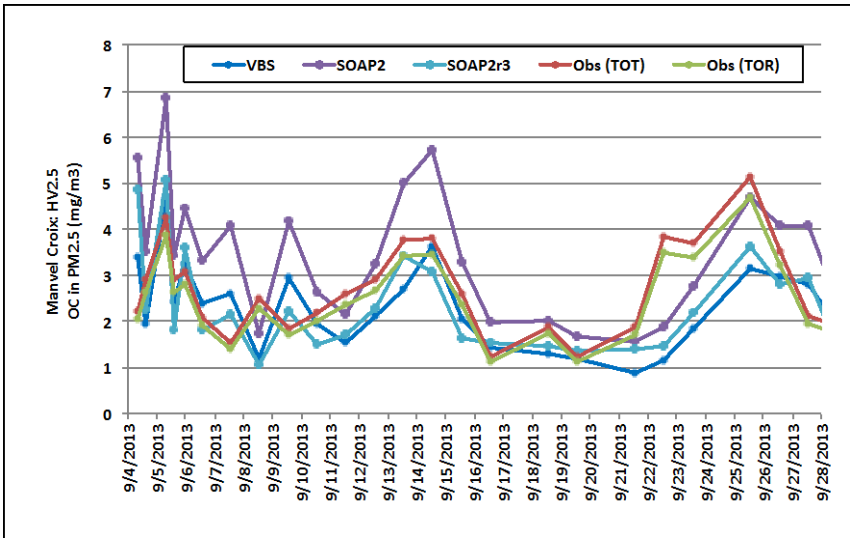
VBS
SOAP2
SOAP2r3
Obs (TOT)
Obs (TOR)
Manvel Croix: HV2.5
OC in PM2.5 (mg/m3)
0
1
2
3
4
5
6
7
8
9/4/2013
9/5/2013
9/6/2013
9/7/2013
9/8/2013
9/9/2013
9/10/2013
9/11/2013
9/12/2013
9/13/2013
9/14/2013
9/15/2013
9/16/2013
9/17/2013
9/18/2013
9/19/2013
9/20/2013
9/21/2013
9/22/2013
9/23/2013
9/24/2013
9/25/2013
9/26/2013
9/27/2013
9/28/2013

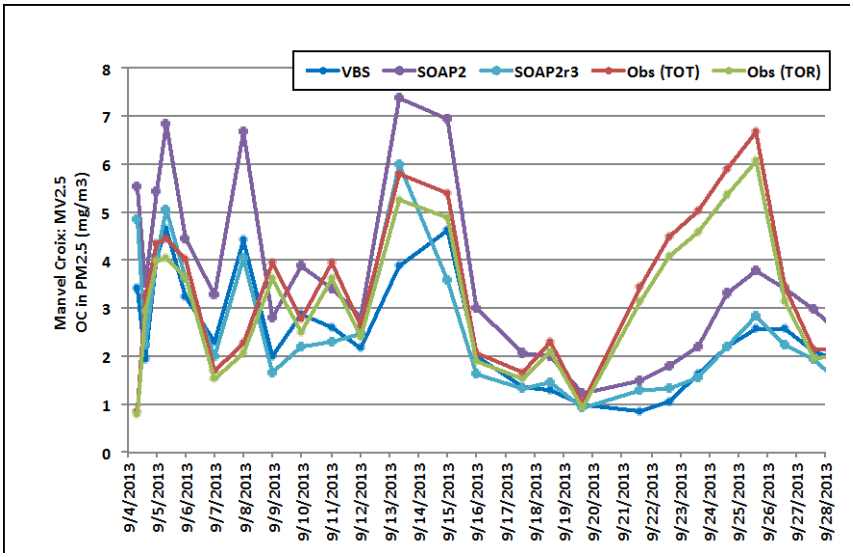
VBS
SOAP2
SOAP2r3
Obs (TOT)
Obs (TOR)
Manvel Croix: MV2.5
OC in PM2.5 (mg/m3)
0
1
2
3
4
5
6
7
8
9/4/2013
9/5/2013
9/6/2013
9/7/2013
9/8/2013
9/9/2013
9/10/2013
9/11/2013
9/12/2013
9/13/2013
9/14/2013
9/15/2013
9/16/2013
9/17/2013
9/18/2013
9/19/2013
9/20/2013
9/21/2013
9/22/2013
9/23/2013
9/24/2013
9/25/2013
9/26/2013
9/27/2013
9/28/2013

(c)

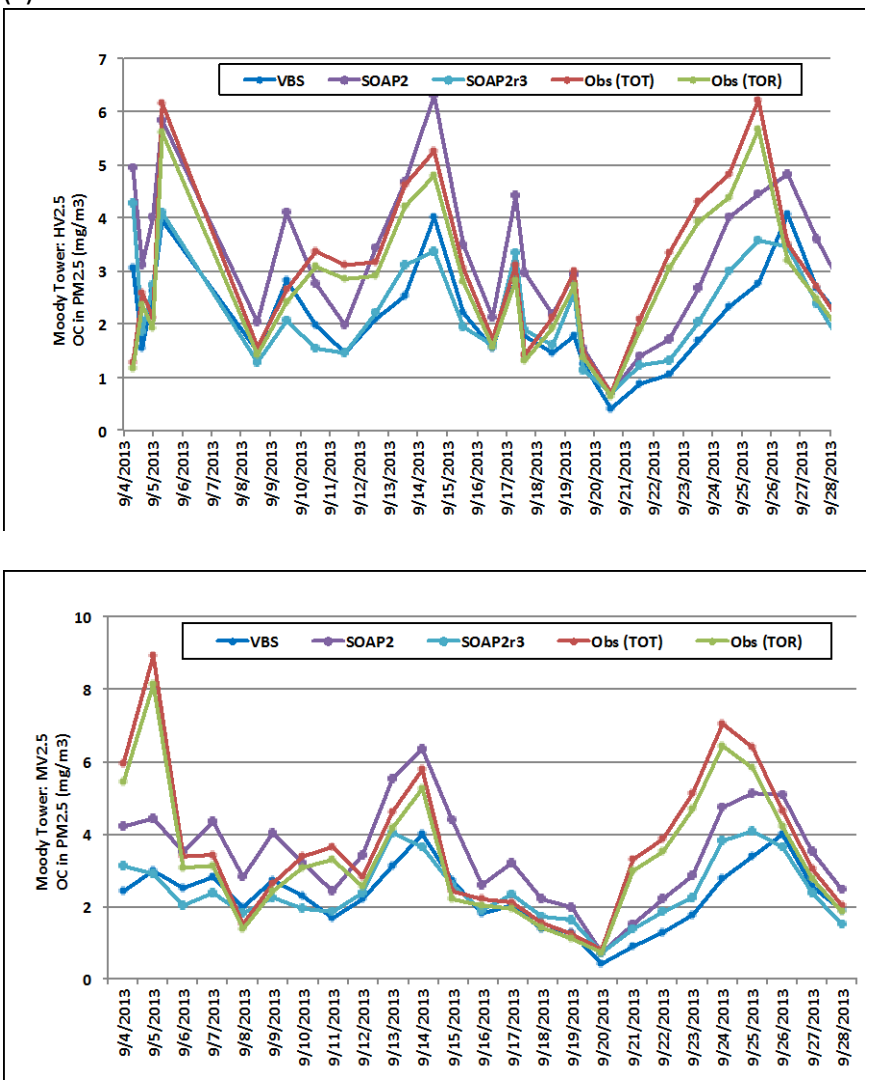

Figure 2-19. Modeled versus observed OC concentrations at (a) Conroe, (b) Manvel Croix, and (c) Moody Tower during September 2013. $PM_{2.5}$ was collected using the TISCH high volume sampler (HV25;) at all three sites and also by the URG medium volume sampler (MV2.5) at the Manvel Croix and Moody Tower sites. OC concentrations were analyzed using thermal optical transmittance (TOT) technique. OC concentrations via thermal optical reflectance (TOR) were estimated using an empirical relationship between TOT and TOR ($OC_{TOR} = 0.91OC_{TOT} + 0.0067$). CAMx model predictions are compared with three organic aerosol-gas partitioning and oxidation schemes: 1.5-D VBS, SOAP2, and SOAP2r3.

(a) Conroe

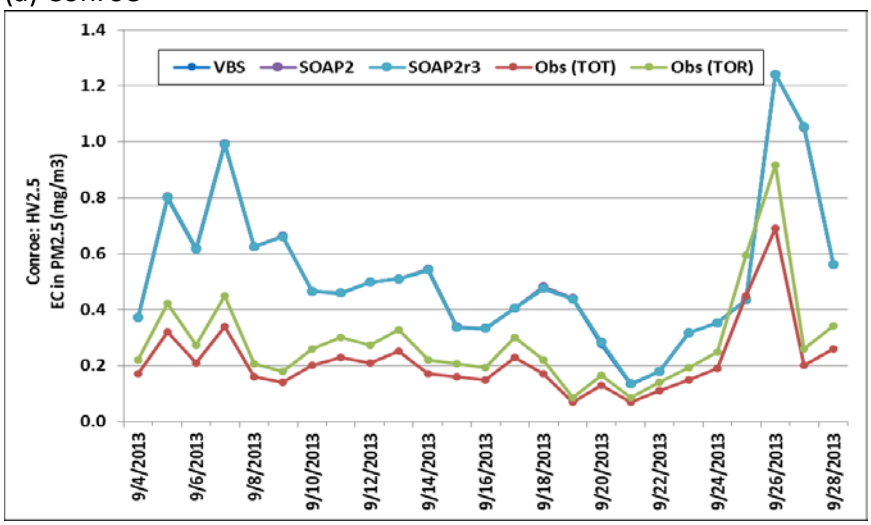
VBS
SOAP2
SOAP2r3
Obs (TOT)
Obs (TOR)
Conroe: HV2.5
EC in PM2.5 (mg/m3)
1.4
1.2
1.0
0.8
0.6
0.4
0.2
0.0
9/4/2013
9/6/2013
9/8/2013
9/10/2013
9/12/2013
9/14/2013
9/16/2013
9/18/2013
9/20/2013
9/22/2013
9/24/2013
9/26/2013
9/28/2013

(b)

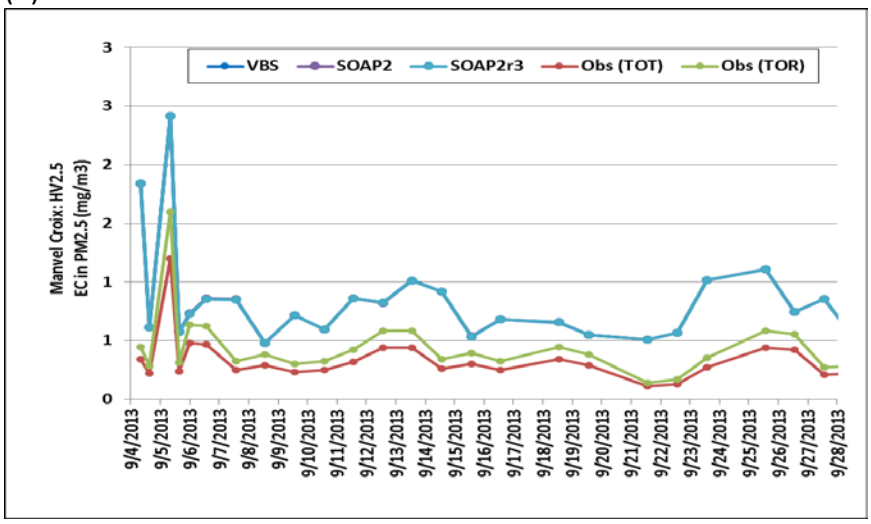
VBS
SOAP2
SOAP2r3
Obs (TOT)
Obs (TOR)
Manvel Croix: HV2.5
EC in PM2.5 (mg/m3)
3
3
2
2
1
1
0
9/4/2013
9/5/2013
9/6/2013
9/7/2013
9/8/2013
9/9/2013
9/10/2013
9/11/2013
9/12/2013
9/13/2013
9/14/2013
9/15/2013
9/16/2013
9/17/2013
9/18/2013
9/19/2013
9/20/2013
9/21/2013
9/22/2013
9/23/2013
9/24/2013
9/25/2013
9/26/2013
9/27/2013
9/28/2013

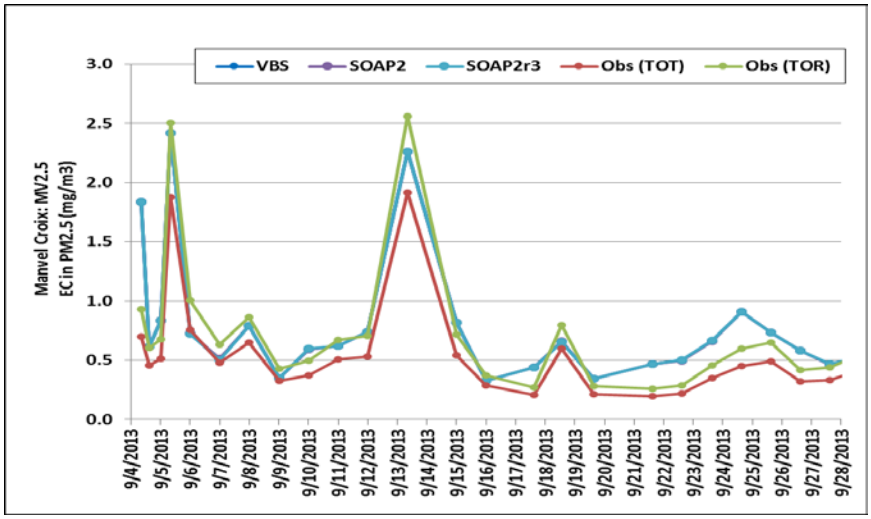
VBS
SOAP2
SOAP2r3
Obs (TOT)
Obs (TOR)
Manvel Croix: MV2.5
EC in PM2.5 (mg/m3)
3.0
2.5
2.0
1.5
1.0
0.5
0.0
9/4/2013
9/5/2013
9/6/2013
9/7/2013
9/8/2013
9/9/2013
9/10/2013
9/11/2013
9/12/2013
9/13/2013
9/14/2013
9/15/2013
9/16/2013
9/17/2013
9/18/2013
9/19/2013
9/20/2013
9/21/2013
9/22/2013
9/23/2013
9/24/2013
9/25/2013
9/26/2013
9/27/2013
9/28/2013

(c)

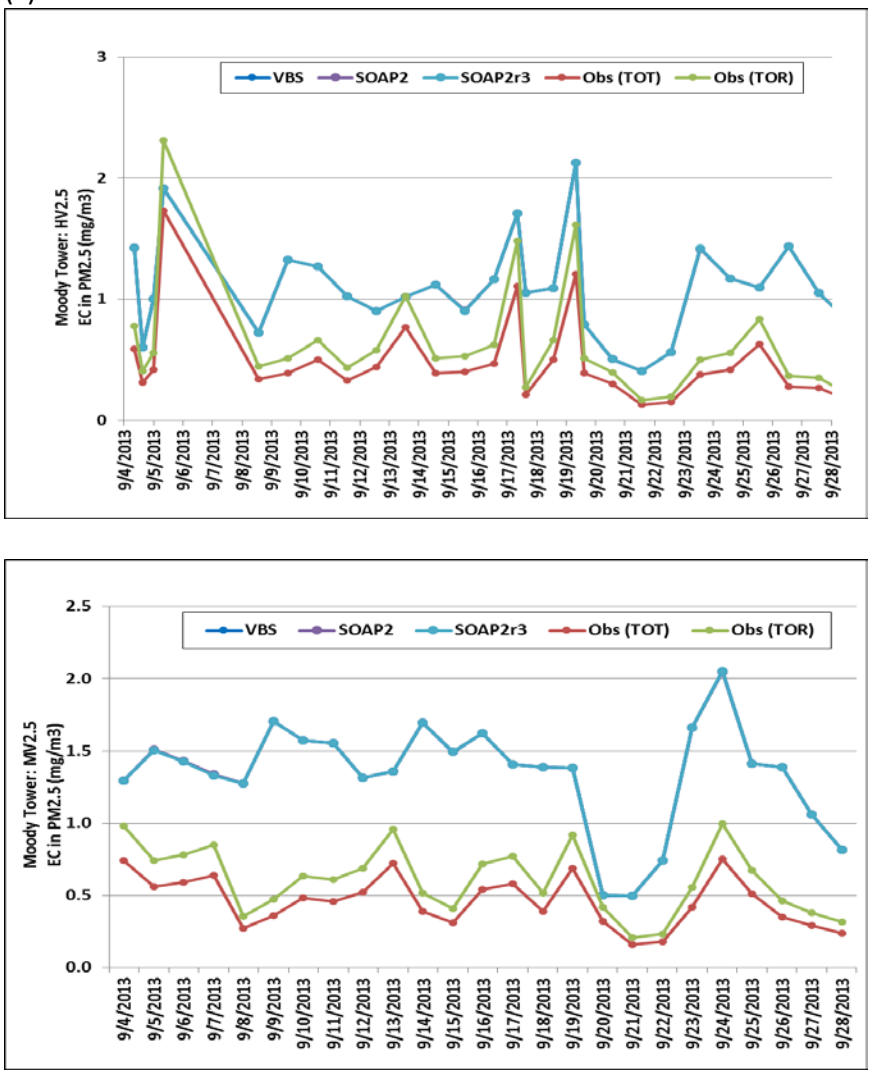

Figure 2-20 Modeled versus observed EC concentrations at (a) Conroe, (b) Manvel Croix, and (c) Moody Tower during September 2013. $PM_{2.5}$ was collected using the TISCH high volume sampler (HV25) at all three sites and also by the URG medium volume sampler (MV2.5) at the Manvel Croix and Moody Tower sites. EC concentrations were analyzed using thermal optical transmittance (TOT) technique. EC concentrations via thermal optical reflectance (TOR) were estimated using an empirical relationship between TOT and TOR ($EC_{TOR} = 1.34EC_{TOT} + 0.0079$). CAMx model predictions are compared with three organic aerosol-gas partitioning and oxidation schemes: 1.5-D VBS, SOAP2, and SOAP2r3. Note that predicted EC concentrations with the three schemes are virtually identical.

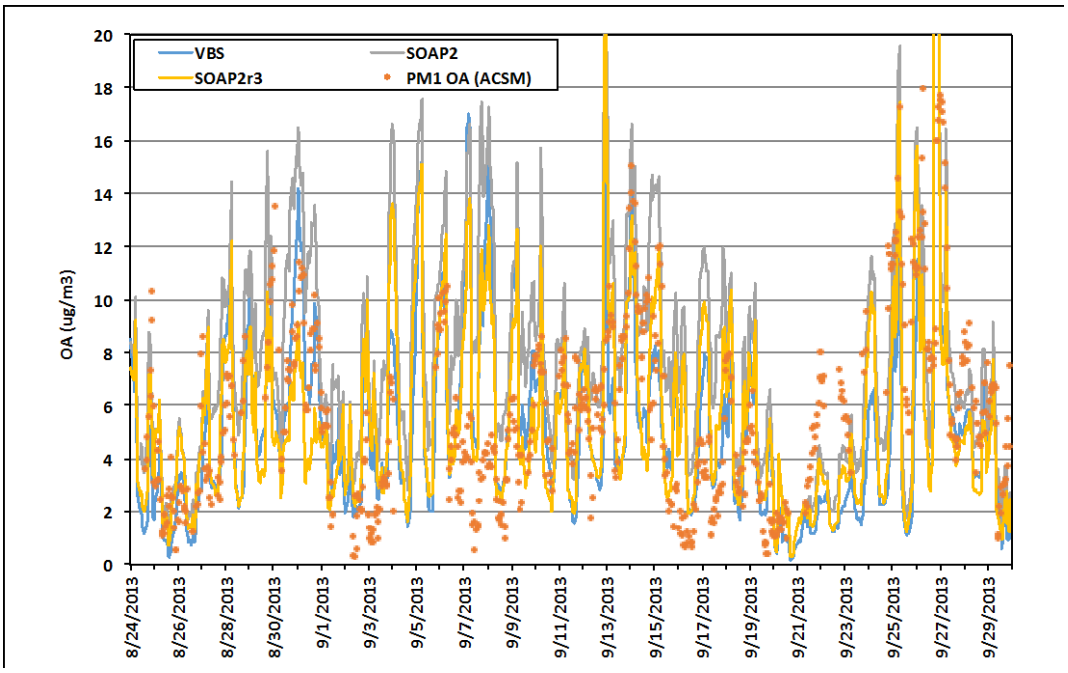

Figure 2-21. Hourly observed PM_1 and modeled $PM_{2.5}$ organic aerosol concentrations at Conroe during the DISCOVER-AQ campaign. Measured PM_1 OA concentrations were obtained from an aerosol chemical speciation monitor (ACSM) at the site. CAMx model predictions are compared with three organic aerosol-gas partitioning and oxidation schemes: 1.5-D VBS, SOAP2, and SOAP2r3. For the 1.5-D VBS scheme, OA is calculated as sum of PAP, PCP, PFP, PAS, PBS (abbreviation denotes the *phase*: P – particle; V – vapor, *source*: A – anthropogenic; B – biogenic: C – cooking; F – fire, and *formation*: P – primary; S – secondary). For SOAP2 and SOAP2r3, OA represents the sum of POA, SOA1, SOA2, SOA2, SOA3, SOA4, SOPA, and SOPB.

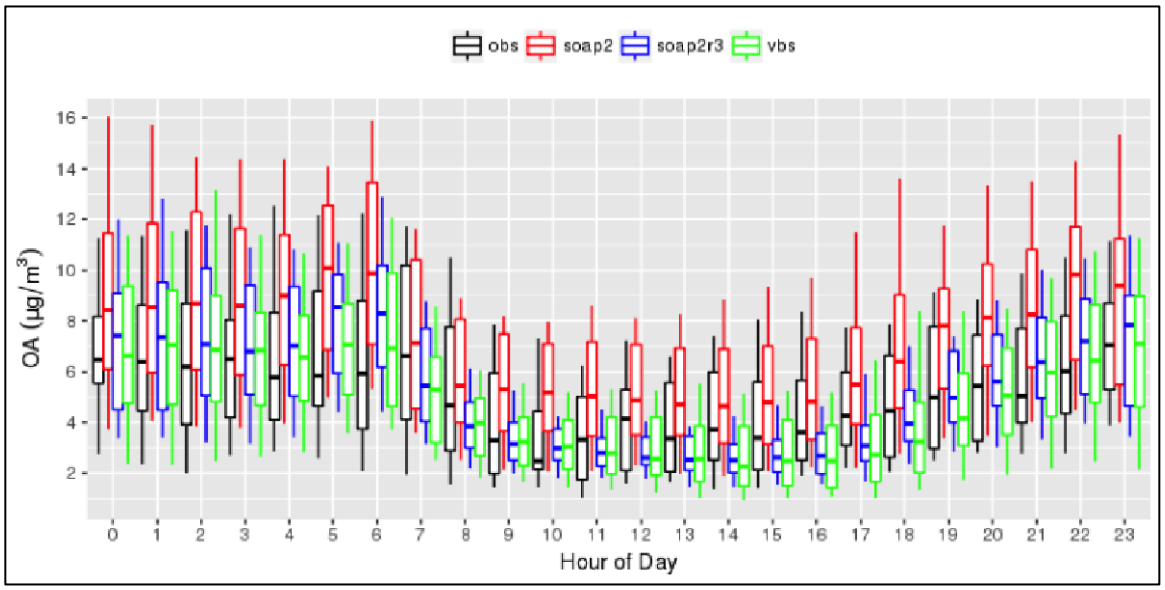

Figure 2-22. Box and whisker plot of the diurnal cycle of observed PM_1 and modeled $PM_{2.5}$ organic aerosol concentration at Conroe obtained from an aerosol chemical speciation monitor (ACSM) at the site. Boxes represent the middle two quartiles, whiskers stretch to 10th to 90th percentile points.

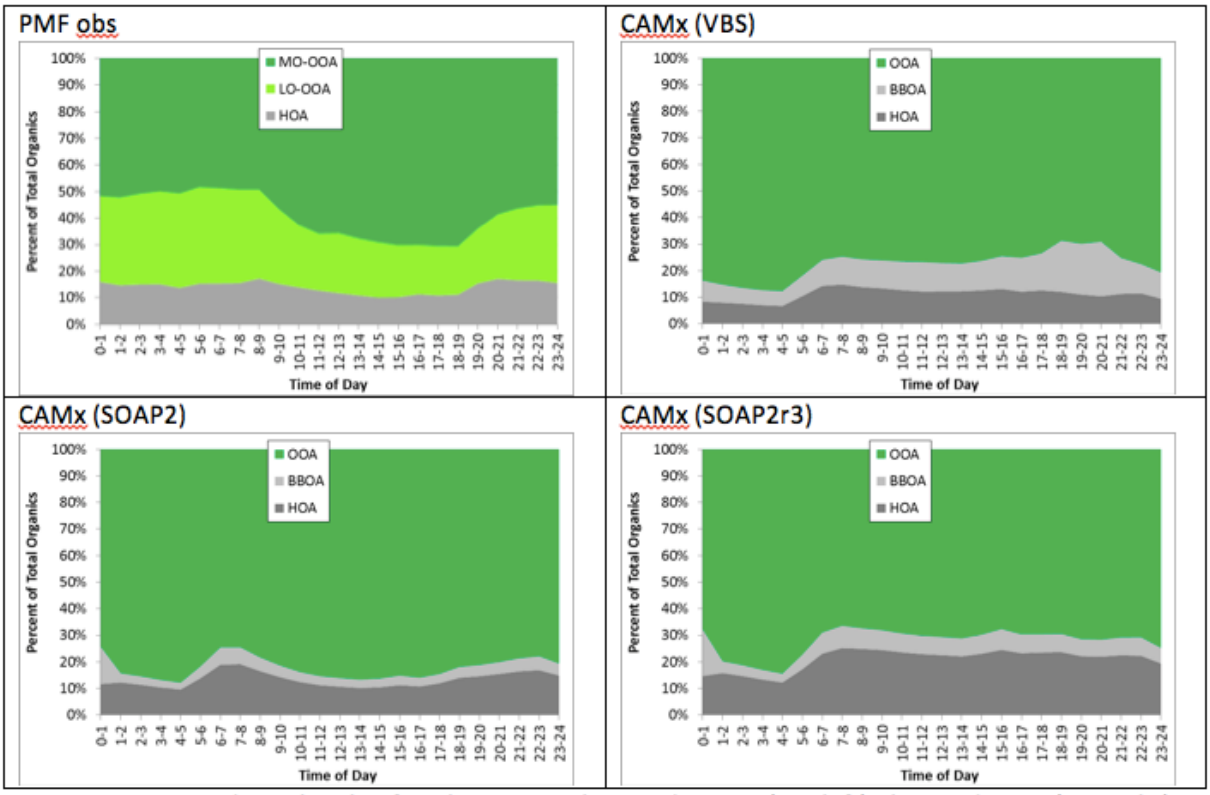

Figure 2-23. Diurnal profile of organic aerosol composition from Positive Matrix Factorization (PMF) analysis of aerosol mass spectrometer (AMS) data collected during the DISCOVER-AQ campaign (top left). CAMx model predictions are compared with three organic aerosol-gas partitioning and oxidation schemes: 1.5-D VBS (top right), SOAP2 (bottom left), and SOAP2r3 (bottom right). HOA represent hydrocarbon-like OA from meat-cooking and other anthropogenic sources. BBOA represents OA from biomass burning OA (BBOA). LO-OOA and MO-OOA refer to less oxidized-oxygenated organic aerosol and more oxidized-oxygenated organic aerosol, respectively. HOA from the PMF analysis represents the sum of HOA and BBOA. OOA from CAMx represents the sum of LO-OOA and MO-OOA. The 1.5-D VBS scheme uses four basis sets to separately track HOA (PAP and PCP), BBOA (PFP), and two OOA groups (PAS and PBS). For the SOAP2 and SOAP2r3 schemes OOA is represented as the sum of SOA1, SOA2, SOA3, SOA4, SOPA, and SOPB, BBOA is the fraction of POA associated with fire emissions, and HOA is the remainder of POA.

(a) Conroe

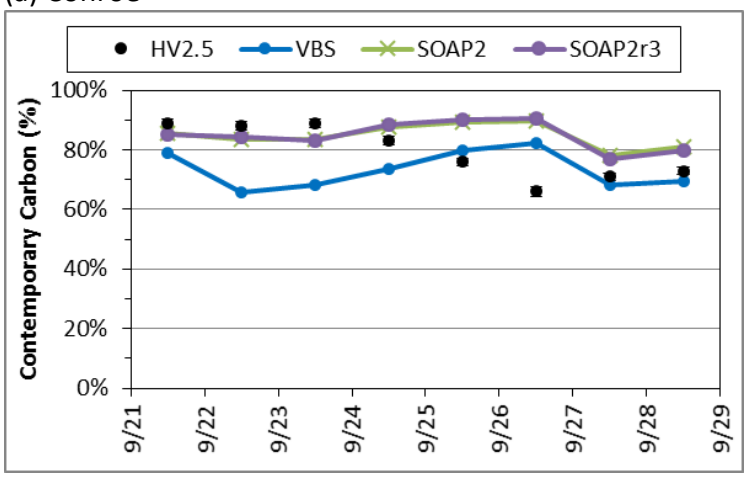

(b) Manvel Croix

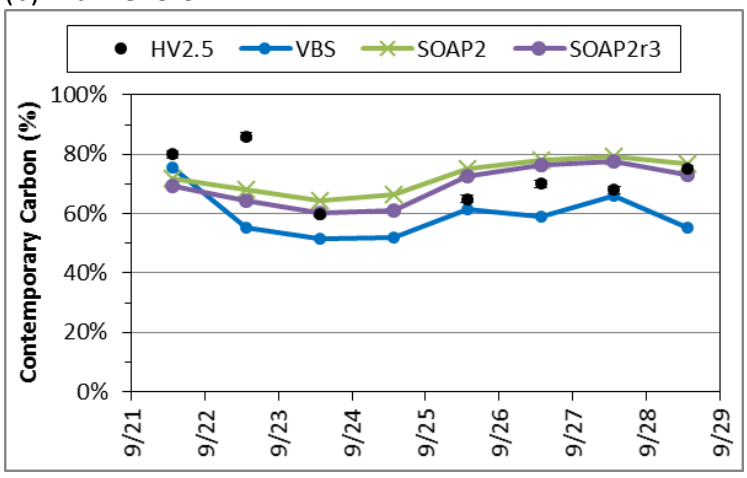

(c) Moody Tower

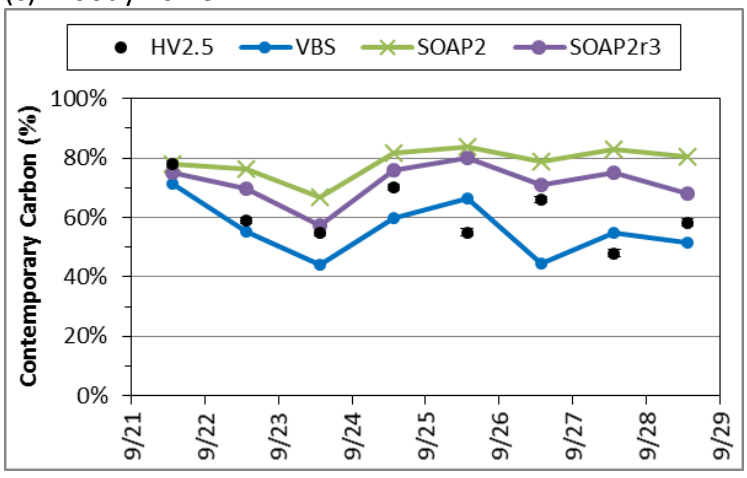

Figure 2-24. Observed and modeled contemporary carbon fractions at (a) Conroe, (b) Manvel Croix, and (c) Moody Tower during September 21-29, 2013. $PM_{2.5}$ was collected

using the TISCH high volume sampler (HV25). CAMx model predictions are compared with three organic aerosol-gas partitioning and oxidation schemes: 1.5-D VBS, SOAP2, and SOAP2r3.

2.6.3 Evaluation of Model Performance with DISCOVER-AQ Aircraft Measurements

Measurements made on-board the National Aeronautics and Space Administration's (NASA's) P-3B aircraft during the DISCOVER-AQ campaign were used to evaluate CAMx predictions of vertical profiles of trace gases and particulate matter components aloft of the Houston metropolitan area. Model performance assessment focused on the locations of aircraft spirals at the locations shown in Figure 2-25 (http://www-air.larc.nasa.gov/missions/discover-aq/discover-aq.html. Flights were conducted on nine days during the campaign as shown in Table 2-11. Measurement data were obtained from NASA's DISCOVER-AQ site: http://www-air.larc.nasa.gov/missions/discover-aq/discover-aq.html.

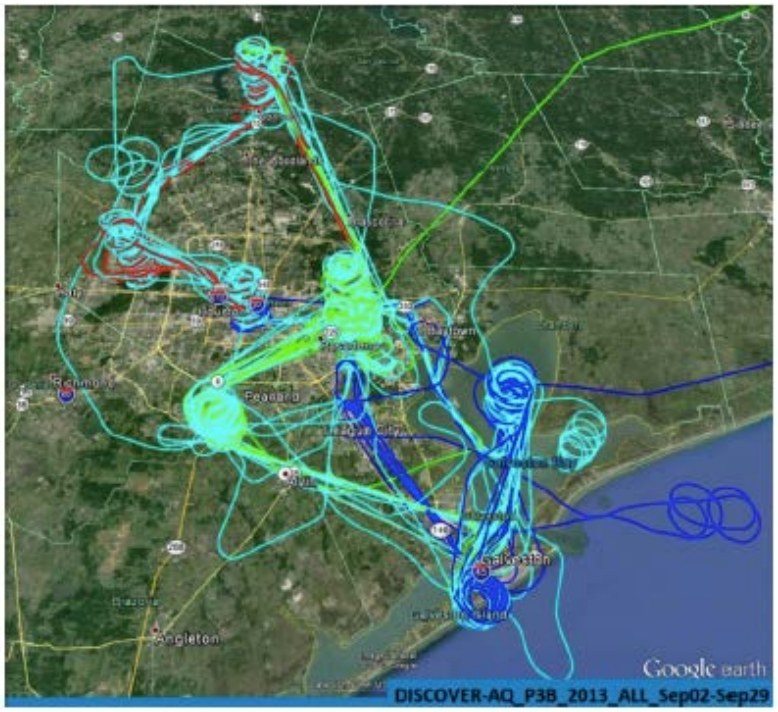

Figure 2-25. Flight paths of NASA's P3-B aircraft during the DISCOVER-AQ campaign.

Table 2-11. P3-B flight dates and measurements during the DISCOVER-AQ campaign

Date	Trace Gases (ppb)								PM Composition (µg/m3)						
	AN	PN	HNO_3	NO_y	NO_x	O_3	Isoprene	Monoterpenes	Nitrate	Sulfate	Sodium	Ammonium	Chloride	BC	WSOC
9/4/13	-	-	-	✓	✓	✓	✓	✓	✓	✓	✓	✓	✓	-	-
9/6/13	-	-	-	✓	✓	✓	✓	✓	✓	✓	✓	✓	✓	✓	✓
9/11/13	-	-	-	✓	✓	✓	✓	✓	-	-	-	-	-	-	-
9/12/13	-	-	-	✓	✓	✓	✓	✓	-	-	-	-	-	✓	✓
9/13/13	-	-	-	✓	-	✓	-	-	-	-	-	-	-	✓	✓
9/14/13	-	-	-	✓	✓	✓	✓	✓	✓	✓	✓	✓	✓	-	-
9/24/13	-	-	-	✓	✓	✓	✓	✓	✓	✓	✓	✓	✓	✓	✓
9/25/13	✓	✓	-	✓	✓	✓	-	-	✓	✓	✓	✓	✓	✓	✓
9/26/13	✓	✓	✓	✓	✓	✓	✓	✓	✓	✓	✓	✓	✓	✓	✓

Figure 2-26 shows vertical profiles of trace gas concentrations measured during P3-B flights and from CAMx base case predictions. Profiles are shown as 25th percentile, 50th percentile, and 75th percentile concentrations in aggregate for all of the nine flight days. These are indicative of overall trends during the time period; model performance for individual flights may vary.

CAMx base case predictions overestimated 25th and 50th percentile ozone concentrations below 1000m and 75th percentile concentrations below 200 m, consistent with trends observed for the region at CAMS surface sites. Predicted 50th percentile ozone concentration exceeded observed concentrations by approximately 10 ppb. Model predictions underestimated observed ozone concentrations at higher altitudes.

Predicted 25th and 50th percentile NO_x concentrations slightly underestimated but were in relatively good agreement with observations below 1000m. The model exhibited a more pronounced underestimation of 75th percentile concentrations. NO_x concentrations declined aloft. Nitric acid observations were limited, with measurements only on September 26. On this day, observed 25th percentile concentrations were well replicated. Predicted 50th percentile concentrations were overestimated below 2000m and underestimated aloft; 75th percentile concentrations overestimated below 500m with reasonably good agreement aloft. CAMx reactive nitrogen, NO_y, included NO_x, nitric acid (HNO_3), nitrous acid (HONO), peroxyl acetyl nitrate (PAN), methyl peroxyl acetyl nitrate (MPAN), peroxyl propionyl nitrate (PPN), and particulate nitrates. Modeled 25th and 50th percentile NO_y concentrations underestimated observations below 1500m and overestimated concentrations aloft; model performance for 75th percentile concentrations was similar with a sharp transition at approximately 300 m.

Modeled isoprene was in reasonably good agreement with observations with a tendency toward overestimation below 200-300m. Predicted 25th percentile concentrations of monoterpenes underpredicted observations with better agreement near the surface. Modeled 50th percentile concentrations below 400m were slightly overestimated but underestimated aloft. Performance for predicted 75th percentile concentration was similar but with a stronger underestimation bias aloft.

Observations of total peroxy nitrates (PNs) and total alkyl nitrates (ANs) were limited to two flight days. Modeled total PN (i.e., the sum of PAN + PANX + OPAN species in the CB mechanism) concentrations were in reasonably good agreement, with a slight underestimation tendency, with observations. In contrast, predicted total AN (the sum of NTR1 + NTR2 + INTR in the CB mechanism) overestimated observed concentrations to 2500m with a rapid decline in predicted and observed concentrations aloft.

Comparisons between CAMx predictions with the SOAP2r3 (base case), SOAP2, and 1.5-D VBS schemes with observed vertical profiles of trace gases are shown in Appendix C.

Differences in the performance of the three CAMx configurations were virtually negligible.

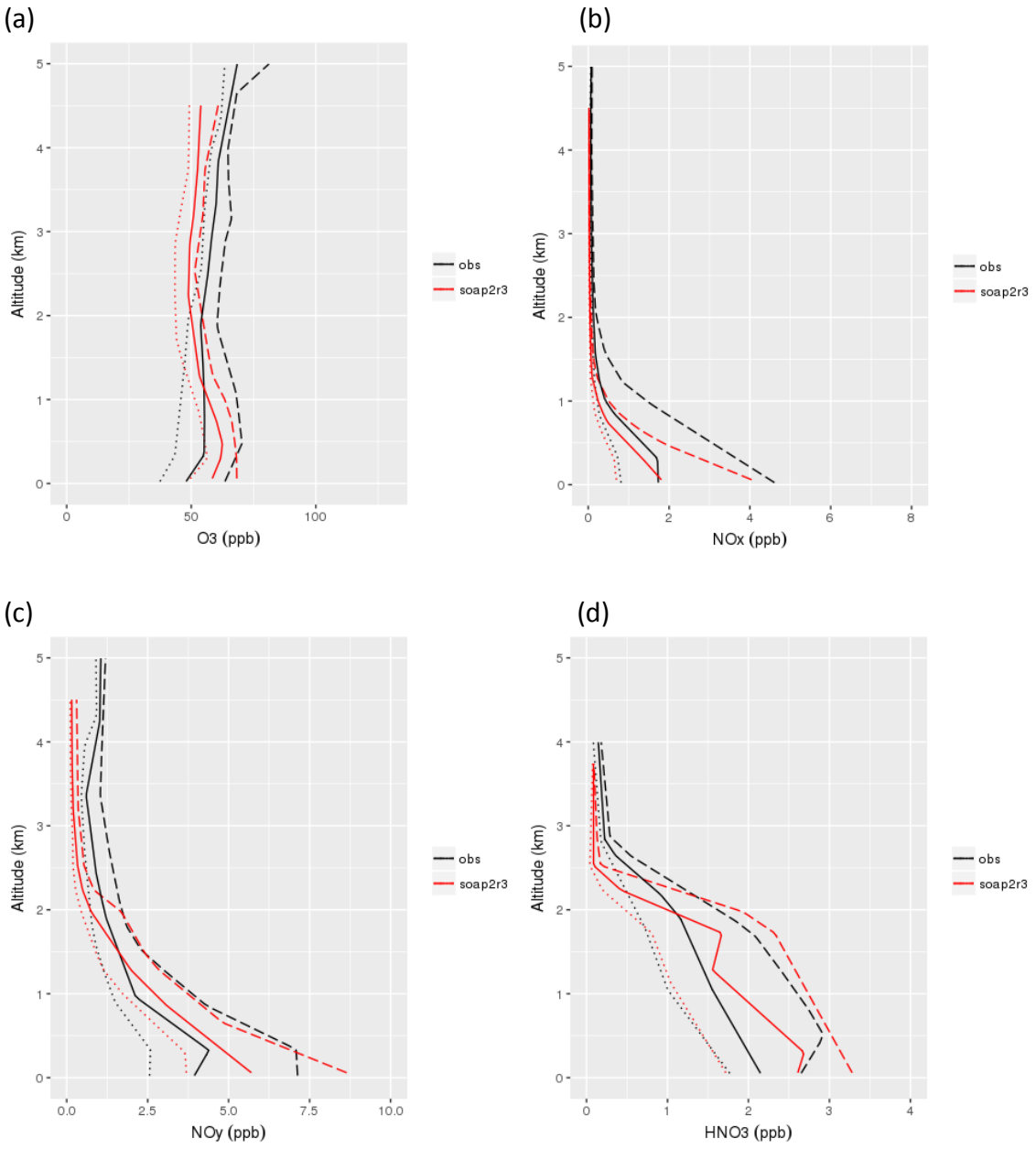

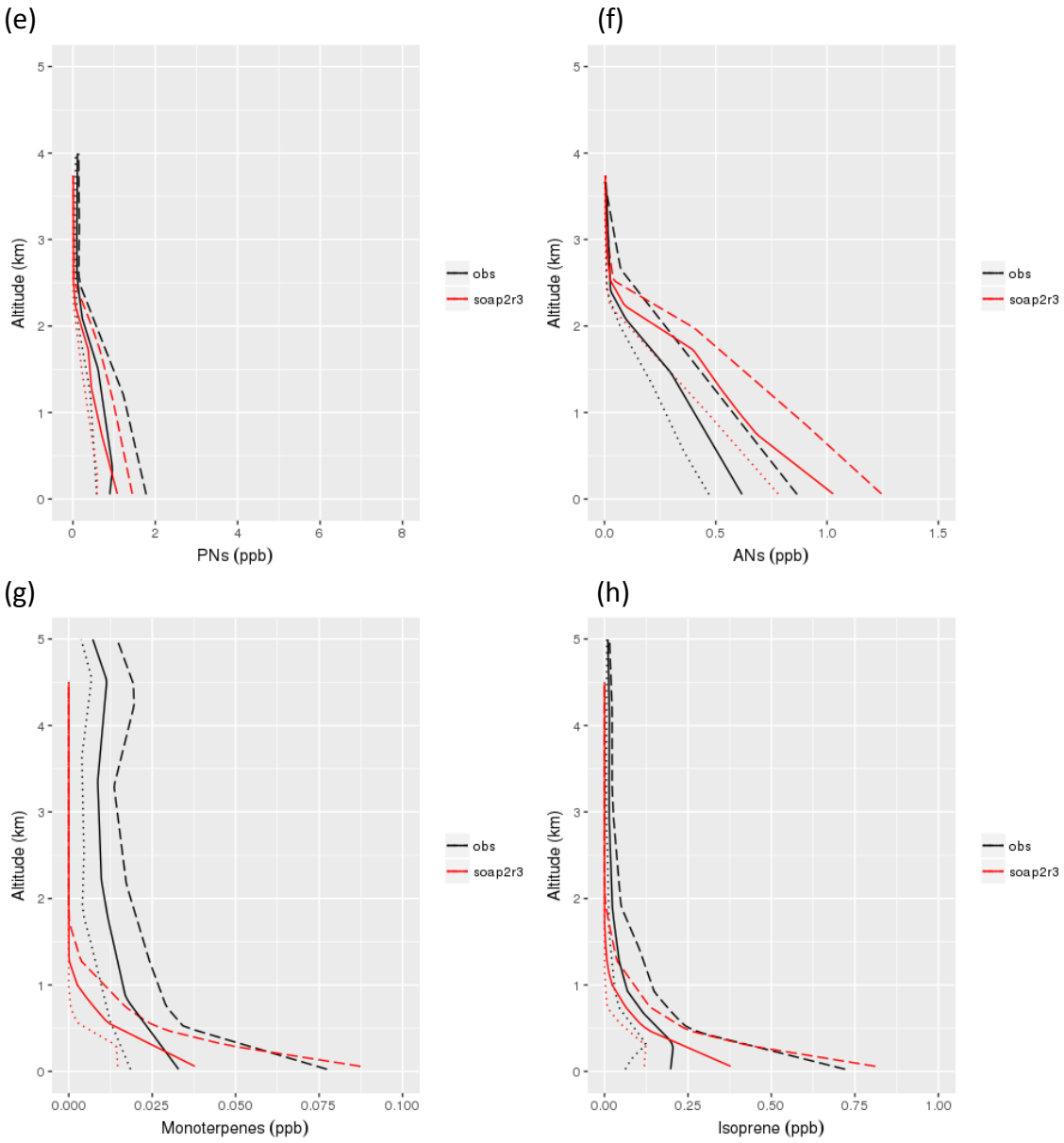

Figure 2-26. Comparison of observed (black) and CAMx base case (red) predicted vertical profiles of (a) ozone, (b) NO_x, (c) NO_y, (d) HNO_3, (e) total peroxy nitrates, (f) alkyl nitrates, (g) monoterpenes, and (h) isoprene concentrations during P3-B flights. Profiles are shown as 25th percentile (small dash), 50th percentile (solid), and 75th percentile (large dash) concentrations. Note that values reported at the lower limit of detection or as negative were not included in the analysis.

Figure 2-27 shows vertical profiles of PM component concentrations measured during P3-B flights and from CAMx base case predictions similar to Figure 2-26.

Modeled sulfate concentrations exhibited a slight underestimation to reasonably good agreement with all observed percentile concentrations below 1000m. More pronounced underestimation of observations aloft could be associated with sensitivity to modeled cloud availability (Nopmongcol et al., 2015). Predicted and observed sulfate concentrations were much higher than those for nitrate during September 2013; observed nitrate was less than 0.2 $\mu g/m^3$ while sulfate was 1-4 $\mu g/m^3$ below 1000m. Ammonia will preferentially bond with sulfate, the stronger acid. Predicted trends in ammonium were similar to those of sulfate. Modeled nitrate concentrations overestimated near surface observations, consistent with performance at CAMx sites.

Modeled sodium profiles exhibited a strong overestimation bias, consistent with the assessment of performance at CAMS sites. In contrast, predicted chloride concentrations exhibited a strong underestimation tendency possibly indicative of missing emission sources.

Predicted black carbon concentrations overestimated observations. Predicted water soluble organic carbon (WSOC) underestimated observed concentrations. Comparisons between CAMx predictions with the SOAP2r3 (base case), SOAP2, and 1.5-D VBS schemes with observed vertical profiles of PM components are shown in Appendix C. The performance of the three CAMx configurations was in excellent agreement for most species with the exception of WSOC. CAMx predictions with SOAP2 were in better agreement with observations of WSOC than either the SOAP2r3 or 1.5-D VBS schemes, which had relatively comparable performance.

2.6.4 Selection of the CAMx Base Case Configuration

CAMx model predictions with the three organic aerosol-gas partitioning and oxidation schemes, 1.5-D VBS, SOAP2, and SOAP2r3, were evaluated against observations at CAMS sites throughout eastern Texas and surface and aircraft observations in southeastern Texas, with a focus on aerosol measurements at the Conroe surface site collected during the DISCOVER-AQ campaign. CAMx predictions of trace gas species at the surface and aloft examined in this work were not sensitive to the selection of the organic aerosol-gas partitioning and oxidation scheme.

CAMx performance for particulate matter mass concentrations and composition remains complex, especially in coastal southeastern Texas. Model performance for $PM_{2.5}$ mass concentrations with the SOAP2r3 scheme was markedly better than with SOAP2 and comparable to that with the 1.5-D VBS scheme at eastern Texas CAMs sites. Predictions of OC and OA concentrations with SOAP2 were consistently higher than either the SOAP2r3 or 1.5-D VBS schemes and frequently, although not always,

exhibited a more pronounced overestimation of these species at the Conroe site. CAMx performance was reasonable for observed contemporary carbon fractions at the Conroe, Manvel Croix, and Moody Tower sites with the three organic aerosol-gas partitioning and oxidation schemes; SOAP2r3 predictions were slightly less than those using SOAP2 and greater than with the 1.5-D VBS scheme, which tended to underestimate observations. The consistent bias in sea salt sodium and particulate nitrate concentrations warrants continued investigation, as do the differences in model performance for WSOC. Attention should continue to focus on SOA yields and removal processes.

The SOAP2r3 and 1.5-D VBS schemes provide generally comparable model performance across the range of trace gases and $PM_{2.5}$ total mass and component concentrations considered here. The VBS scheme requires greater computational intensity and emissions inventory processing than the SOAP scheme and, as such, is expected to be used less frequently in modeling efforts that support of air quality planning and management. However, it is considered to be more representative of the state of the science that should lead to better performance in $PM_{2.5}$ and OA statistics. Evolution of the original SOAP scheme such as that considered here with the modifications for SOAP2r3 may result in performance more comparable to that of the VBS approach. This study proceeded with the use of SOAP2r3 for the CAMx base case.

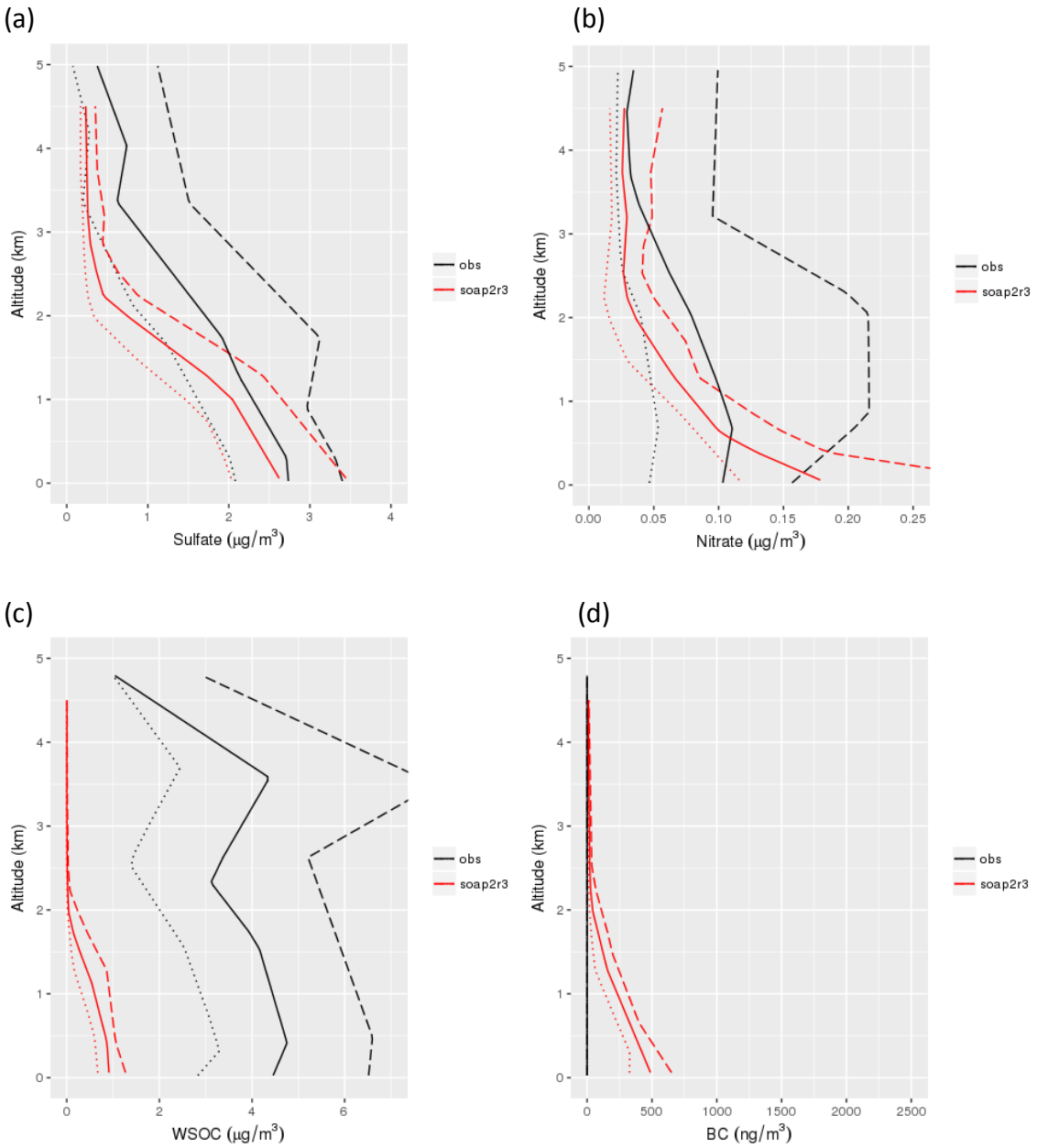
(a)
(b)
(c)
(d)
Altitude (km)
Sulfate (μg/m³)
Nitrate (μg/m³)
WSOC (μg/m³)
BC (ng/m³)
obs
soap2r3

(e)

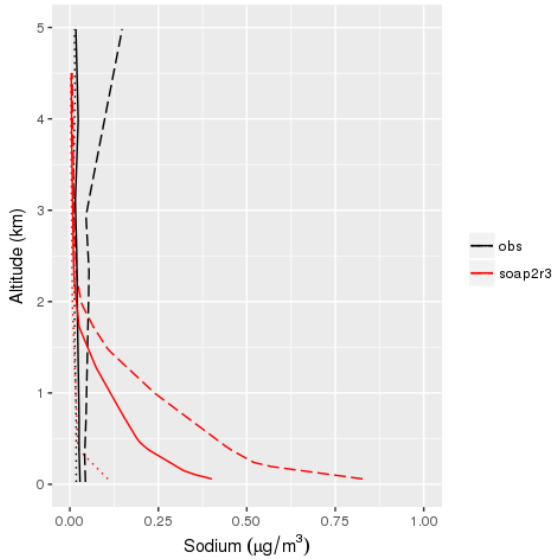

(f)

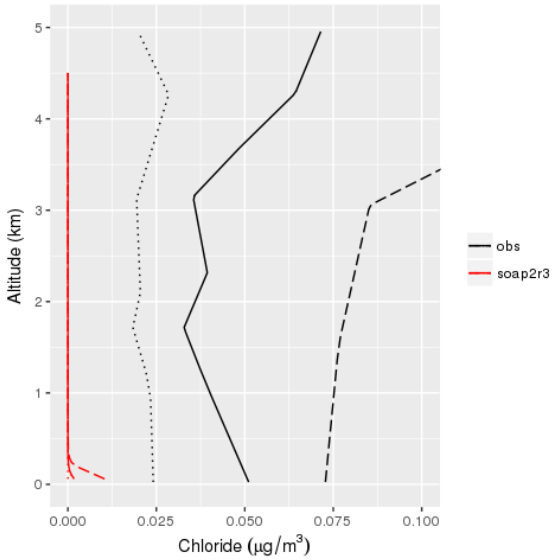

(g)

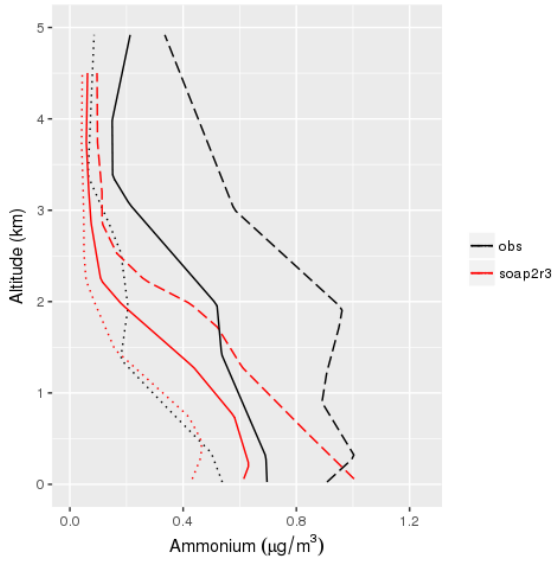

Figure 2-27. Comparison of observed (black) and CAMx base case (red) predicted vertical profiles of (a) sulfate, (b) nitrate, (c) WSOC, (d) BC, (e) sodium, (f) chloride, and (g) ammonium concentrations during P3-B flights. Profiles are shown as 25th percentile (small dash), 50th percentile (solid), and 75th percentile (large dash) concentrations. Note that values reported at the lower limit of detection or as negative were not included in the analysis.

3. CAMx Chemical Mechanism Updates

The starting point for mechanism improvements was revision 4 of the Carbon Bond 6 mechanism, called CB6r4. The TCEQ has been using CB6r4 since March 2017. Compared to the previous CB6r3 mechanism, CB6r4 has AN yields from alkanes that depend upon temperature and atmospheric pressure, and a compact mechanism for ozone destruction by iodine intended for modeling oceanic environments such as the Gulf of Mexico. The updated mechanisms are revision 6, CB6r6, because revision 5, CB6r5, is bypassed. Development version 4 of CB6r6, CB6r6d4, is mainly discussed.

In the CB6r4 mechanism, the species, NTR2, represents organic nitrates that can partition significantly to organic aerosol. These include large multifunctional organic nitrates formed from aromatics, alkenes, and the chemical processing of the NTR1 species. The NTR1 species in the CB6r4 mechanism represents organic nitrates that primarily exist in the gas-phase, such as alkyl nitrates and hydroxyalkyl nitrates. Reaction with OH converts NTR1 to NTR2 in the CB6r4 mechanism. CB6r6d4 does not change the identities of NTR1 and NTR2, but does change their formation and removal.

3.1 Hydrolysis of Organic Nitrates

In the CB6r4 mechanism, the sole fate of NTR2 is assumed to be hydrolysis within the particle phase. Loss of organic nitrates via hydrolysis in the particle phase is thought to depend on their structures, with tertiary organic nitrates undergoing rapid hydrolysis while primary and secondary nitrates are relatively stable. The gas-particle partitioning of NTR2 and its subsequent hydrolysis in the particle phase were implemented as a pseudo gas-phase reaction in the CB6r4 mechanism in CAMX v.6.40. The particle-phase NTR2 hydrolysis lifetime was set to 6-hours based on Liu et al. (2012), as described by Hildebrandt Ruiz and Yarwood (2013: AQRP Project No. 12-012)

Recent laboratory experiments as well as findings from the Southeast Atmosphere Studies have indicated that very short atmospheric lifetimes against hydrolysis are appropriate for acidic aerosols. Rindelaub et al. (2016) examined the effects of solution acidity on hydrolysis rates of simple alkyl nitrates and an organic nitrate derived from α-pinene oxidation by hydroxyl radical. Hydrolysis rate constants increased with solution acidity for all organic nitrates studied, with shorter hydrolysis lifetimes for α-pinene-derived organic nitrate than the simple alkyl nitrates. Hydrolysis of the tertiary α-pinene-derived organic nitrate at low pH was found to be a unimolecular specific acid-catalyzed mechanism forming pinol.

Fisher et al. (2016) modified the organic nitrate simulation in GEOS-Chem based on surface and aircraft measurements of BVOC-derived organic nitrates in the southeastern United States. They assumed a bulk lifetime against hydrolysis of 1 hour, which improved model performance for particulate organic nitrates (pRONO2) relative to longer lifetimes and provided reasonable agreement with aerosol mass spectrometer (AMS) measurements of total $pRONO_2$ at the surface during SOAS and $SEAC^4RS$. They noted that the 1-hour bulk hydrolysis lifetime was shorter than the 2–4 h lifetime found

in analysis of SOAS data and laboratory experiments (Boyd et al., 2015; Lee et al., 2016; Pye et al., 2015). Formation of pRONO2 via aerosol uptake, followed by particle-phase hydrolysis, was found to be the dominant loss process for gas-phase $RONO_2$ in the southeastern United States.

Pye et al. (2015) conducted CMAQ simulations focusing on the formation and aerosol-phase partitioning of organic nitrates from isoprene and monoterpenes in the southeastern United States. Particulate organic nitrates were assumed to undergo rapid pseudohydrolysis with lifetime of 3 hours, representative of tertiary nitrates, or slow pseudohydrolysis with a lifetime 30 hours, resulting in nitric acid and nonvolatile secondary organic aerosol. Pye et al. (2015) found that the rate of organic nitrate pseudohydrolysis in the particle phase affected the magnitude and speciation of organic aerosol. Predicted concentrations of organic aerosol and gas-phase organic nitrates were improved, and a greater fraction (60% vs. 30%) of less oxidized-oxygenated organic aerosol (LO-OOA) could be accounted for via organic nitrate mediated chemistry during the Southern Oxidants and Aerosol Study (SOAS) when particulate organic nitrates were assumed to undergo rapid pseudohydrolysis with τ = 3 hours.

Aerosol pH, derived by the inorganic thermodynamic model ISORROPIA in CAMx and obtained via the Chemical Process Analysis (CPA) tool, was investigated in the 4-km eastern Texas domain. Daily mean aerosol pH was generally acidic in nature throughout the region as shown in Figure 3-1. Sensitivity studies were conducted that reduced the particle-phase NTR2 hydrolysis lifetime in the CB6r4 mechanism from 6-hours to 1-hour or 3 hours.

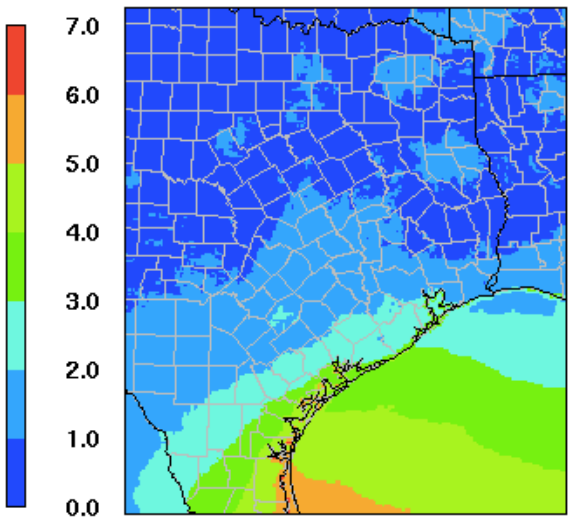

Figure 3-1. Mean aerosol pH in eastern Texas for the CAMx base case with the SOAP2r3 during September 2013 determined via the chemical process analysis (CPA) tool.

3.2 Monoterpene Chemistry

In Texas and other regions of the United States such as the southeast, BVOC emissions are abundant and interactions with NO_x emissions primarily of anthropogenic origin can affect air quality (Xu et al, 2015; Bean et al., 2016). Nitrate radical (NO_3) is a strong oxidant of unsaturated organic compounds including the biogenic alkenes: isoprene, monoterpenes, and sesquiterpenes. Ng et al. (2017) recently provide a comprehensive review of findings regarding BVOC-NO_3 chemistry.

Recent measurement campaigns indicate the importance of the contribution of monotoerpene-NO_3 chemistry to SOA formation. In the southeastern U.S., less oxidized-oxygenated organic aerosol (LO-OOA) and organic nitrates are enhanced at night suggesting that LO-OOA is produced from the NO_3- initiated oxidation of monoterpenes (Xu et al., 2015). The prevalence of LO-OOA indicated an important contribution of monoterpene SOA to total OA. Organic nitrates were found to account for 5-25% of total OA in the southeastern U.S (Xu et al., 2015).

The contribution of NO_3-initiated oxidation of monoterpenes as a source for nighttime organic nitrates and SOA has been found in other areas of the United States (Fry et al. 2013; Rollins et al., 2012; Ng et al., 2017). Bean et al. (2016) found that on average 64% of submicron non-refractory particulate matter (NR-PM1) was organic material, with a high fraction (27-41%) of organic nitrates in Conroe, Texas, during DISCOVER-AQ. The ecosystem near Conroe transitions from prairie and marsh to piney woods, and the area is influenced by transport from Houston urban and industrial sources. Gas-phase monoterpene organic nitrates were elevated at night and just after sunrise. LO-OOA exhibited a diurnal cycle with higher concentrations at night than during the day.

Chamber experiments have indicated that SOA yields from the NO_3-initiated oxidation of different monoterpenes are variable, in particular between α-pinene and other monoterpenes (Ng et al., 2017). Fry et al., (2014) investigated SOA mass yields from the NO_3-initiated oxidation of five monoterpenes and one sesquiterpene: α-pinene, β-pinene, Δ-3-carene, limonene, sabinene, and β-caryophyllene. SOA yields ranged from zero for α-pinene to 38−65% for Δ-3-carene and 86% for β-caryophyllene at a mass loading of 10 μg m^{-3}. Nah et al. (2016) found that organic nitrates formed by NO_3+monoterpene chemistry could serve as either permanent or temporary NO_x sinks depending on the monoterpene precursor. High SOA mass loadings were produced from the NO_3+β-pinene reaction. First generation gas-phase organic nitrate compounds had low volatilities and condensed efficiently onto seed particles. In contrast, NO_3+α-pinene chemistry produced low SOA mass loadings. Ng et al. (2017) summarize oxidation products and SOA yields observed in studies of NO_3-BVOC reactions (ref. Table 2). They note that SOA yields from monoterpenes are variable but consistently above 20% with the exception of alpha-pinene that has yields of 0-15%.

In this study, the CB6r4 mechanism was updated to split terpenes to α-pinene (APIN) and other terpenes (TERP). Gas-phase reactions of TERP and APIN with OH, O_3, NO_3 as

well as SOA yields for TERP and APIN reactions with NO_3 were revised. APIN and TERP emissions estimates were separated in the MEGAN inventory.

The chemical reactions for terpenes are shown for CB6r4 in Table 3-1 and CB6r6d4 in Table 3-2. In addition to updating rate constants and AN yields, product yields of PAR and ALDX with ISPD were replaced to improve separation between anthropogenic and biogenic model species. The same composition profile for emitted terpenes as in the SAPRC-07 mechanism (Carter, 2010) was used to develop the lumped terpene mechanism, namely 40% α-pinene, 25% β-pinene, 15% Δ-3-carene, 10% limonene and 10% sabinene, with α-pinene excluded and remaining terpenes renormalized. Rate constants for terpene reactions with OH, O_3 and NO_3 were obtained from data compilations provided by IUPAC (2017) and Calvert et al. (2000). Product yields for terpene reactions were based on data compilations reported by Lee et al. (2016) and Atkinson and Arey (2003) and with reference to the corresponding reactions in SAPRC-07 (Carter, 2010).

Table 3-1. Reactions for lumped terpenes (TERP) in CB6r4.

Reactants and Products	**Rate Constant Expression**	**k_{298}**
TERP + OH = 0.75 XO2H + 0.5 XO2 + 0.25 XO2N + 1.5 RO2 + 0.28 FORM + 1.66 PAR + 0.47 ALDX	k = 1.50E-11 exp(449/T)	6.77E-11
TERP + O3 = 0.57 OH + 0.07 XO2H + 0.69 XO2 + 0.18 XO2N + 0.94 RO2 + 0.24 FORM + 0.001 CO + 7 PAR + 0.21 ALDX + 0.39 CXO3	k = 1.20E-15 exp(-821/T)	7.63E-17
TERP + NO3 = 0.47 NO2 + 0.28 XO2H + 0.75 XO2 + 0.25 XO2N + 1.28 RO2 + 0.47 ALDX + 0.53 NTR2	k = 3.70E-12 exp(175/T)	6.66E-12

Table 3-2. Reactions for α-pinene (APIN) and other lumped terpenes (TERP) in CB6r6d4.

Reactants and Products	**Rate Constant Expression**	**k_{298}**
TERP + OH = 0.75 XO2H + 0.3 XO2 + 0.2 YO2N + 1.25 RO2 + 0.37 FORM + 0.33 ISPD + 0.1 ACET	k = 7.62E-11 exp(90/T)	1.03E-10
TERP + O3 = 0.53 OH + 0.1 HO2 + 0.93 XO2 + 0.2 YO2N + 1.13 RO2 + 0.37 FORM + 0.33 ISPD + 0.25 C2O3 + 0.05 OPO3 + 0.05 ACET	k = 1.21E-15 exp(-310/T)	4.28E-16
TERP + NO3 = 0.4 NO2 + 0.6 NTR2 + 0.2 HO2 + 1. XO2 + 1. RO2 + 0.35 ISPD + 0.1 FORM	k = 4.89E-11 exp(-580/T)	6.98E-12
APIN + OH = 0.75 XO2H + 0.3 XO2 + 0.2 YO2N + 1.25 RO2 + 0.2 FORM + 0.5 ISPD + 0.1 ACET	k = 1.20E-11 exp(440/T)	5.25E-11
APIN + O3 = 0.85 OH + 0.1 HO2 + 1.1 XO2 + 0.2 YO2N + 1.3 RO2 + 0.2 FORM + 0.4 ISPD + 0.3 OPO3 + 0.05 ACET	k = 8.05E-16 exp(-640/T)	9.40E-17
APIN + NO3 = 0.85 NO2 + 0.15 NTR2 + 0.2 HO2 + 1. XO2 + 1. RO2 + 0.6 ISPD + 0.1 FORM	k = 1.20E-12 exp(490/T)	6.21E-12

3.3 Alkane Chemistry

Alkanes account for the largest fraction of anthropogenic non-methane organic compound (NMOC) emissions in urban areas because they are the dominant constituents of hydrocarbon fuels including gasoline, diesel and liquid petroleum gas (LPG). Laboratory studies have shown that long-chain alkanes (C8 and higher) can contribute to SOA formation under high-NO_x conditions (Lim and Ziemann, 2005; Jordan et al., 2008; Presto et al., 2010) by forming condensable reaction products including organic nitrates.

3.3.1 SOA Formation Potential from Alkanes

In CAMx, SOA formation from long-chain alkanes is modeled through IVOC (e.g., PAHs and C12 and higher n-alkanes) but SOA formation from smaller alkanes (C11 and smaller) is omitted. To evaluate the validity of this methodology, a screening comparison of SOA-forming potential of n-octane (C8) and IVOC based on available data was performed. C8 was used to represent the collective SOA-forming potential of alkanes C11 and smaller. This assessment confirmed that SOA formation from alkanes is expected to be dominated by C12 and higher n-alkanes with the implication that efforts to improve the representation of SOA formation from alkanes should focus on quantifying alkane IVOCs. SOA formation from smaller alkanes (C11 and smaller) continues to be omitted from CAMx.

Figure 3.2 compares SOA yield curves for C8 and IVOC. The SOA yield from C8 was measured by Jordan et al. (2008) at a high OA loading (C_{OA} = 139 μg/m^3). The yield curve for C8 was fitted to the experimental yield using an absorptive partitioning model (Pankow, 1994) with an effective saturation concentration (C*) of 10 μg/m^3 (similar to ALK5 in Murphy and Pandis, 2009). At an atmospherically more relevant C_{OA} level of 10 μg/m^3, the SOA yield from C8 was 2.2%. The SOA yield curve for IVOC was given by Hodzic et al. (2016). At C_{OA} = 10 μg/m^3, the SOA yield from IVOC was 35%, which is about 16 times higher than the yield from C8.

Emissions of C8 and IVOC were estimated based on the TCEQ data described in Section 2.3. Emissions of C8 were derived from the PARH emissions with n-octane represented as 5 PARH and 3 PAR in the revised mechanism. For mobile source emissions, PARH was set to 20% of PAR + PARH emissions, which resulted in average daily total C8 emissions of 1831 tons per day (tpd) over the continental US during the modeling period of September 2013. IVOC emissions were scaled from total NMOC emissions. For mobile emissions, Jathar et al. (2014) estimated that IVOC would account for either 25% (gasoline engines) or 20% (diesel engines) of total NMOC emissions, resulting in daily average total IVOC emissions of 3423 tpd. Combining 1.9 times higher emissions with 16 times higher SOA yield, the SOA-forming potential of IVOC is about 30 times higher than that of C8 for mobile sources (i.e., SOA formed from C8 would account for only about 3% of total SOA from mobile source alkanes).

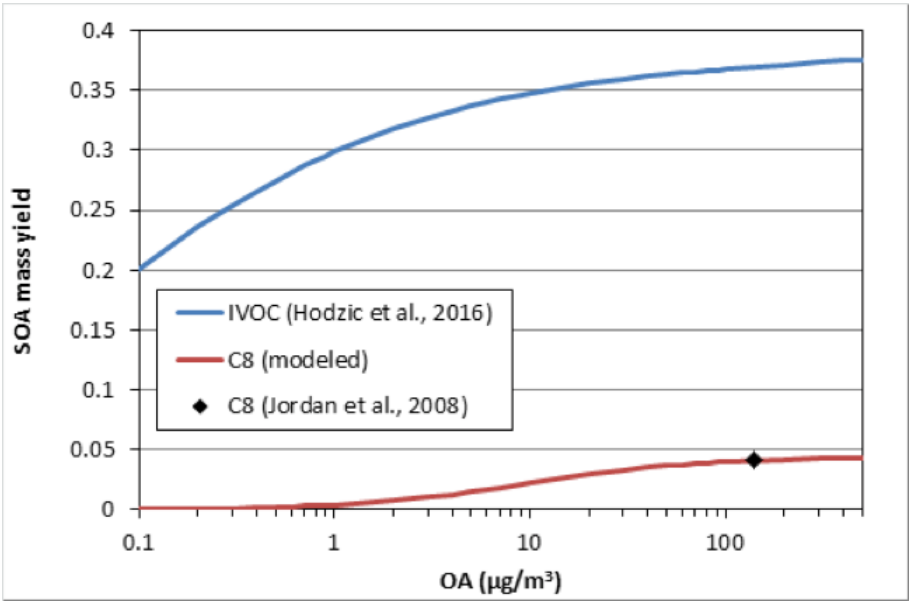

Figure 3-2. SOA yield curves for C8 and IVOC under high-NO_x conditions.

3.3.2 Gas-Phase Mechanism Updates for Alkanes

Alkanes larger than propane are all represented by the model species PAR in CR6r4. PAR also represents alkyl chains in other VOC classes, also referred to as paraffinic carbon, in CB6r4. The AN yield from PAR is 12% (at 298 K and 1 atmosphere pressure) representing an overall average for paraffinic carbon. However, AN yields for alkanes represented by PAR vary widely from 2% for iso-butane to 38% for n-dodecane (Table 3-3), according to the Master Chemical Mechanism (MCM). Secondary carbons (CH_2 groups) are known to have higher yields of ANs than either primary or tertiary carbons (CH_3 and CH groups, respectively). In CB6r6 we implemented a scheme that represents paraffinic carbon using two model species called PAR and PARH. The AN yield from PARH is 50% whereas PAR is 4%, and the PAR:PARH split varies between alkanes as shown in Table 3-3. The number of alkane carbon atoms represented as PARH is the number of secondary carbons minus 2, and minus 4 when a ring is present. For non-alkanes PARH would be zero. The PAR/PARH scheme in CB6r6d4 improves upon CB6r4 for representing both the OH rate constant (kOH) and AN yield for alkanes (Table 3-3, Figure 3-3).

Table 3-3. Attributes of alkane mechanisms in the MCM, CB6r4 and CB6r6d4.

Alkane	**Carbon Atoms**			**AN Yield at 298 K & 1 atm**			**k_{OH} at 298 K & 1 atm**		
	# C	**# PARH**	**# PAR**	**MCM**	**CB6r4**	**CB6r6d4**	**MCM**	**CB6r4**	**CB6r6d4**
n-butane	4	0	4	6.4%	12.0%	4.2%	2.36E-12	3.10E-12	2.28E-12
2-methyl-propane	4	0	4	1.9%	12.0%	4.2%	2.19E-12	3.10E-12	2.28E-12
n-pentane	5	1	4	9.8%	12.0%	13.3%	4.00E-12	3.88E-12	3.85E-12
2-methylbutane	5	0	5	6.5%	12.0%	4.2%	3.70E-12	3.88E-12	2.84E-12
2,2-dimethylpropane	5	0	5	5.3%	12.0%	4.2%	8.48E-13	3.88E-12	2.84E-12
n-hexane	6	2	4	17.4%	12.0%	19.4%	5.44E-12	4.66E-12	5.43E-12
2-methylpentane	6	0	6	9.1%	12.0%	4.2%	5.31E-12	4.66E-12	3.41E-12
3-methylpentane	6	0	6	9.0%	12.0%	4.2%	5.40E-12	4.66E-12	3.41E-12
2,2-dimethylbutane	6	0	6	11.5%	12.0%	4.2%	2.34E-12	4.66E-12	3.41E-12
2,3-dimethylbutane	6	0	6	6.9%	12.0%	4.2%	5.78E-12	4.66E-12	3.41E-12
cyclohexane	6	2	4	12.8%	12.0%	19.4%	7.21E-12	4.66E-12	5.43E-12
n-heptane	7	3	4	25.1%	12.0%	23.8%	7.02E-12	5.43E-12	7.01E-12
2-methylhexane	7	1	6	18.8%	12.0%	10.7%	6.86E-12	5.43E-12	4.99E-12
3-methylhexane	7	1	6	17.9%	12.0%	10.7%	7.15E-12	5.43E-12	4.99E-12
n-octane	8	4	4	30.5%	12.0%	27.1%	8.71E-12	6.21E-12	8.59E-12
n-nonane	9	5	4	34.2%	12.0%	29.6%	9.99E-12	6.99E-12	1.02E-11
n-decane	10	6	4	36.0%	12.0%	31.7%	1.12E-11	7.76E-12	1.17E-11
n-hendecane	11	7	4	37.0%	12.0%	33.3%	1.29E-11	8.54E-12	1.33E-11
n-dodecane	12	8	4	37.7%	12.0%	34.7%	1.39E-11	9.31E-12	1.49E-11

(a)

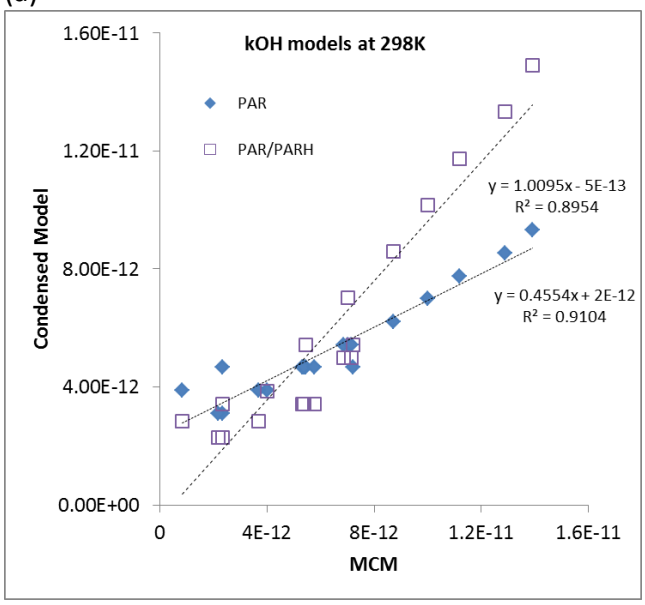

(b)

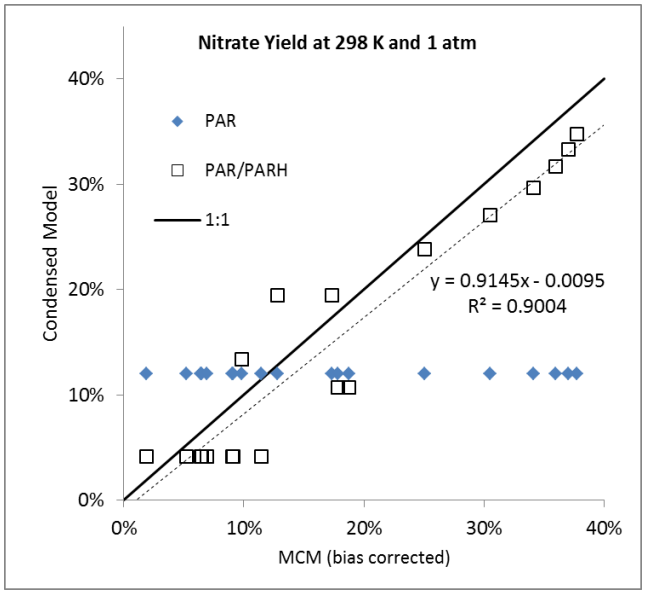

Figure 3-3. Comparison of the CB6r4 (PAR) and CB6r6d4 (PAR/PARH) schemes to MCM for representing (a) OH rate constant (k_{OH}, cm^3 $molecule^{-1}$ s^{-1}) and (b) AN yield for alkanes listed in Table 3-3.

The main chemical reactions for higher alkanes are shown for CB6r4 in Table 3-4 and CB6r6d4 in Table 3-5. In CB6r4, ANs are formed from PAR when XO2N (an operator representing RO2 radicals) reacts with NO. The operator XPAR enables the yield of XO2N to vary with temperature and pressure. Because PAR must represent all types of paraffinic carbon, the AN products from XO2N are a mixture (assumed equal) of NTR1

and NTR2. OH-reaction with NTR1 is assumed to add functional groups, rather than causing loss of NO_2, making the AN less volatile and therefore represented by NTR2. The sole fate of NTR2 is assumed to be hydrolysis in the aerosol phase forming nitric acid (HNO_3) with a default reaction lifetime of 12-hours that can be over-ridden with an estimate that explicitly considers how NTR2 partitions to aerosol. Changes introduced in CB6r6d4 are as follows:

- Paraffinic carbon is represented by PAR and PARH where PARH has much higher AN yield (50% at 298 K and 1 atmosphere)
- Operator YPAR is needed in addition to XPAR to enable AN yields to vary with temperature and pressure.
- AN formation from PAR occurs through operator XO2N forming NTR, whereas PARH forms NTR2 via YO2N; this update eliminates the assumption of equal yields of NTR1 and NTR2 from XO2N in CB6r4
- OH reaction with NTR1 is assumed to liberate NO_2 which is more consistent with MCM; aerosol-phase hydrolysis continues to be the sole fate of NTR2
- When alkanes react with OH both PAR and PARH are transformed to products by the operator DPAR; this update eliminates negative product yields of PAR present in CB6r4
- OH reaction is added for ketones (KET) correcting an omission in CB6r4

Table 3-4. The main chemical reactions for higher alkanes in CB6r4.

Reactants and Products	**Rate Constant Expression**	**k_{298}**
PAR + OH = XPAR	k = 8.10E-13	8.10E-13
ROR = 0.2 KET + 0.42 ACET + 0.74 ALD2 + 0.37 ALDX + 0.04 XO2N + 0.94 XO2H + 0.98 RO2 + 0.02 ROR - 2.7 PAR	k = 5.70E+12 exp(-5780/T)	2.15E+4
ROR + O2 = KET + HO2	k = 1.50E-14 exp(-200/T)	7.67E-15
ROR + NO2 = NTR1	k = 8.60E-12 exp(400/T)	3.29E-11
KET = 0.5 ALD2 + 0.5 C2O3 + 0.5 XO2H + 0.5 CXO3 + 0.5 MEO2 + RO2 - 2.5 PAR	Photolysis	2.27E-7
XPAR = XO2N + RO2	Falloff: F=0.41; n=1 k(0) = 4.81E-20 k(inf) = 4.30E-1 (T/298)^-8	1.49E-1
XPAR = 0.126 ALDX + 0.874 ROR + 0.126 XO2H + 0.874 XO2 + RO2 - 0.126 PAR	k = 1.00E+0	1.00E+0
XO2N + NO = 0.5 NTR1 + 0.5 NTR2	k = 2.70E-12 exp(360/T)	9.04E-12

NTR1 + OH = NTR2	k = 2.00E-12	2.00E-12
NTR1 = NO2	Photolysis	1.06E-6
NTR2 = HNO3	k = 2.30E-5	2.30E-5

Table 3-5. The main chemical reactions for higher alkanes in CB6r6d4.

Reactants and Products	**Rate Constant Expression**	**k_{298}**
PAR + OH = XPAR	k = 4.87E-12 exp(-640/T)	5.69E-13
PARH + OH = YPAR	k = 1.33E-12 exp(50/T)	1.57E-12
XPAR = 0.3 KET + 0.3 ACET + 0.2 ALDX + 0.4 ALD2 + 0.2 MEO2 + 0.8 XO2H + 0.7 XO2 + 1.7 RO2 + 1.6 DPAR	k = 2.64E+0	2.64E+0
XPAR = 0.5 XO2N + 0.5 YO2N + RO2 + 2. DPAR	Falloff: F=0.41; n=1 k(0) = 2.97E-20 k(inf) = 4.30E-1 (T/298)^-8	1.16E-1
YPAR = KET + XO2H + XO2 + 2. RO2 + 4. PAR + 4. DPAR	k = 3.20E-1	3.20E-1
YPAR = YO2N + RO2 + 4. DPAR	Falloff: F=0.41; n=1 k(0) = 5.96E-19 k(inf) = 4.30E-1 (T/298)^-8	3.20E-1
DPAR + PAR =	k = 1.00E+0	1.00E+0
DPAR + PARH =	k = 1.00E+0	1.00E+0
KET + OH = 0.3 KET + 0.1 ACET + 0.3 ALDX + 0.15 ALD2 + 0.1 MEO2 + 0.1 CXO3 + 0.2 C2O3 + 0.56 XO2H + 0.04 YO2N + 0.6 RO2 + 1.2 DPAR	k = 4.00E-12	4.00E-12
KET = 0.5 ALD2 + 0.5 C2O3 + 0.5 XO2H + 0.5 CXO3 + 0.5 MEO2 + RO2 + 3 DPAR	Photolysis	2.27E-7
XO2N + NO = NTR1	k = 2.70E-12 exp(360/T)	9.04E-12
YO2N + NO = NTR2	k = 2.70E-12 exp(360/T)	9.04E-12
NTR1 + OH = NO2	k = 1.00E-12	1.00E-12
NTR1 = NO2	Photolysis	1.06E-6
NTR2 = HNO3	k = 1.39E-4	1.39E-4

The CAMx-ready emission inventory for the PAR/PARH scheme in CB6r6d4 was updated as shown in Table 3-6. Relative proportions of PARH and PAR were derived by analyzing speciation profiles to represent major source sectors and leading to lower AN yields for alkane emissions from the biogenic, wildfire and the oil and gas sectors, slightly higher AN yield for mobile sources, and essentially no change for other sectors. If the CB6r6d4

mechanism is used in future studies, the PARH fraction of alkane emissions can be determined by re-processing emission inventories for modeling. The approach implemented here is simple and transparent which is helpful in interpreting simulation results.

Table 3-6. PAR:PARH split factors by source sector and resulting AN yields with CB6r6d4 compared to CB6r4.

Source Category	PAR:PARH	AN Yield	
		CB6r4	CB6r6d4
On-road/Non-road/Off-road	0.8:0.2	12%	13%
Area/Mexico_Canada/Low Point/Elevated_Point_Anthro	0.85:0.15	12%	11%
Oil_Gas	0.9:0.1	12%	9%
MEGAN/FINN_fires	1.0:0.0	12%	4%

4. Evaluation of the Effects of Chemical Mechanism Updates

Updates made to the CB6r4 mechanism in CAMx were applied to evaluate the effects on regional ozone and fine particulate matter concentrations. New versions of the mechanism included:

- **CB6r4 with τ = 3 h or τ = 1 h pseudohydrolysis of NTR2**. The lifetime of NTR2 against hydrolysis was reduced to τ = 1-h or 3-h from 6-h in the base case.
- **CB6r6d1.** Hydrolysis of NTR2 with τ = 1 h and updates to TERP and APIN gas-phase chemistry and SOA yields.
- **CB6r6d4.** All updates that were part of CB6r6d1 as well as revised PAR/PARH and other gas-phase reactions.

Four CAMx simulations were performed with each of the revised mechanisms and associated emissions inventories. The CB6r6d1 and CB6r6d4 versions of the mechanism included multiple updates relative to the base case. Therefore the effects of the mechanism changes were first evaluated incrementally relative to each other and then the net effects of the CB6r6d4 mechanism were compared to the base case. Effects of mechanism updates were investigated for ozone, total $PM_{2.5}$ mass, particulate nitrate, HNO_3, total alkyl nitrate, NO, NO_2, NO_x, NO_y NTR1, NTR2, peroxyacetyl nitrate (PAN), C3 and higher peroxyacyl nitrate (PANX), total peroxy nitrates (PNs), formaldehyde (FORM), acetaldehyde (ALD), propionaldehyde and higher aldehydes (ALDX), and organic aerosol. Results are reported below for ozone and total $PM_{2.5}$ mass concentrations and are shown for other species if mean differences > 0.1 ppb.

4.1 NTR2 Hydrolysis

Figure 4-1 shows mean and maximum (positive or negative) differences in predicted ozone, total $PM_{2.5}$ mass, particulate nitrate concentrations, NTR2, HNO_3, total alkyl nitrate, and NO_y concentrations assuming a NTR2 hydrolysis lifetime of 1 hour in the CB6r4 mechanism relative to the base case. Similar plots showing the effects of a reduction in in the NTR2 hydrolysis lifetime to 3 hours are shown in Appendix D.

Predicted ozone concentrations were insensitive to a reduction in the hydrolysis rate from 6-h to 1-h (differences of less than 0.1 ppb across the 12-km domain on average). Effects on total $PM_{2.5}$ mass and particulate nitrate concentrations were more significant, particularly in northeastern and southeastern Texas, Arkansas, Mississippi, and Louisiana. NTR2 concentrations were highest in these areas of the domain (Figure 4-2). Increases in hourly total $PM_{2.5}$ mass concentrations due to particulate NO_3 (pNO3) were up to 0.5 μg/m^3 on average with maximum differences of approximately 6 μg/m^3. Maximum differences were coincident with areas where NTR2 sensitivity to BVOC emissions (by DDM) dominated anthropogenic emissions (Figure 4-3). NTR2, total alkyl nitrates, and NO_y concentrations decreased, while HNO_3 concentrations increased in these areas consistent with the reduction in the NTR2 lifetime against hydrolysis.

(a)

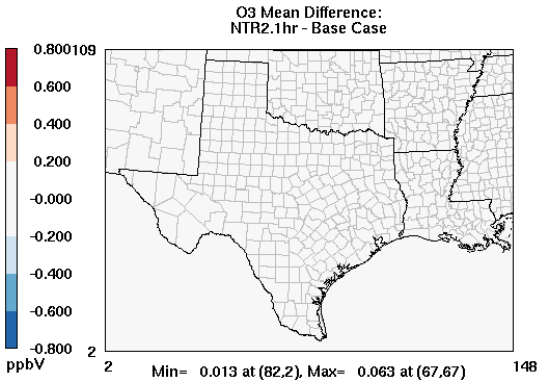
O3 Mean Difference:
NTR2.1hr - Base Case
0.800109
0.600
0.400
0.200
-0.000
-0.200
-0.400
-0.600
-0.800
ppbV
2
2
148
Min= 0.013 at (82,2), Max= 0.063 at (67,67)

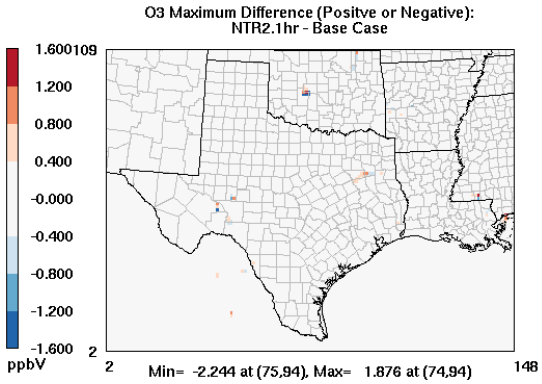
O3 Maximum Difference (Positve or Negative):
NTR2.1hr - Base Case
1.600109
1.200
0.800
0.400
-0.000
-0.400
-0.800
-1.200
-1.600
ppbV
2
2
148
Min= -2.244 at (75,94), Max= 1.876 at (74,94)

(b)

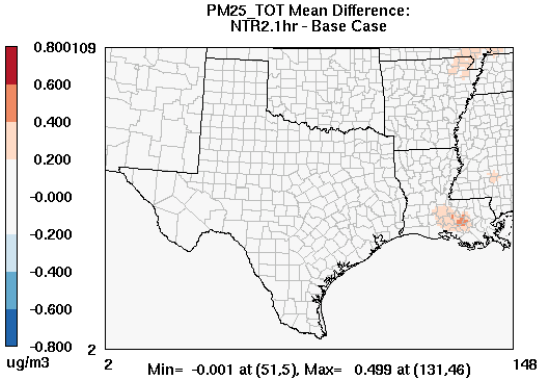
PM25_TOT Mean Difference:
NTR2.1hr - Base Case
0.800109
0.600
0.400
0.200
-0.000
-0.200
-0.400
-0.600
-0.800
ug/m3
2
2
148
Min= -0.001 at (51,5), Max= 0.499 at (131,46)

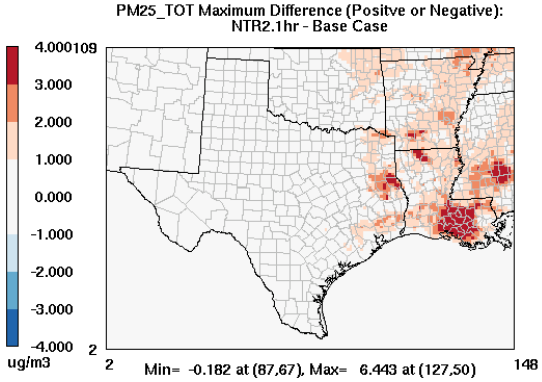
PM25_TOT Maximum Difference (Positve or Negative):
NTR2.1hr - Base Case
4.000109
3.000
2.000
1.000
0.000
-1.000
-2.000
-3.000
-4.000
ug/m3
2
2
148
Min= -0.182 at (87,67), Max= 6.443 at (127,50)

(c)

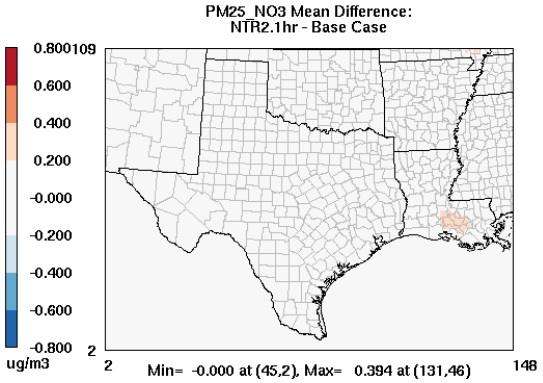
PM25_NO3 Mean Difference:
NTR2.1hr - Base Case
0.800109
0.600
0.400
0.200
-0.000
-0.200
-0.400
-0.600
-0.800
ug/m3
2
2
148
Min= -0.000 at (45,2), Max= 0.394 at (131,46)

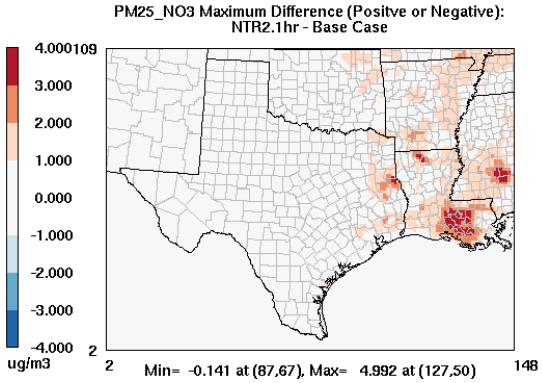
PM25_NO3 Maximum Difference (Positve or Negative):
NTR2.1hr - Base Case
4.000109
3.000
2.000
1.000
0.000
-1.000
-2.000
-3.000
-4.000
ug/m3
2
2
148
Min= -0.141 at (87,67), Max= 4.992 at (127,50)

(d)

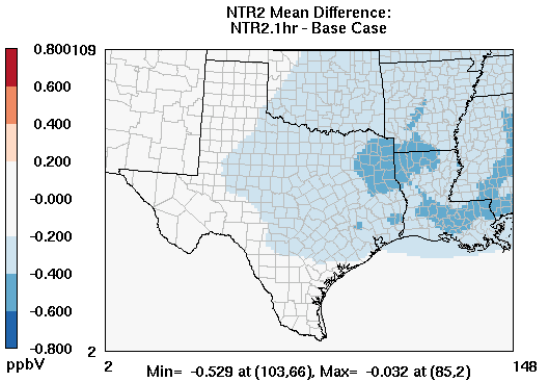
NTR2 Mean Difference:
NTR2.1hr - Base Case
0.800109
0.600
0.400
0.200
-0.000
-0.200
-0.400
-0.600
-0.800
ppbV
2
2
148
Min= -0.529 at (103,66), Max= -0.032 at (85,2)

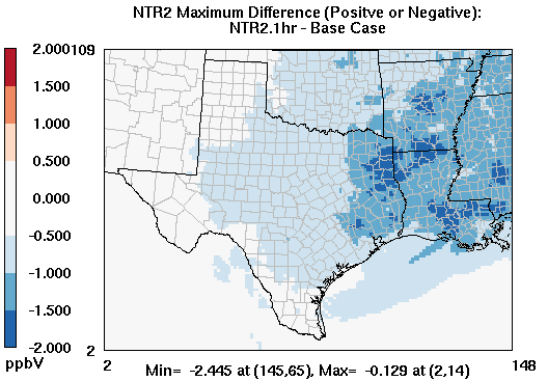
NTR2 Maximum Difference (Positve or Negative):
NTR2.1hr - Base Case
2.000109
1.500
1.000
0.500
0.000
-0.500
-1.000
-1.500
-2.000
ppbV
2
2
148
Min= -2.445 at (145,65), Max= -0.129 at (2,14)

(e)

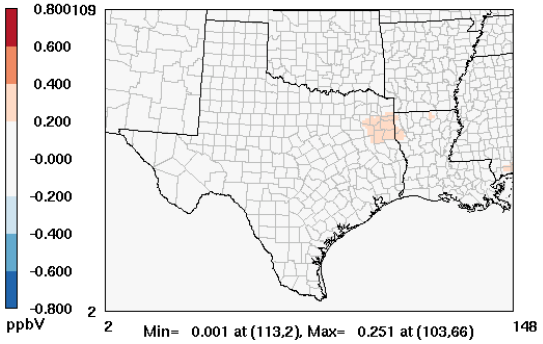
HNO3 Mean Difference:
NTR2.1hr - Base Case
0.800109
0.600
0.400
0.200
-0.000
-0.200
-0.400
-0.600
-0.800
ppbV
2
2
148
Min= 0.001 at (113,2), Max= 0.251 at (103,66)

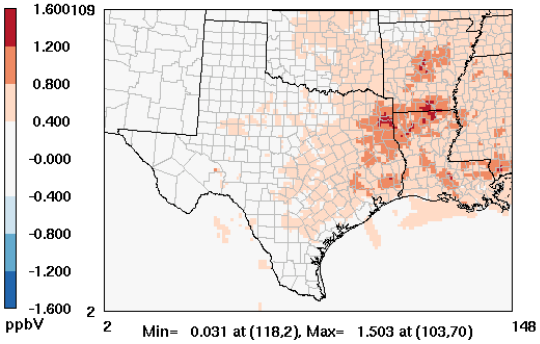
HNO3 Maximum Difference (Positve or Negative):
NTR2.1hr - Base Case
1.600109
1.200
0.800
0.400
-0.000
-0.400
-0.800
-1.200
-1.600
ppbV
2
2
148
Min= 0.031 at (118,2), Max= 1.503 at (103,70)

(f)

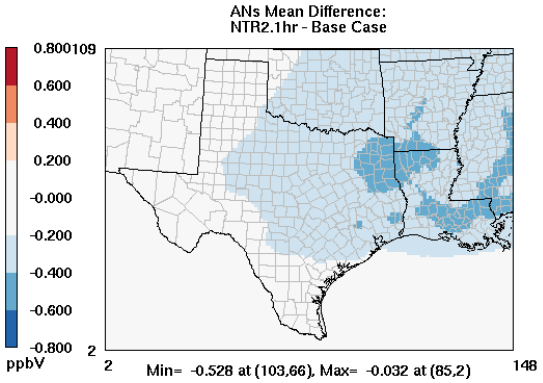
ANs Mean Difference:
NTR2.1hr - Base Case
0.800109
0.600
0.400
0.200
-0.000
-0.200
-0.400
-0.600
-0.800
ppbV
2
2
148
Min= -0.528 at (103,66), Max= -0.032 at (85,2)

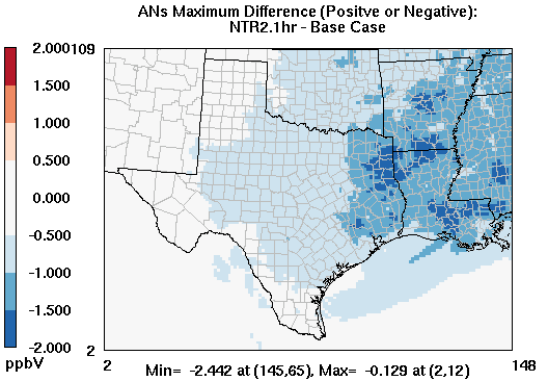
ANs Maximum Difference (Positve or Negative):
NTR2.1hr - Base Case
2.000109
1.500
1.000
0.500
0.000
-0.500
-1.000
-1.500
-2.000
ppbV
2
2
148
Min= -2.442 at (145,65), Max= -0.129 at (2,12)

(g)

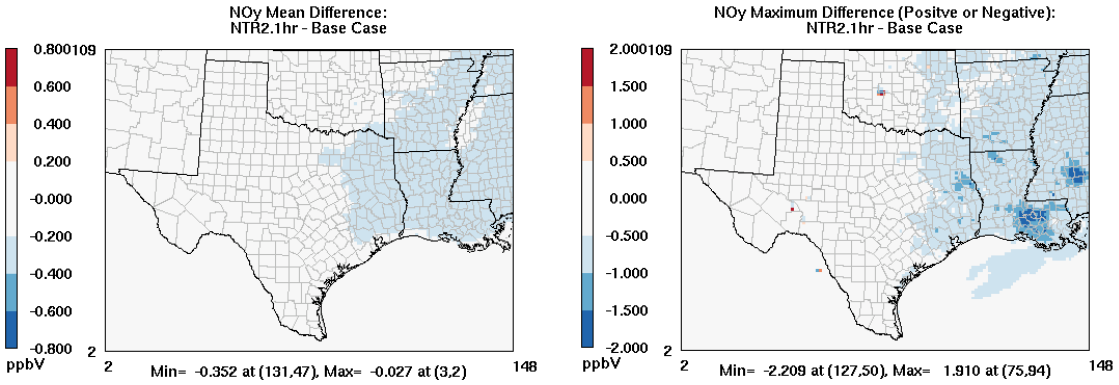

Figure 4-1. Mean (left) and maximum (positive or negative) differences (right) between CAMx predictions with NTR2 hydrolysis lifetimes of 1 hour and 6-hrs (base case) in the CB6r4 mechanism: (a) ozone, (b) total $PM_{2.5}$ mass, (c) particulate nitrate, (d) NTR2, (e) HNO_3, (f) total alkyl nitrate, and (g) NO_y concentrations. Note differences in scales between plots.

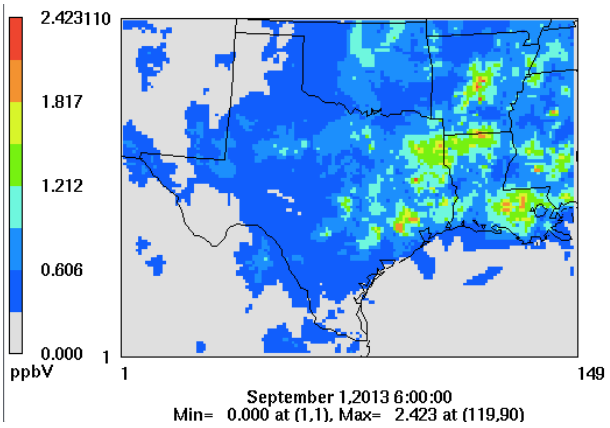

Figure 4-2. Monthly average predictions of NTR2 concentrations during September 2013.

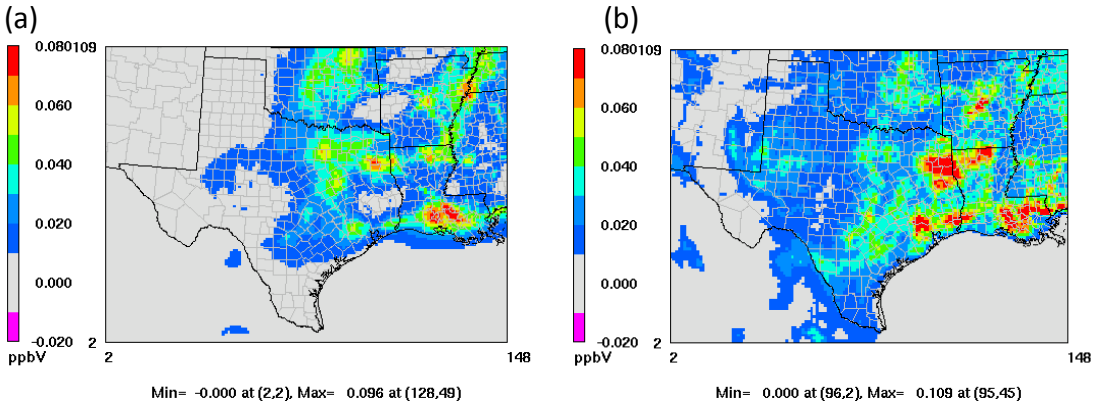

Figure 4-3. DDM NTR2 sensitivity to (a) isoprene and (b) terpene emissions.

4.2 Monoterpene Chemistry and SOA Yields

The CB6r6d1 mechanism included hydrolysis of NTR2 with τ = 1 h and revisions to the TERP and APIN gas-phase chemistry and SOA yields. Predicted α-pinene and other terpene concentrations from the CB6r6d1 mechanisms are shown in Figure 4-4. Figure 4-5 shows mean and maximum (positive or negative) differences in ozone, total $PM_{2.5}$ mass, organic aerosol, formaldehyde, acetaldehyde, propionaldehyde and higher aldehyde, NO_2, PAN, PANX, NTR2, and total alkyl nitrate concentrations between CAMx predictions with the CB6r6d1 mechanism and with the simulation described in Section 4.1 in which the only change was a reduction in the NTR2 hydrolysis lifetime to 1-hour. Thus, the results shown in Figure 4-5 approximate the effects of the monoterpene chemistry updates alone.

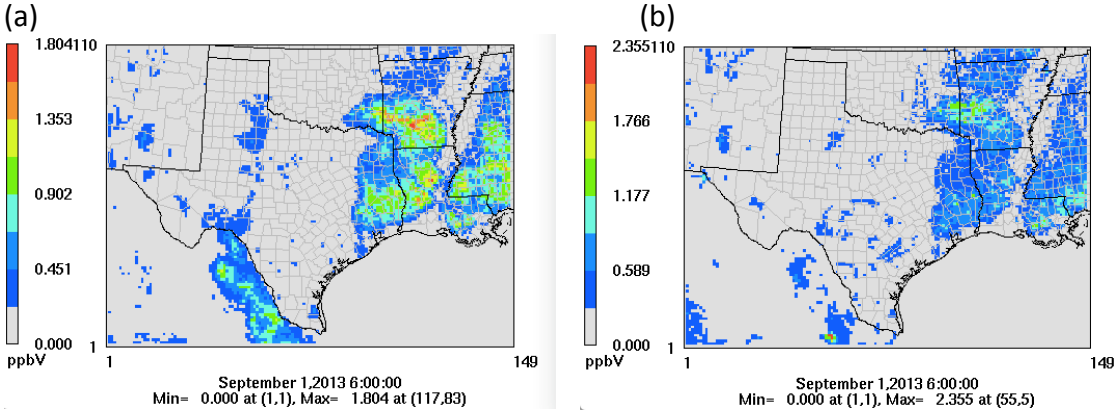

Figure 4-4. Monthly average predictions of (a) α-pinene and (b) other terpene concentrations during September 2013. Note differences in scales between plots.

Average decreases in ozone were 0.5 ppb with maximum decreases of 1-2 ppb in terpene-rich areas including much of northeastern Texas, western Louisiana, southwestern Arkansas, and southern Mississippi. The ozone differences have similar spatial patterns to differences for ALDX (higher aldehydes) and PANX (PAN-type compounds from higher aldehydes) caused by representing larger terpene degradation products as ISPD in CB6r6d4 as opposed to PAR and ALDX in CB6r4. Formaldehyde concentrations increased but concentrations of acetaldehyde and higher aldehydes decreased in terpene-rich areas. Differences in other species were relatively smaller with increases in concentrations of PAN and NO_2 and decreases in PANX, NTR2 and total alkyl nitrates. Differences in total $PM_{2.5}$ mass and organic aerosol concentrations were within ±0.5 µg/m^3 on average with maximum differences of -2 to +5 µg/m^3.

(a)

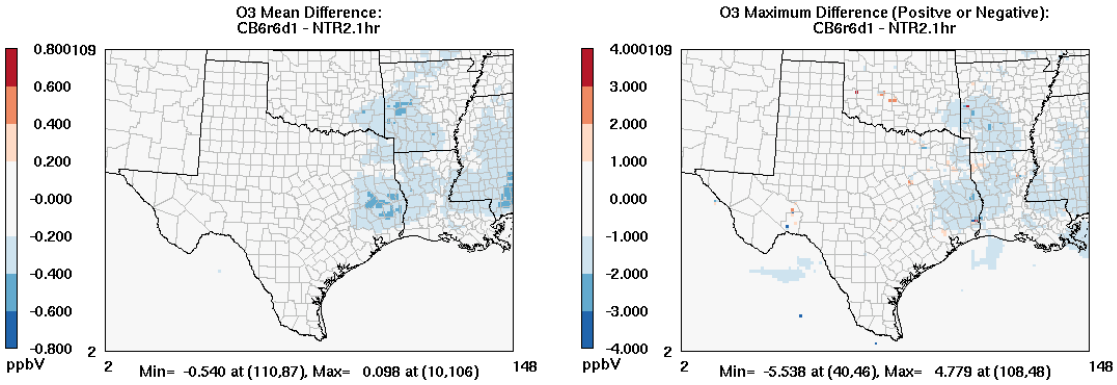

(b)

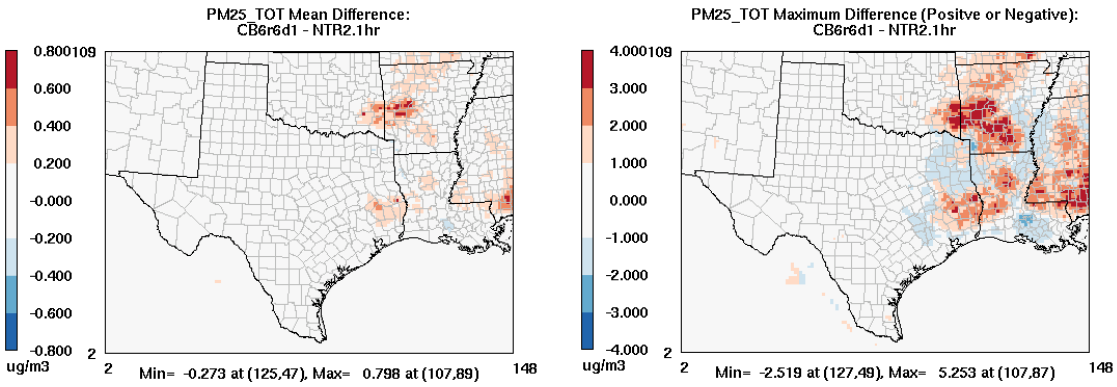

(c)

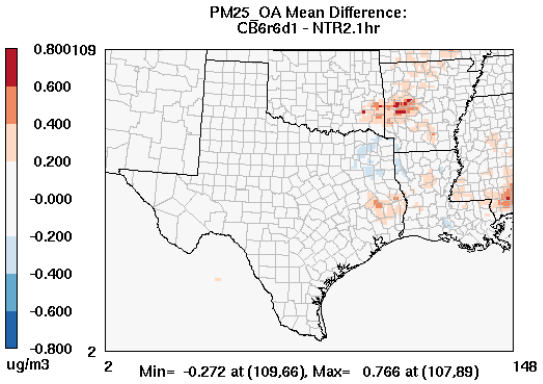
PM25_OA Mean Difference:
CB6r6d1 - NTR2.1hr
0.800109
0.600
0.400
0.200
-0.000
-0.200
-0.400
-0.600
-0.800
ug/m3
2
2
148
Min= -0.272 at (109,66), Max= 0.766 at (107,89)

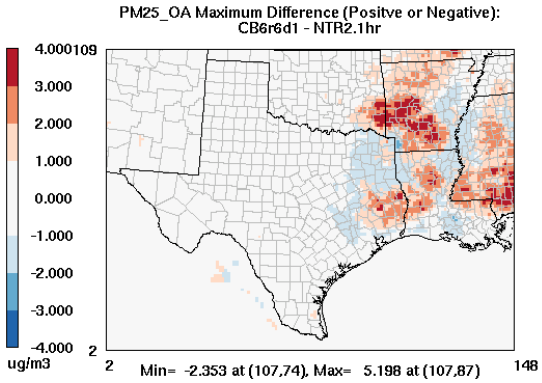
PM25_OA Maximum Difference (Positve or Negative):
CB6r6d1 - NTR2.1hr
4.000109
3.000
2.000
1.000
0.000
-1.000
-2.000
-3.000
-4.000
ug/m3
2
2
148
Min= -2.353 at (107,74), Max= 5.198 at (107,87)

(d)

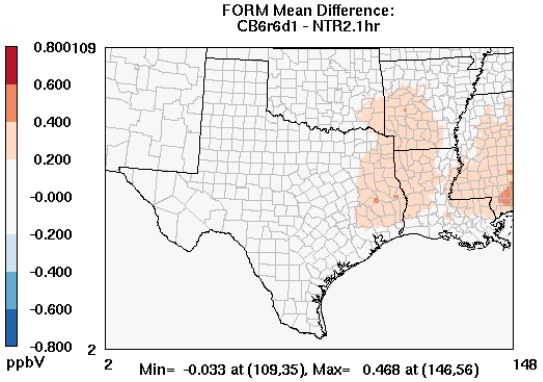
FORM Mean Difference:
CB6r6d1 - NTR2.1hr
0.800109
0.600
0.400
0.200
-0.000
-0.200
-0.400
-0.600
-0.800
ppbV
2
2
148
Min= -0.033 at (109,35), Max= 0.468 at (146,56)

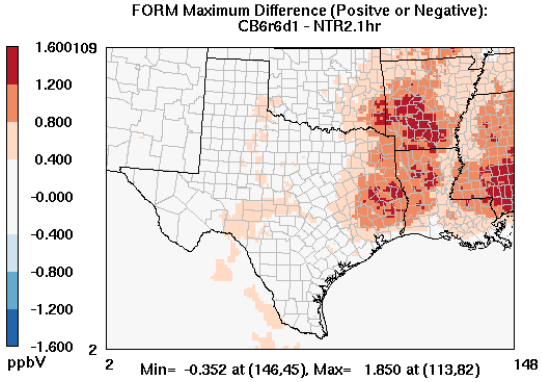
FORM Maximum Difference (Positve or Negative):
CB6r6d1 - NTR2.1hr
1.600109
1.200
0.800
0.400
-0.000
-0.400
-0.800
-1.200
-1.600
ppbV
2
2
148
Min= -0.352 at (146,45), Max= 1.850 at (113,82)

(e)

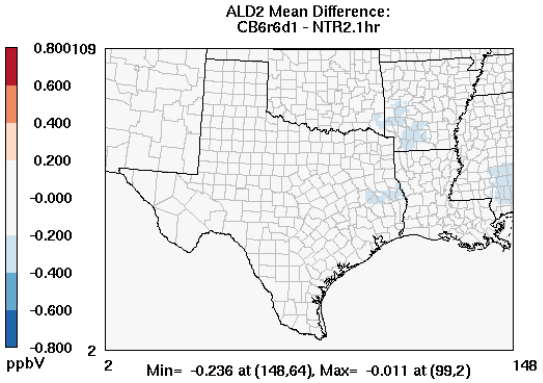
ALD2 Mean Difference:
CB6r6d1 - NTR2.1hr
0.800109
0.600
0.400
0.200
-0.000
-0.200
-0.400
-0.600
-0.800
ppbV
2
2
148
Min= -0.236 at (148,64), Max= -0.011 at (99,2)

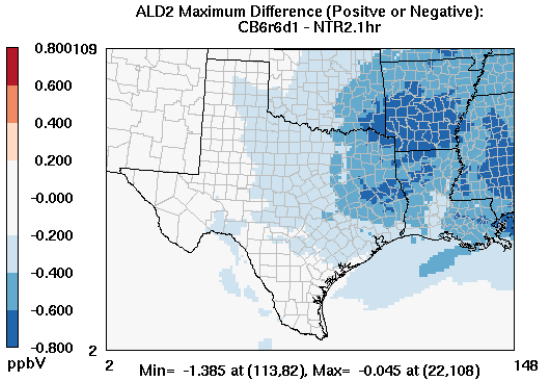
ALD2 Maximum Difference (Positve or Negative):
CB6r6d1 - NTR2.1hr
0.800109
0.600
0.400
0.200
-0.000
-0.200
-0.400
-0.600
-0.800
ppbV
2
2
148
Min= -1.385 at (113,82), Max= -0.045 at (22,108)

(f)

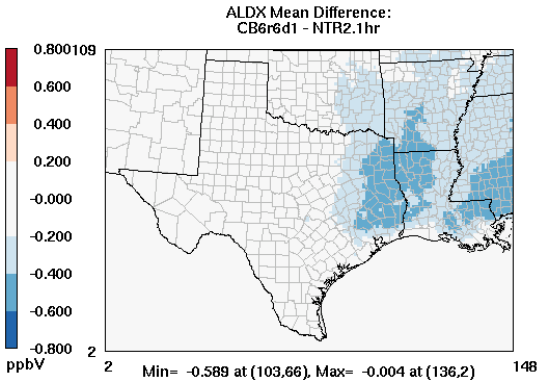
ALDX Mean Difference:
CB6r6d1 - NTR2.1hr
0.800109
0.600
0.400
0.200
-0.000
-0.200
-0.400
-0.600
-0.800
ppbV
2
2
Min= -0.589 at (103,66), Max= -0.004 at (136,2)
148

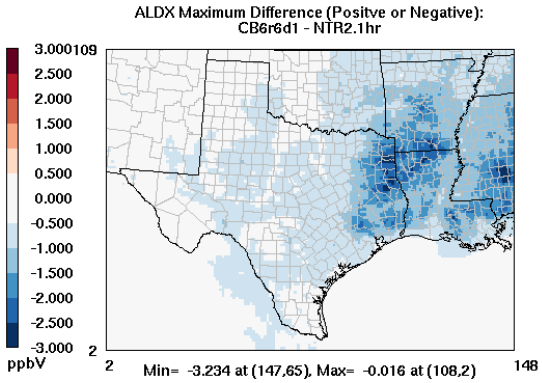
ALDX Maximum Difference (Positve or Negative):
CB6r6d1 - NTR2.1hr
3.000109
2.500
2.000
1.500
1.000
0.500
0.000
-0.500
-1.000
-1.500
-2.000
-2.500
-3.000
ppbV
2
2
Min= -3.234 at (147,65), Max= -0.016 at (108,2)
148

(g)

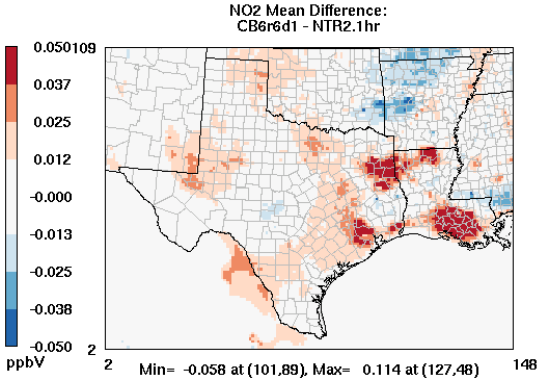
NO2 Mean Difference:
CB6r6d1 - NTR2.1hr
0.050109
0.037
0.025
0.012
-0.000
-0.013
-0.025
-0.038
-0.050
ppbV
2
2
Min= -0.058 at (101,89), Max= 0.114 at (127,48)
148

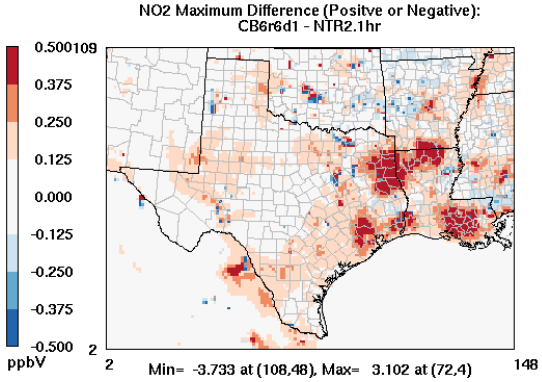
NO2 Maximum Difference (Positve or Negative):
CB6r6d1 - NTR2.1hr
0.500109
0.375
0.250
0.125
0.000
-0.125
-0.250
-0.375
-0.500
ppbV
2
2
Min= -3.733 at (108,48), Max= 3.102 at (72,4)
148

(h)

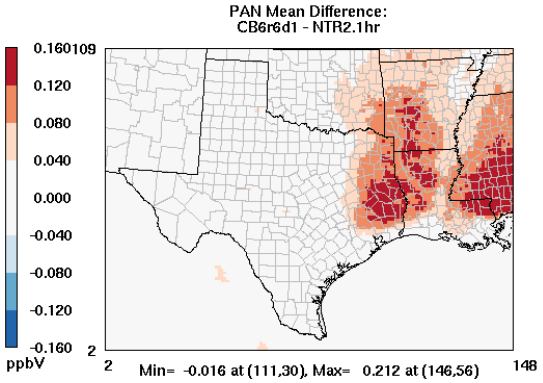
PAN Mean Difference:
CB6r6d1 - NTR2.1hr
0.160109
0.120
0.080
0.040
0.000
-0.040
-0.080
-0.120
-0.160
ppbV
2
2
Min= -0.016 at (111,30), Max= 0.212 at (146,56)
148

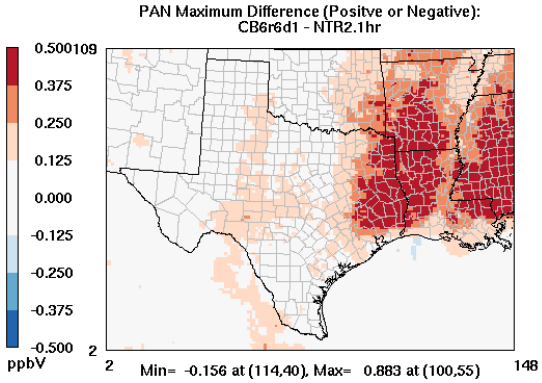
PAN Maximum Difference (Positve or Negative):
CB6r6d1 - NTR2.1hr
0.500109
0.375
0.250
0.125
0.000
-0.125
-0.250
-0.375
-0.500
ppbV
2
2
Min= -0.156 at (114,40), Max= 0.883 at (100,55)
148

(i)

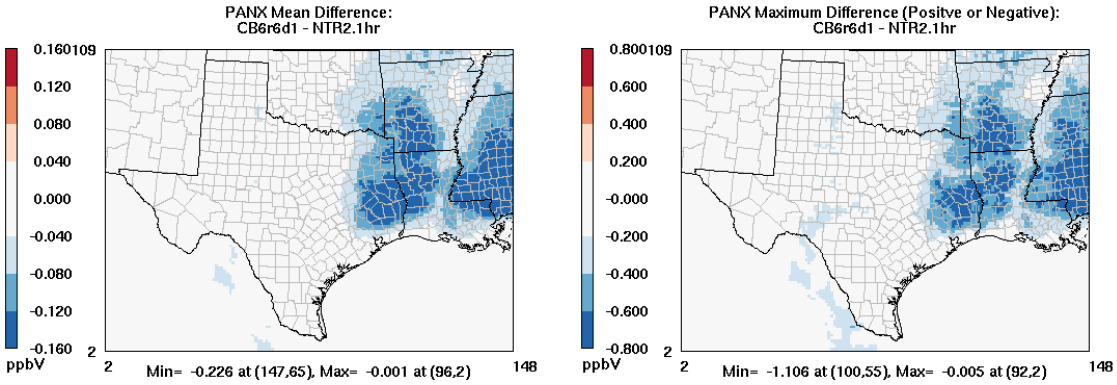

(j)

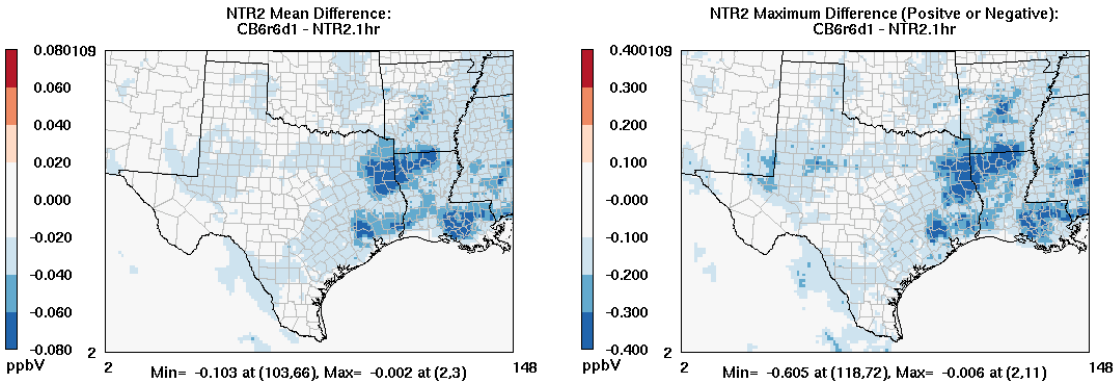

(k)

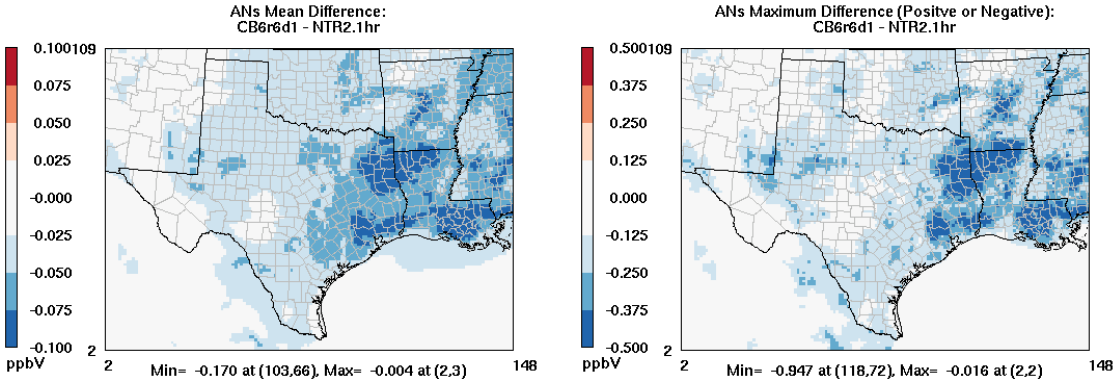

Figure 4-5. Mean (left) and maximum (positive or negative) differences (right) between CAMx predictions with the CB6r6d1 mechanism and the CB6r4 mechanism with a NTR2 hydrolysis lifetime of 1-hour: (a) ozone, (b) total $PM_{2.5}$ mass, (c) organic aerosol, (d) formaldehyde, (e) acetaldehyde, (f) propionaldehyde and higher aldehyde, (g) NO_2, (h) PAN, (i) PANX, (j) NTR2, and (k) total alkyl nitrate concentrations. Note differences in scales between plots.

4.3 Alkane Chemistry

The CB6r6d4 mechanism included all updates that were part of CB6r6d1 as well as revisions associated with the PAR/PARH reactions. Predicted PAR and PARH concentrations with the CB6r6d4 mechanisms are shown in Figure 4-6. Figure 4-7 shows mean and maximum (positive or negative) differences in ozone, total $PM_{2.5}$ mass, NTR1, NTR2, and total alkyl nitrate concentrations between CAMx predictions with the CB6r6d4 and CB6r6d1 mechanisms. The results shown in Figure 4-7 approximate the effects associated with the updates to the PAR/PARH chemistry.

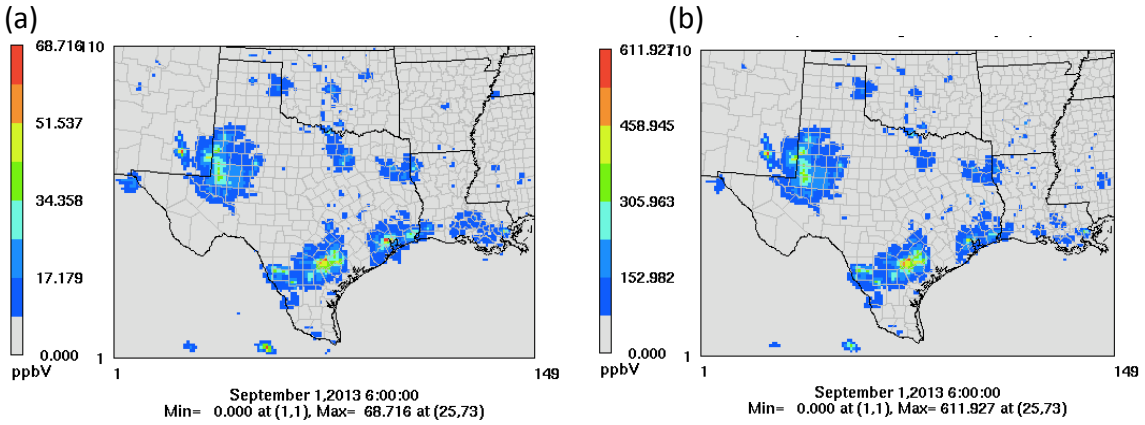

Figure 4-6. Monthly average predictions of (a) PARH and (b) PAR concentrations during September 2013.

Widespread increases in ozone concentrations were within 0.5 ppb on average with maximum increases of 1-2 ppb. The total AN (NTR1+NTR2) burden decreased slightly overall primarily driven by the reduction in NTR1. PAR is the primary precursor to NTR1 in the CB6r4 mechanism, while PARH is a precursor to NTR2. Mean differences in total $PM_{2.5}$ mass concentrations were less than 0.5 ppb for the 12-km domain indicating little sensitivity to the revised PAR/PARH chemistry.

The DDM tool was used to investigate ozone sensitivities to NO_x and VOC emissions from four source sectors, oil and gas, mobile, other anthropogenic, and natural sources, for the base case and for the CAMx simulation with the CB6r4 mechanism. DDM ozone sensitivities to NO_x and VOC emissions by source sector for the 12-km domain during September 2013 are shown in Figure 4-8. DDM ozone sensitivities for both simulations indicate the relative importance of mobile and other anthropogenic NO_x sources and natural sources of VOCs. Scatter plots of ozone sensitivities by NO_x or VOC emission source sector for the CB6r6d4 mechanism versus the base case are shown in Figure 4-9. Updating AN yields from alkanes using the PARH scheme increased and altered the spatial distributions of ozone sensitivities to VOC emissions from the oil and gas, mobile, and other anthropogenic source sectors. DDM ozone sensitivities averaged across only

daytime hours, defined as 1000 - 1800 local time, are shown in Appendix E. Ozone sensitivities were larger in magnitude than those averaged over all hours but otherwise exhibited similar trends.

(a)

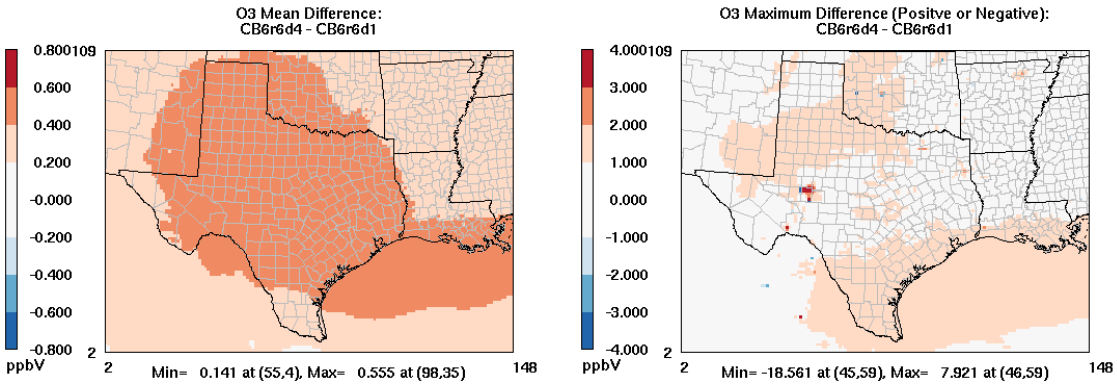

(b)

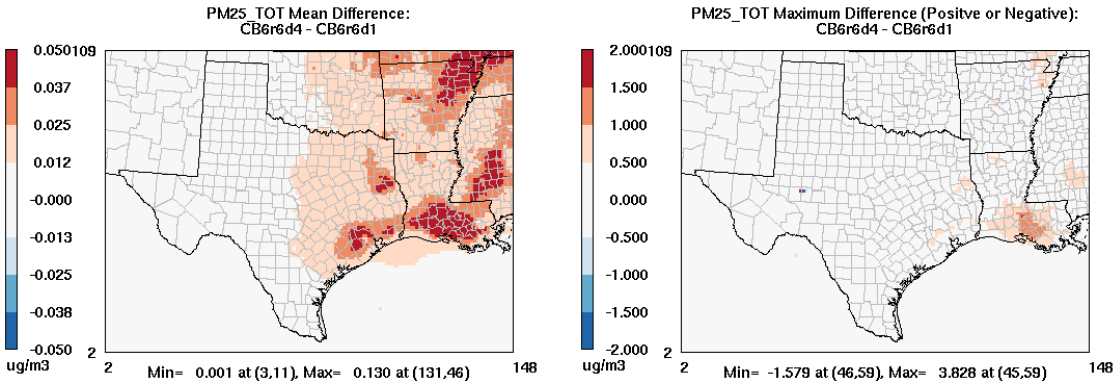

(c)

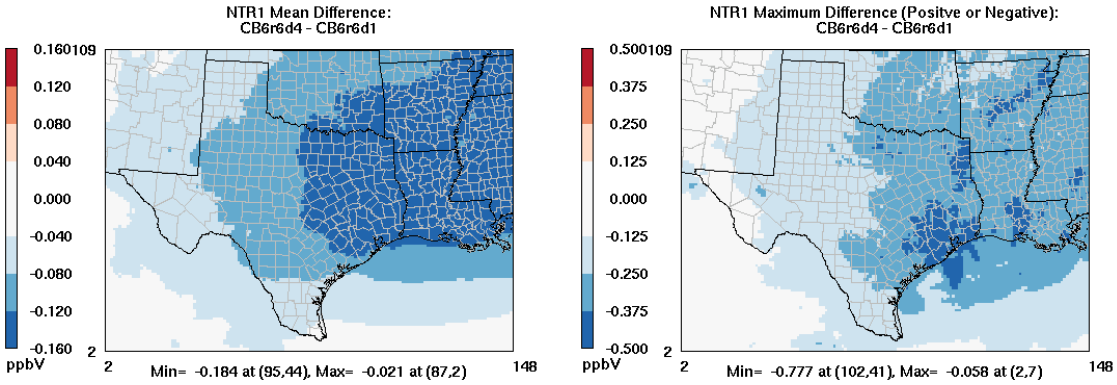

(d)

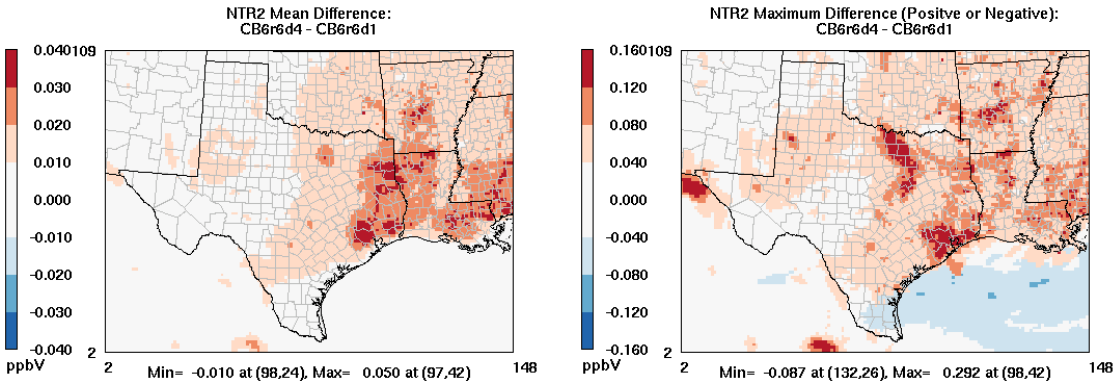

(e)

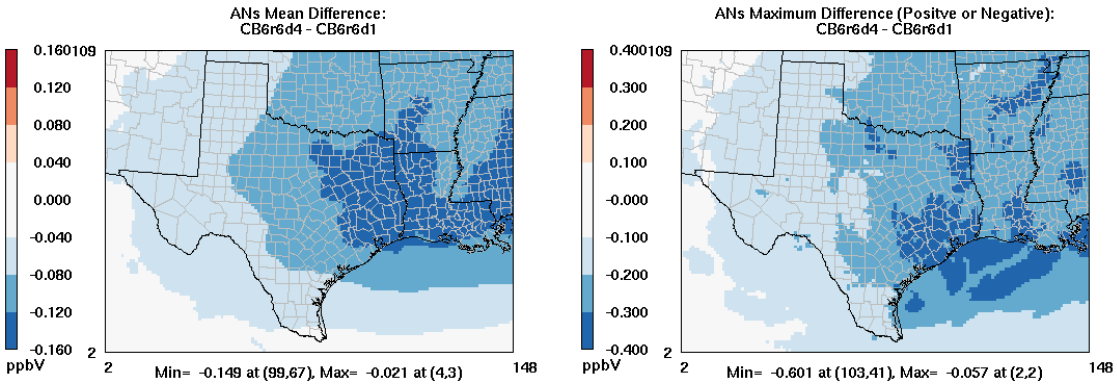

Figure 4-7. Mean (left) and maximum (positive or negative) differences (right) between CAMx predictions with the CB6r6d4 and CB6r6d1 mechanisms: (a) ozone, (b) total $PM_{2.5}$ mass, (c) NTR1, (d) NTR2, and (e) AN concentrations. Note differences in scales between plots.

(a)

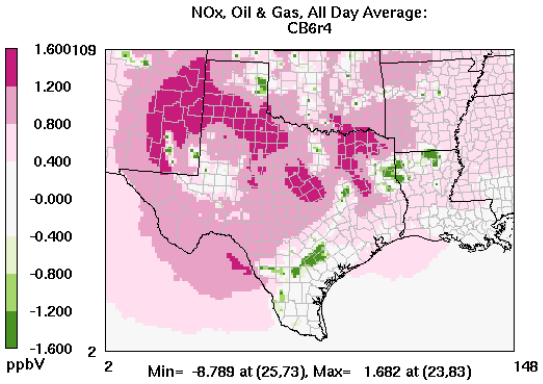
NOx, Oil & Gas, All Day Average:
CB6r4
1.600109
1.200
0.800
0.400
-0.000
-0.400
-0.800
-1.200
-1.600
ppbV
2
2
148
Min= -8.789 at (25,73), Max= 1.682 at (23,83)

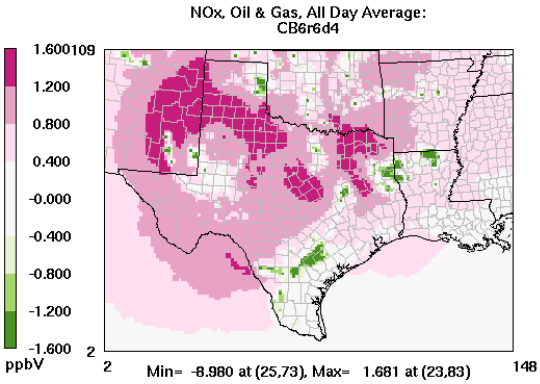
NOx, Oil & Gas, All Day Average:
CB6r6d4
1.600109
1.200
0.800
0.400
-0.000
-0.400
-0.800
-1.200
-1.600
ppbV
2
2
148
Min= -8.980 at (25,73), Max= 1.681 at (23,83)

(b)

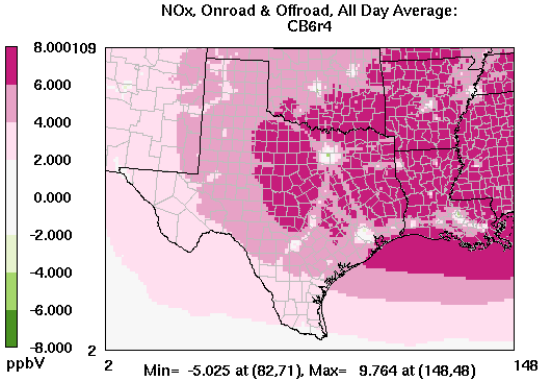
NOx, Onroad & Offroad, All Day Average:
CB6r4
8.000109
6.000
4.000
2.000
0.000
-2.000
-4.000
-6.000
-8.000
ppbV
2
2
148
Min= -5.025 at (82,71), Max= 9.764 at (148,48)

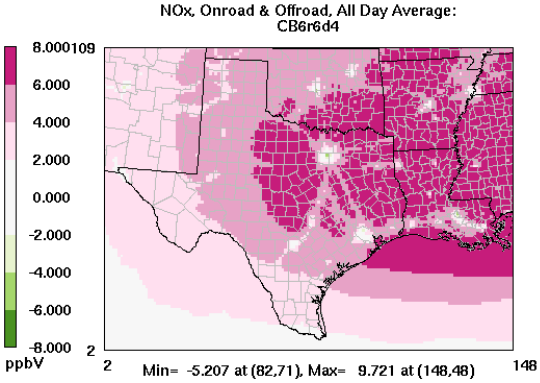
NOx, Onroad & Offroad, All Day Average:
CB6r6d4
8.000109
6.000
4.000
2.000
0.000
-2.000
-4.000
-6.000
-8.000
ppbV
2
2
148
Min= -5.207 at (82,71), Max= 9.721 at (148,48)

(c)

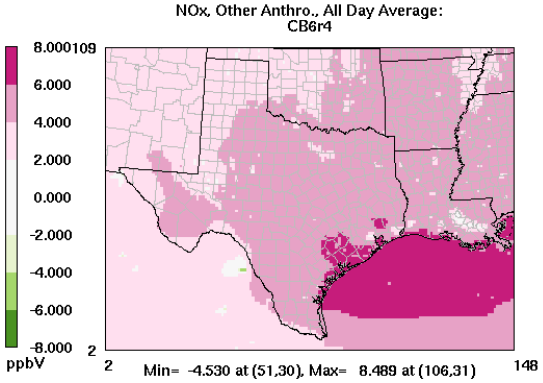
NOx, Other Anthro., All Day Average:
CB6r4
8.000109
6.000
4.000
2.000
0.000
-2.000
-4.000
-6.000
-8.000
ppbV
2
2
148
Min= -4.530 at (51,30), Max= 8.489 at (106,31)

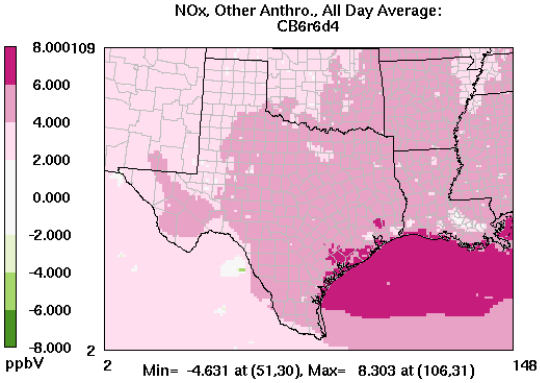
NOx, Other Anthro., All Day Average:
CB6r6d4
8.000109
6.000
4.000
2.000
0.000
-2.000
-4.000
-6.000
-8.000
ppbV
2
2
148
Min= -4.631 at (51,30), Max= 8.303 at (106,31)

(d)

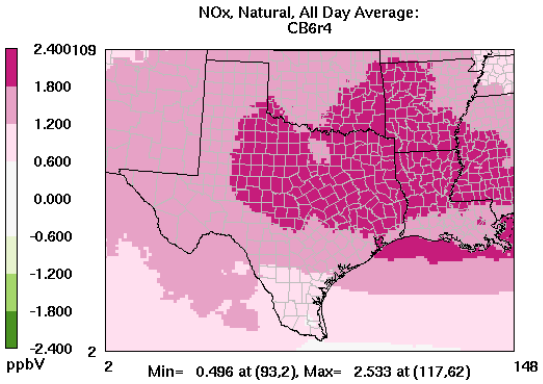
NOx, Natural, All Day Average:
CB6r4
2.400109
1.800
1.200
0.600
0.000
-0.600
-1.200
-1.800
-2.400
ppbV
2
2
Min= 0.496 at (93,2), Max= 2.533 at (117,62)
148

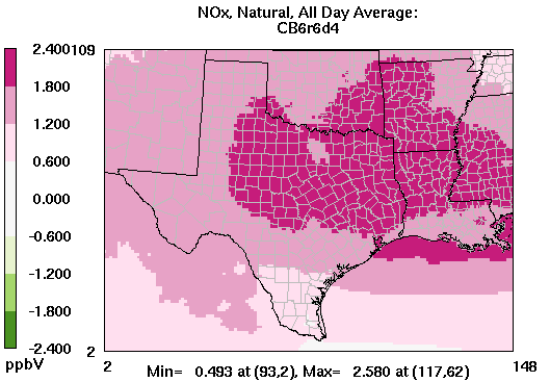
NOx, Natural, All Day Average:
CB6r6d4
2.400109
1.800
1.200
0.600
0.000
-0.600
-1.200
-1.800
-2.400
ppbV
2
2
Min= 0.493 at (93,2), Max= 2.580 at (117,62)
148

(e)

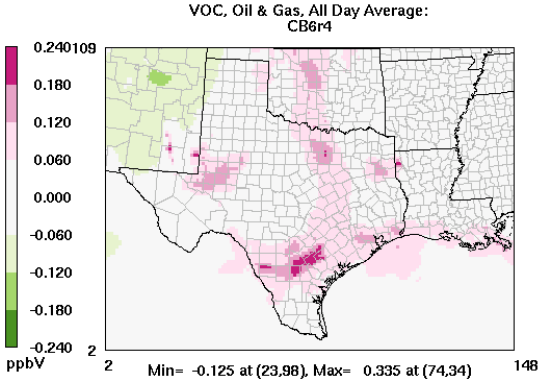
VOC, Oil & Gas, All Day Average:
CB6r4
0.240109
0.180
0.120
0.060
0.000
-0.060
-0.120
-0.180
-0.240
ppbV
2
2
Min= -0.125 at (23,98), Max= 0.335 at (74,34)
148

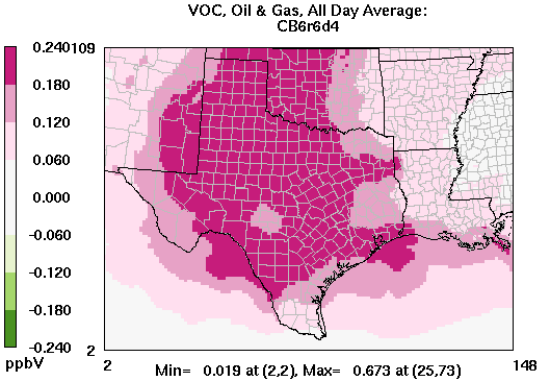
VOC, Oil & Gas, All Day Average:
CB6r6d4
0.240109
0.180
0.120
0.060
0.000
-0.060
-0.120
-0.180
-0.240
ppbV
2
2
Min= 0.019 at (2,2), Max= 0.673 at (25,73)
148

(f)

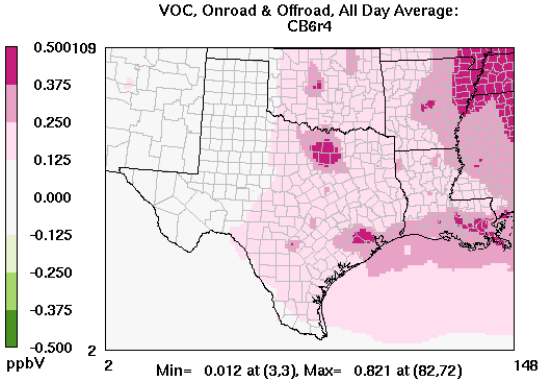
VOC, Onroad & Offroad, All Day Average:
CB6r4
0.500109
0.375
0.250
0.125
0.000
-0.125
-0.250
-0.375
-0.500
ppbV
2
2
Min= 0.012 at (3,3), Max= 0.821 at (82,72)
148

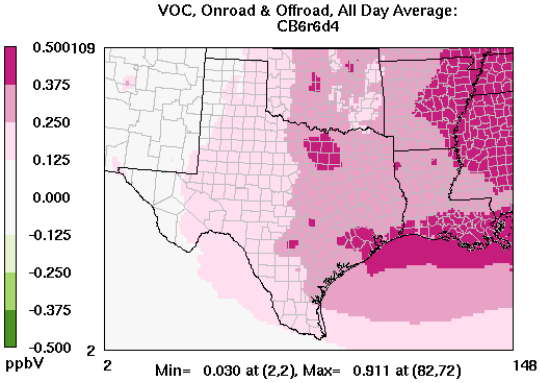
VOC, Onroad & Offroad, All Day Average:
CB6r6d4
0.500109
0.375
0.250
0.125
0.000
-0.125
-0.250
-0.375
-0.500
ppbV
2
2
Min= 0.030 at (2,2), Max= 0.911 at (82,72)
148

(g)

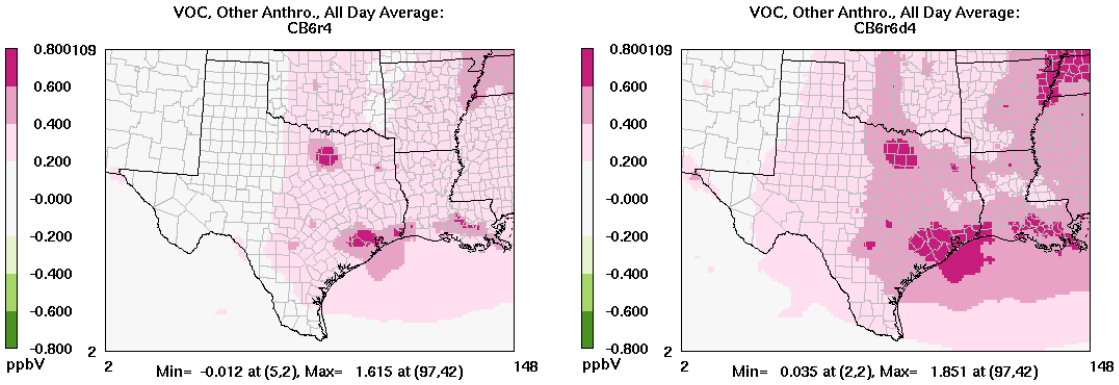

(h)

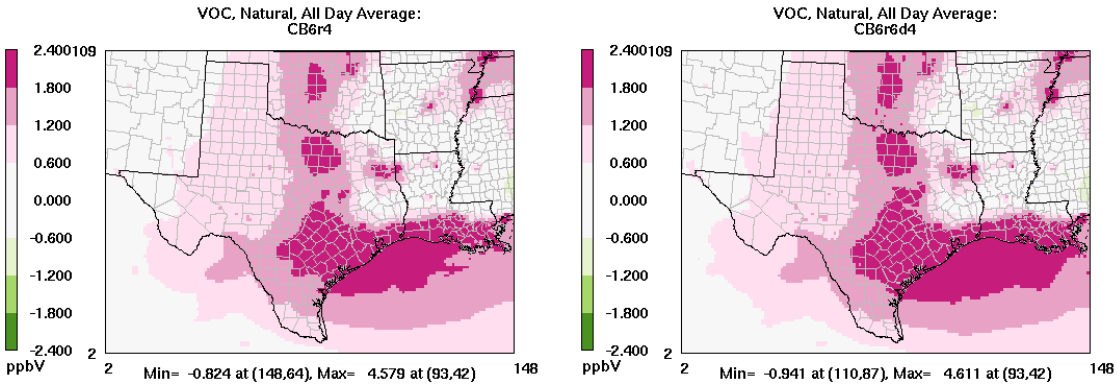

Figure 4-8. DDM ozone sensitivity to NOx or VOC emissions by source sector for the base case (left) and for CAMx with the CB6r6d4 mechanism (right): (a) oil and gas NO_x, (b) on-road and non-road mobile NO_x, (c) other anthropogenic NO_x, (d) natural NO_x, (e) oil and gas VOC, (f) on-road and non-road mobile VOC, (g) other anthropogenic VOC, and (h) natural VOC. Note differences in scales between plots.

(a)

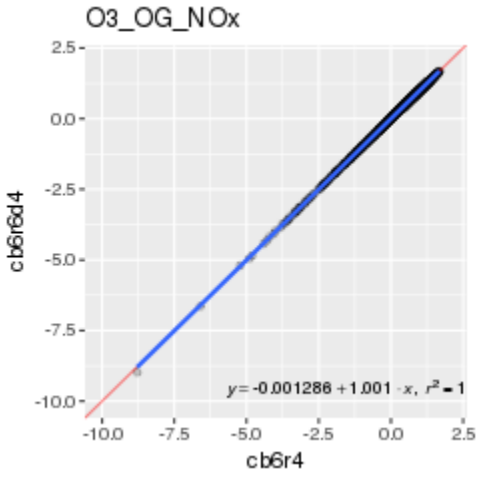
O3_OG_NOx
cb6r6d4
cb6r4
y = -0.001286 + 1.001 · x, r² = 1
2.5
0.0
-2.5
-5.0
-7.5
-10.0

(b)

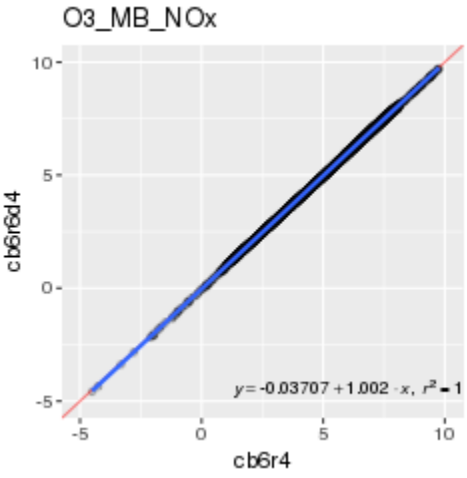
O3_MB_NOx
cb6r6d4
cb6r4
y = -0.03707 + 1.002 · x, r² = 1
10
5
0
-5

(c)

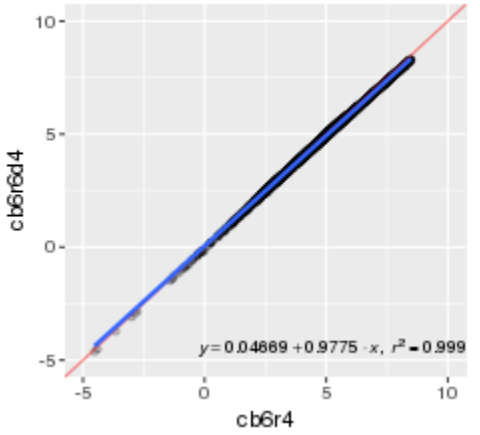
O3_AT_NOx
cb6r6d4
cb6r4
y = 0.04869 + 0.9775 · x, r² = 0.999
10
5
0
-5

(d)

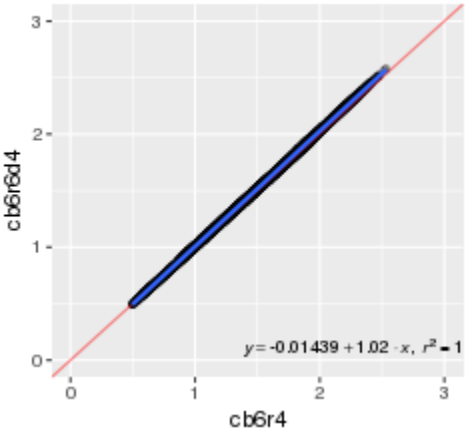
O3_NT_NOx
cb6r6d4
cb6r4
y = -0.01439 + 1.02 · x, r² = 1
3
2
1
0

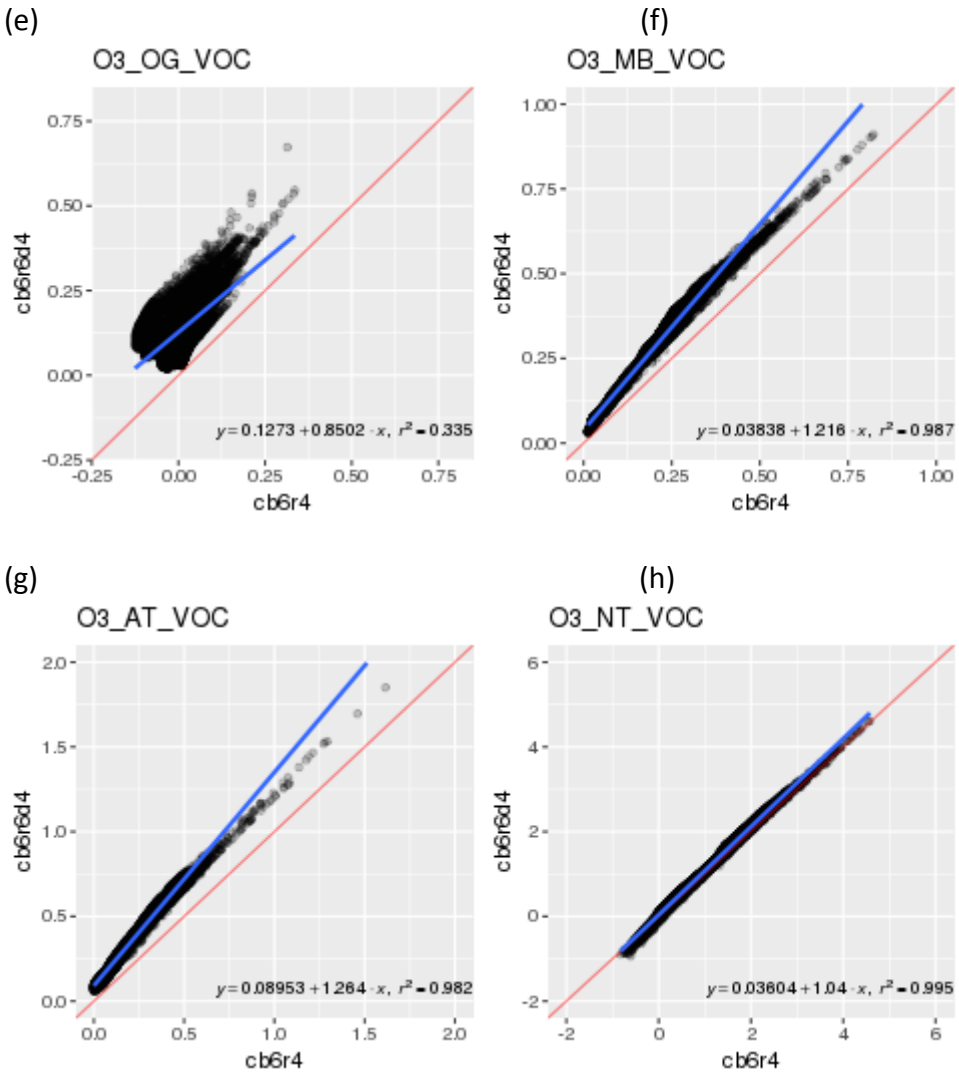

Figure 4-9. Scatter plots of DDM ozone sensitivities to NO_x or VOC emissions by source sector for CAMx with the CB6r6d4 mechanism versus the base case (CB6r4 mechanism): (a) oil and gas NO_x, (b) on-road and non-road mobile NO_x, (c) other anthropogenic NO_x, (d) natural NO_x, (e) oil and gas VOC, (f) on-road and non-road mobile VOC, (g) other anthropogenic VOC, and (h) natural VOC. The linear regression (blue) and 1:1 (red) lines are shown. Note differences in scales between plots.

4.4 Net Effects of Mechanism Updates on Model Performance

Figure 4-10 shows the net effects of the mechanism changes relative to the base case. CAMx hourly ozone, MDA8 ozone, and hourly $PM_{2.5}$ performance at CAMS surface sites with the CB6r6d4 mechanism and the base case are shown in Figures 4-11 through 4-15. Overall the collective mechanism changes do not significantly affect model performance for these metrics.

(a)

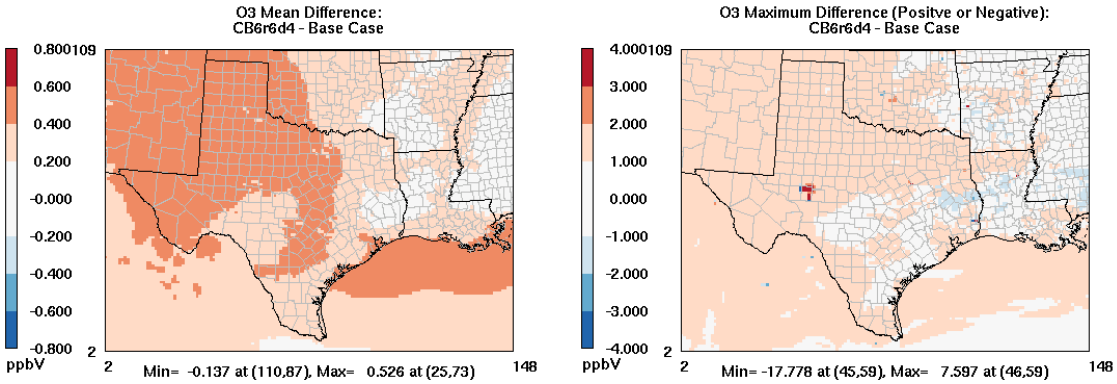

(b)

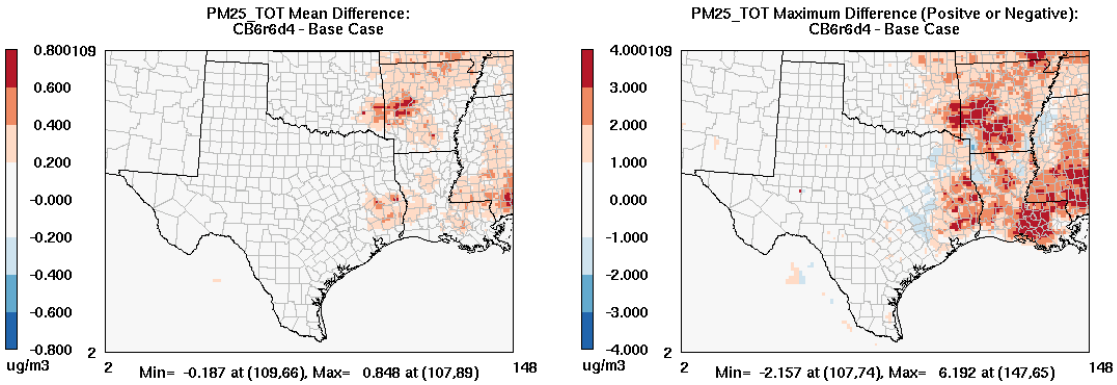

(c)

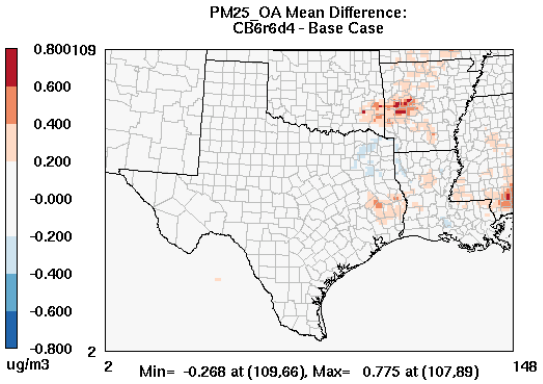
PM25_OA Mean Difference:
CB6r6d4 - Base Case
0.800109
0.600
0.400
0.200
-0.000
-0.200
-0.400
-0.600
-0.800
ug/m3
2
2
148
Min= -0.268 at (109,66), Max= 0.775 at (107,89)

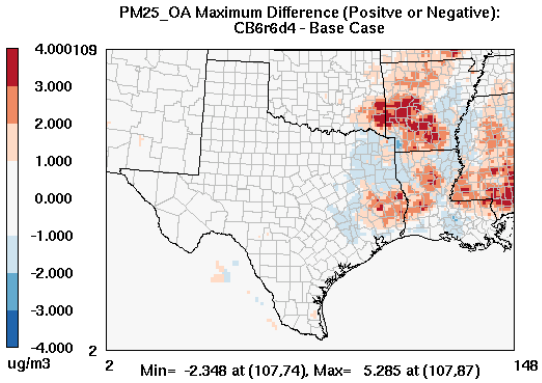
PM25_OA Maximum Difference (Positve or Negative):
CB6r6d4 - Base Case
4.000109
3.000
2.000
1.000
0.000
-1.000
-2.000
-3.000
-4.000
ug/m3
2
2
148
Min= -2.348 at (107,74), Max= 5.285 at (107,87)

(d)

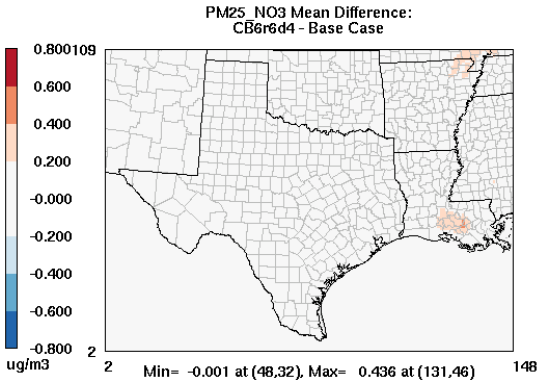
PM25_NO3 Mean Difference:
CB6r6d4 - Base Case
0.800109
0.600
0.400
0.200
-0.000
-0.200
-0.400
-0.600
-0.800
ug/m3
2
2
148
Min= -0.001 at (48,32), Max= 0.436 at (131,46)

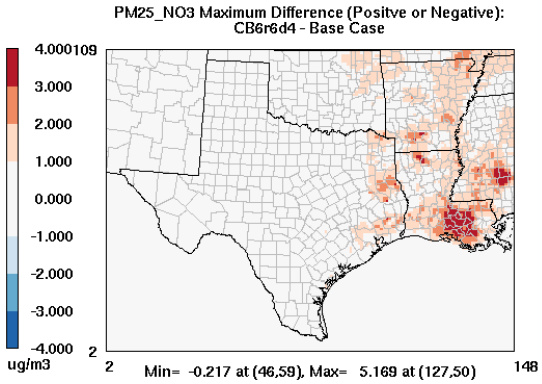
PM25_NO3 Maximum Difference (Positve or Negative):
CB6r6d4 - Base Case
4.000109
3.000
2.000
1.000
0.000
-1.000
-2.000
-3.000
-4.000
ug/m3
2
2
148
Min= -0.217 at (46,59), Max= 5.169 at (127,50)

(e)

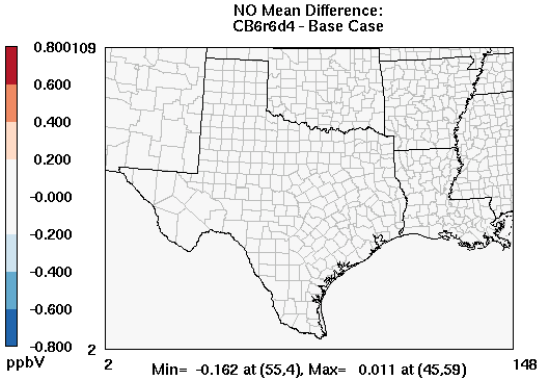
NO Mean Difference:
CB6r6d4 - Base Case
0.800109
0.600
0.400
0.200
-0.000
-0.200
-0.400
-0.600
-0.800
ppbV
2
2
148
Min= -0.162 at (55,4), Max= 0.011 at (45,59)

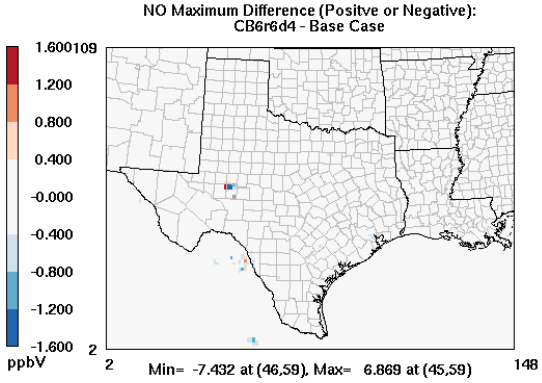
NO Maximum Difference (Positve or Negative):
CB6r6d4 - Base Case
1.600109
1.200
0.800
0.400
-0.000
-0.400
-0.800
-1.200
-1.600
ppbV
2
2
148
Min= -7.432 at (46,59), Max= 6.869 at (45,59)

(f)

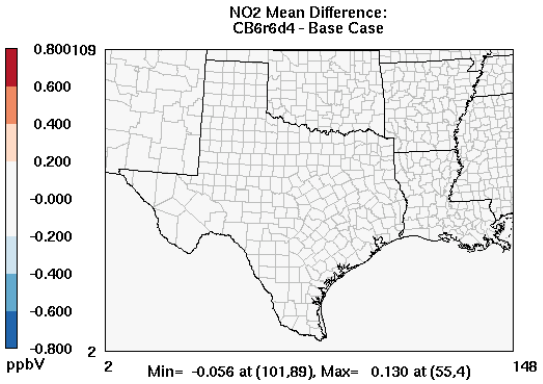
NO2 Mean Difference:
CB6r6d4 - Base Case
0.800109
0.600
0.400
0.200
-0.000
-0.200
-0.400
-0.600
-0.800
ppbV
2
2
148
Min= -0.056 at (101,89), Max= 0.130 at (55,4)

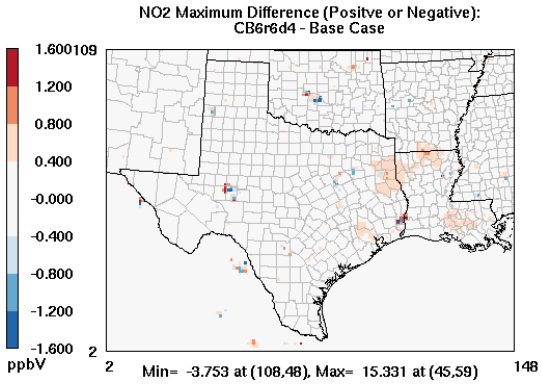
NO2 Maximum Difference (Positve or Negative):
CB6r6d4 - Base Case
1.600109
1.200
0.800
0.400
-0.000
-0.400
-0.800
-1.200
-1.600
ppbV
2
2
148
Min= -3.753 at (108,48), Max= 15.331 at (45,59)

(g)

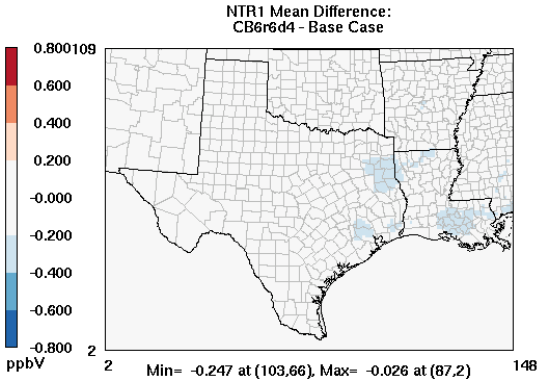
NTR1 Mean Difference:
CB6r6d4 - Base Case
0.800109
0.600
0.400
0.200
-0.000
-0.200
-0.400
-0.600
-0.800
ppbV
2
2
148
Min= -0.247 at (103,66), Max= -0.026 at (87,2)

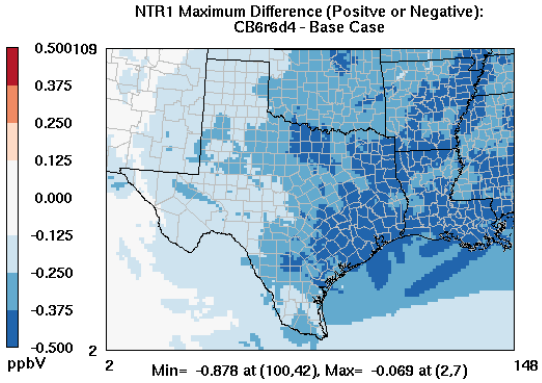
NTR1 Maximum Difference (Positve or Negative):
CB6r6d4 - Base Case
0.500109
0.375
0.250
0.125
0.000
-0.125
-0.250
-0.375
-0.500
ppbV
2
2
148
Min= -0.878 at (100,42), Max= -0.069 at (2,7)

(h)

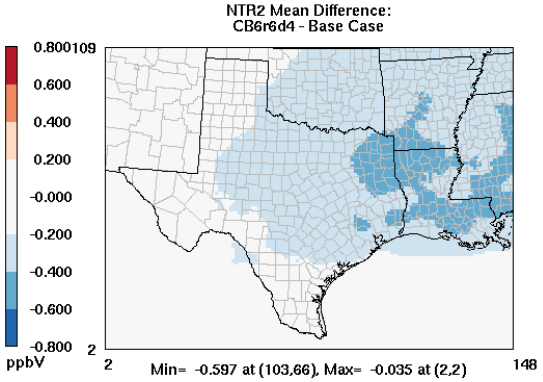
NTR2 Mean Difference:
CB6r6d4 - Base Case
0.800109
0.600
0.400
0.200
-0.000
-0.200
-0.400
-0.600
-0.800
ppbV
2
2
148
Min= -0.597 at (103,66), Max= -0.035 at (2,2)

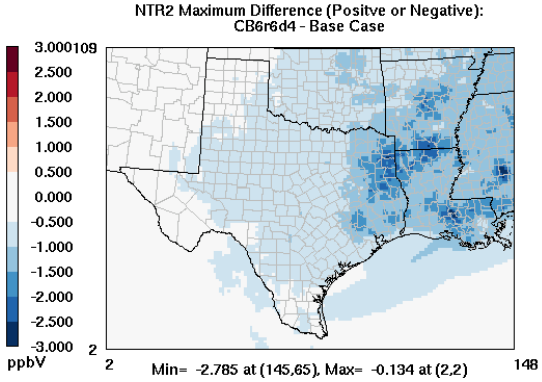
NTR2 Maximum Difference (Positve or Negative):
CB6r6d4 - Base Case
3.000109
2.500
2.000
1.500
1.000
0.500
0.000
-0.500
-1.000
-1.500
-2.000
-2.500
-3.000
ppbV
2
2
148
Min= -2.785 at (145,65), Max= -0.134 at (2,2)

(i)

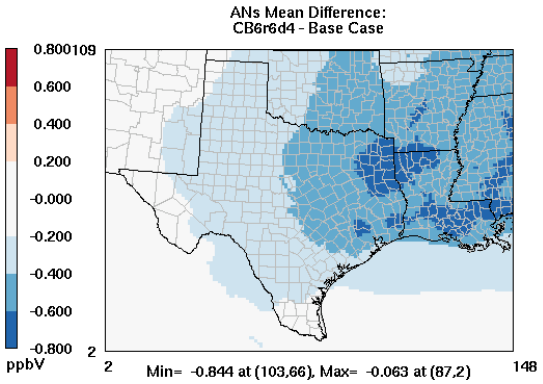
ANs Mean Difference:
CB6r6d4 - Base Case
0.800109
0.600
0.400
0.200
-0.000
-0.200
-0.400
-0.600
-0.800
ppbV
2
2
148
Min= -0.844 at (103,66), Max= -0.063 at (87,2)

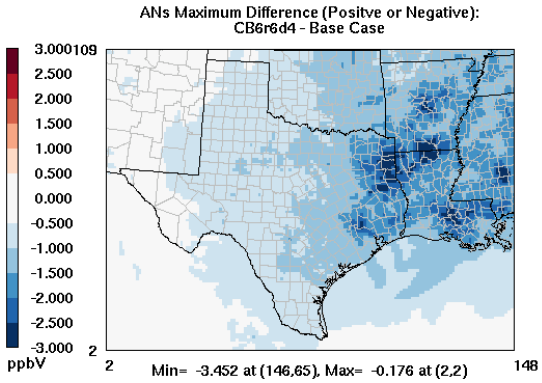
ANs Maximum Difference (Positve or Negative):
CB6r6d4 - Base Case
3.000109
2.500
2.000
1.500
1.000
0.500
0.000
-0.500
-1.000
-1.500
-2.000
-2.500
-3.000
ppbV
2
2
148
Min= -3.452 at (146,65), Max= -0.176 at (2,2)

(j)

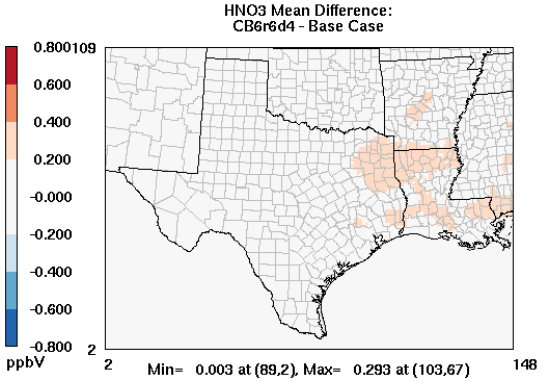
HNO3 Mean Difference:
CB6r6d4 - Base Case
0.800109
0.600
0.400
0.200
-0.000
-0.200
-0.400
-0.600
-0.800
ppbV
2
2
148
Min= 0.003 at (89,2), Max= 0.293 at (103,67)

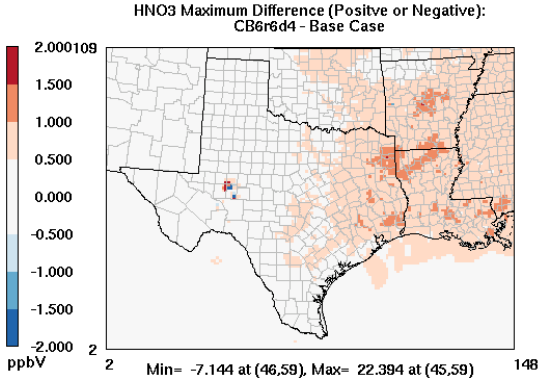
HNO3 Maximum Difference (Positve or Negative):
CB6r6d4 - Base Case
2.000109
1.500
1.000
0.500
0.000
-0.500
-1.000
-1.500
-2.000
ppbV
2
2
148
Min= -7.144 at (46,59), Max= 22.394 at (45,59)

(k)

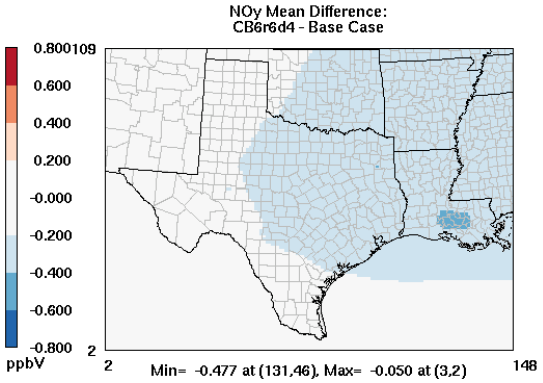
NOy Mean Difference:
CB6r6d4 - Base Case
0.800109
0.600
0.400
0.200
-0.000
-0.200
-0.400
-0.600
-0.800
ppbV
2
2
148
Min= -0.477 at (131,46), Max= -0.050 at (3,2)

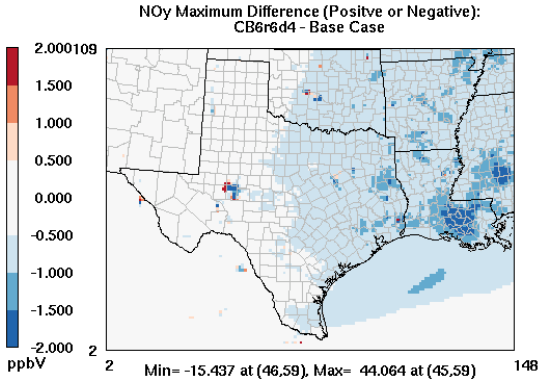
NOy Maximum Difference (Positve or Negative):
CB6r6d4 - Base Case
2.000109
1.500
1.000
0.500
0.000
-0.500
-1.000
-1.500
-2.000
ppbV
2
2
148
Min= -15.437 at (46,59), Max= 44.064 at (45,59)

(l)

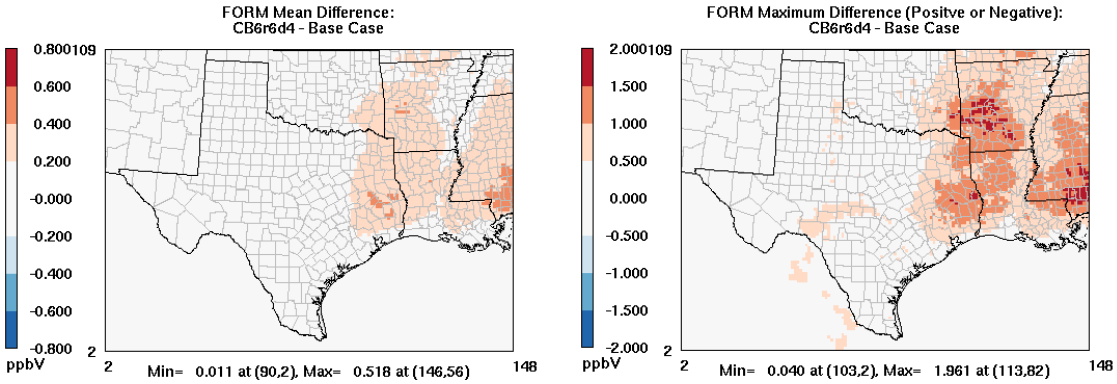

(m)

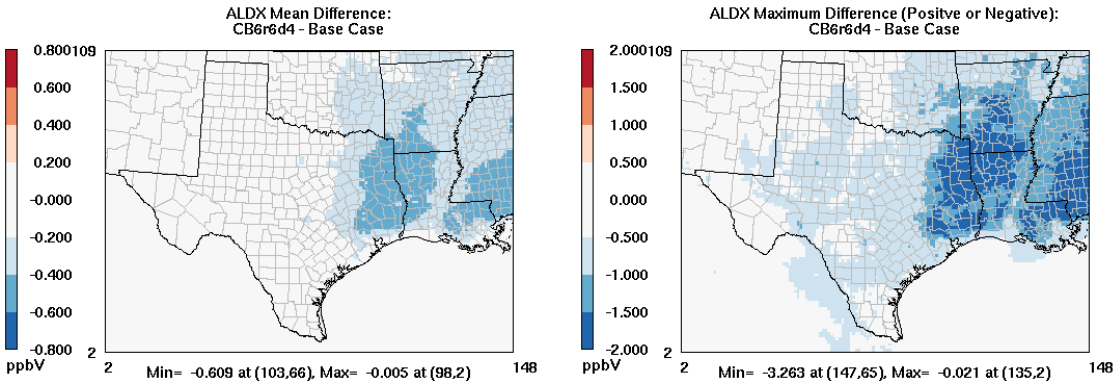

(n)

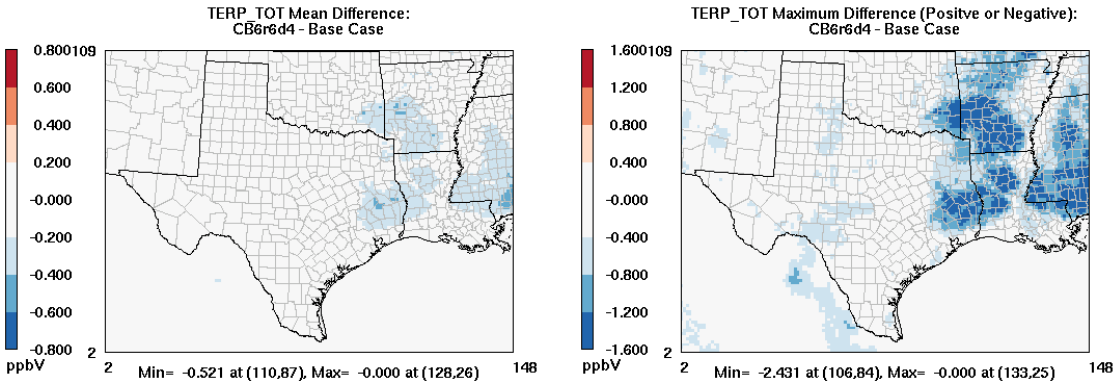

Figure 4-10. Mean (left) and maximum (positive or negative) differences (right) between CAMx predictions with the CB6r4 mechanism and the base case: (a) ozone, (b) total $PM_{2.5}$ mass, (c) organic aerosol, (d) particulate nitrate, (e) NO, (f) NO_2, (g) NTR1, (h) NTR2, (i) total alkyl nitrates, (j) HNO_3, (k) NO_y, (l) formaldehyde, (m) propionaldehyde and higher aldehyde, and (n) terpene concentrations. Note differences in scales between plots.

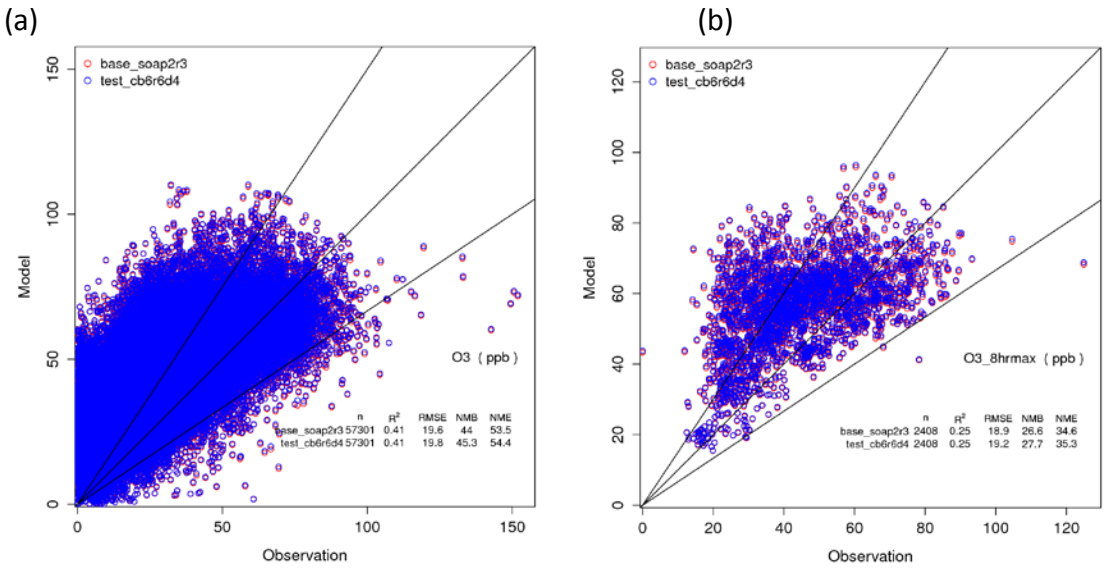

Figure 4-11. Scatter plots of modeled and observed (a) hourly ozone and (b) maximum daily average 8-hour (MDA8) ozone concentrations, paired in space and time, at CAMS monitoring sites within the 4-km eastern Texas domain. Modeled concentrations are shown for CAMx with the CB6r4 mechanism and for the base case.

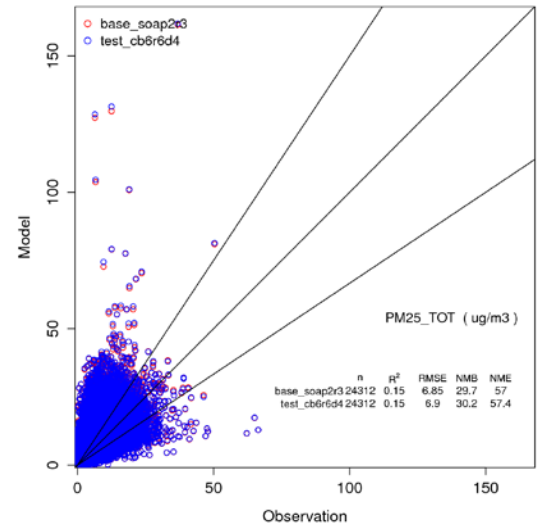

Figure 4-12. Scatter plots of modeled and observed hourly $PM_{2.5}$ concentrations, paired in space and time, at CAMS monitoring sites within the 4-km eastern Texas domain. Modeled concentrations are shown for CAMx with the CB6r4 mechanism and for the base case.

(a)

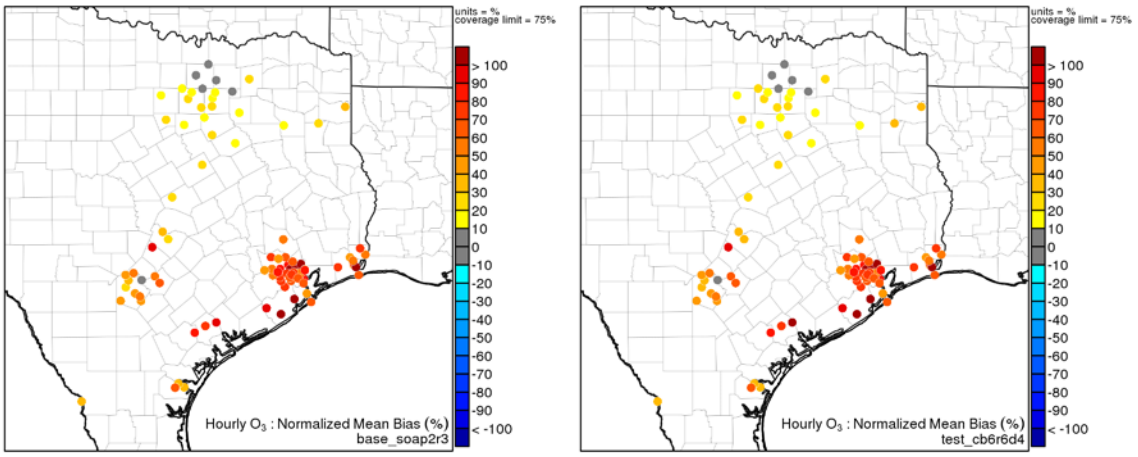

(b)

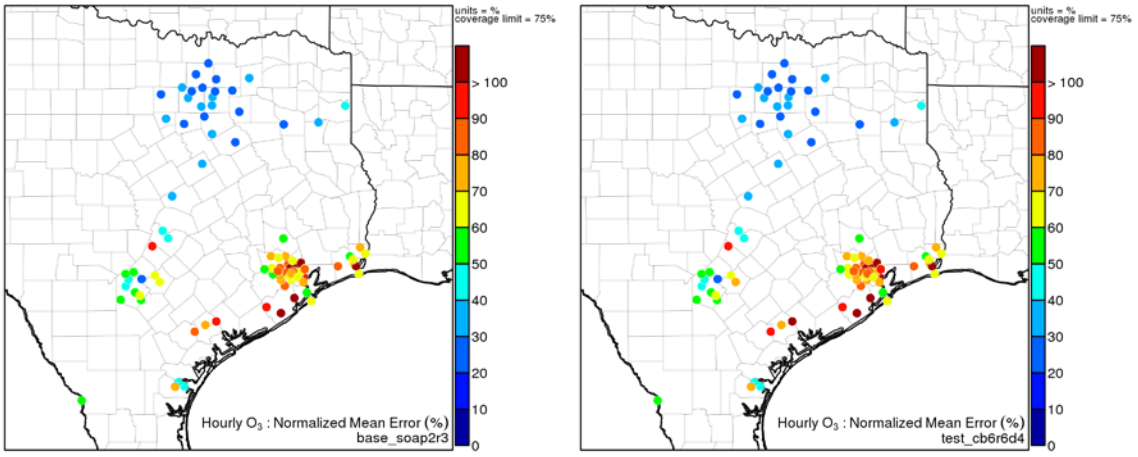

Figure 4-13. (a) Normalized mean bias and (b) normalized mean error for modeled hourly ozone concentrations at CAMS monitoring sites in eastern Texas during the episode time period for the base case (left) and for CAMx with the CB6r4 mechanism (right).

(a)

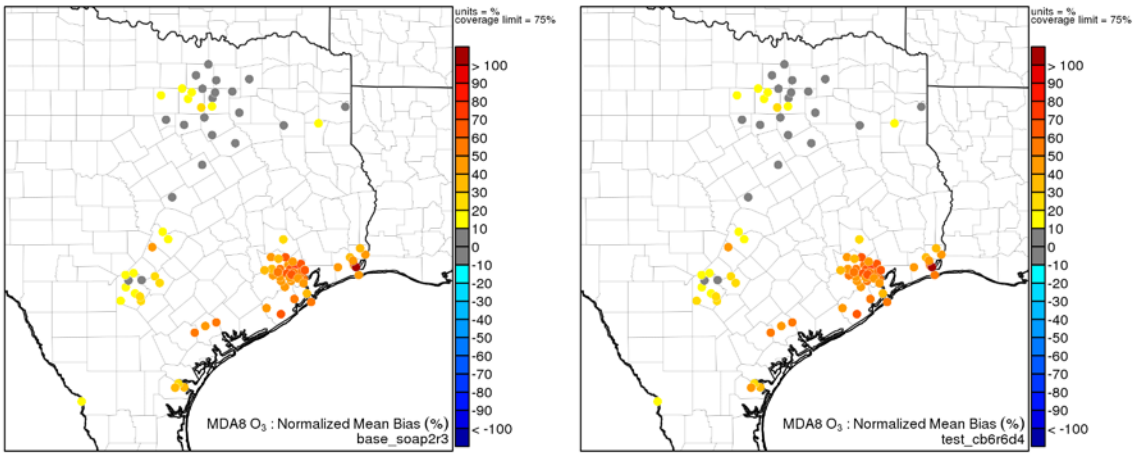

(b)

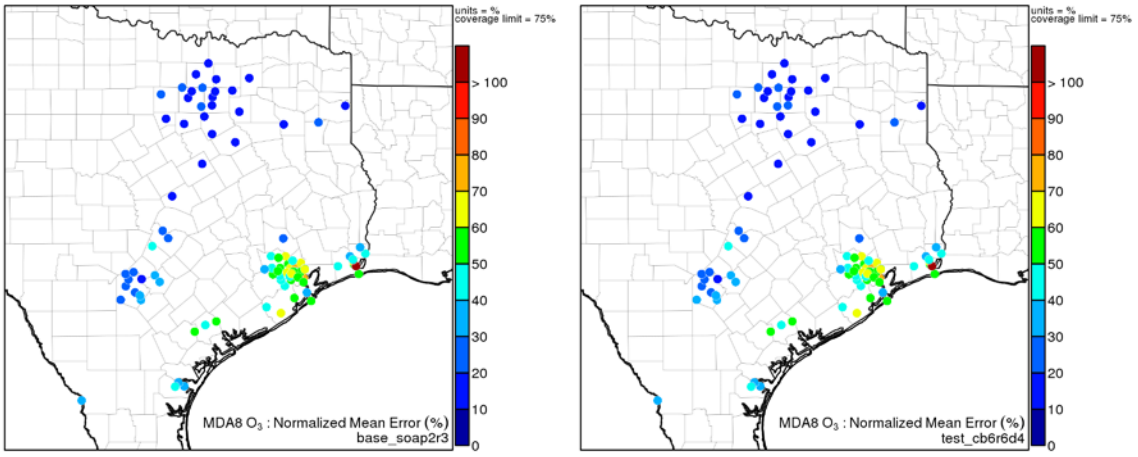

Figure 4-14. (a) Normalized mean bias and (b) normalized mean error for modeled MDA8 ozone concentrations at CAMS monitoring sites in eastern Texas during the episode time period for the base case (left) and for CAMx with the CB6r4 mechanism (right).

(a)

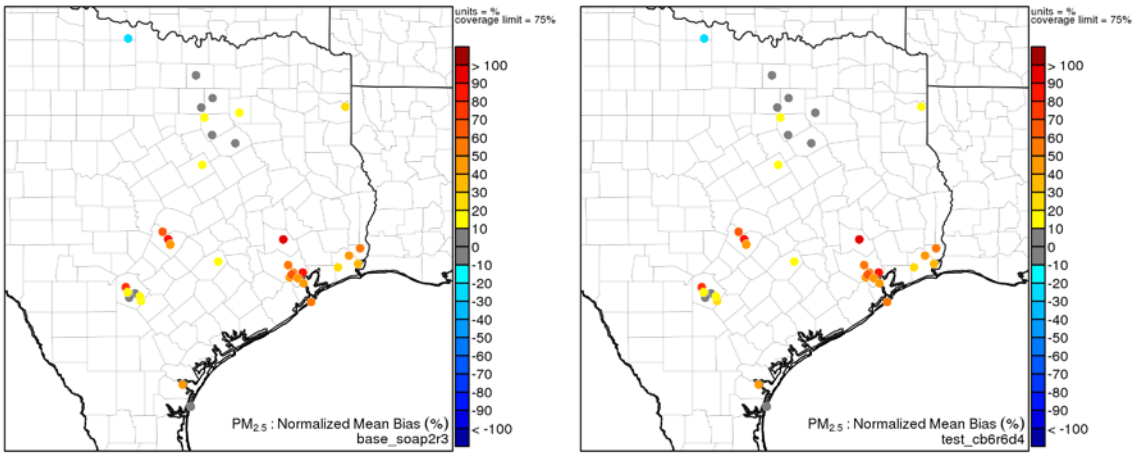

(b)

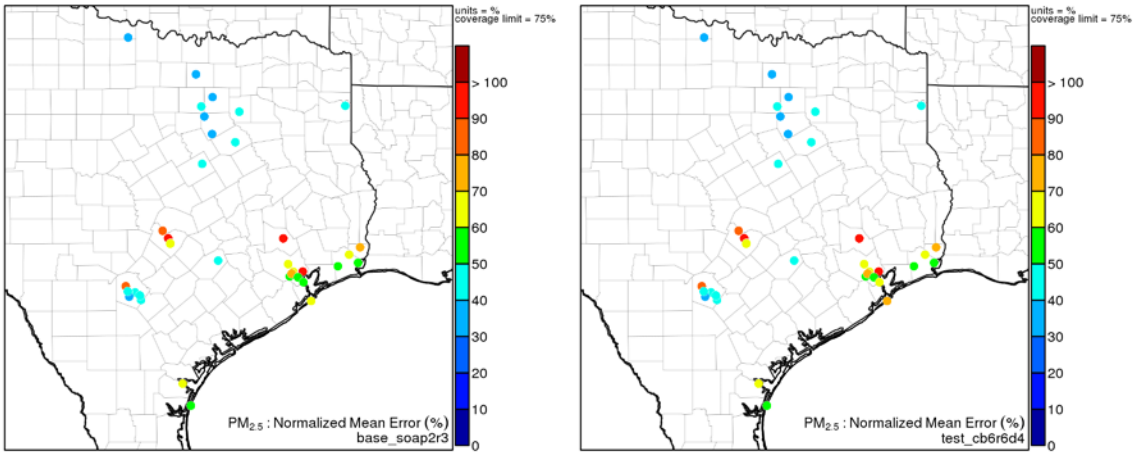

Figure 4-15. (a) Normalized mean bias and (b) normalized mean error for modeled hourly $PM_{2.5}$ concentrations at CAMS monitoring sites in eastern Texas during the episode time period for the base case (left) and for CAMx with the CB6r4 mechanism (right).

5. Audits of Data Quality

Quality assurance was addressed throughout the project.

5.1 CAMx Base Case Development and Evaluation

As described in Chapter 2, the CAMx configuration leveraged the work of Nopmongcol et al. (2015) at Ramboll Environ as a starting point. CAMx modeling input and supplementary data and scripts for model performance evaluation from this previous effort were transferred to the University of Texas at Austin, specifically to the Texas Advanced Computing Center where all model simulations for the project were performed. The initial CAMx run was replicated on the TACC's Lonestar5 system using the files provided. The results were evaluated using visualization and statistical software to confirm reasonable reproducibility.

Model performance evaluation was conducted using the Atmospheric Model Evaluation Tool (AMET) inputs and scripts for CAMS surface monitors (Section 2.6.1), in-house Microsoft Excel file for DISCOVER-AQ surface observations (Section 2.6.2), and an in-house python script for DISCOVER-AQ aloft observations (Section 2.6.3). Surface network observations were retrieved from the Texas Air Monitoring Information System (TAMIS: http://www17.tceq.texas.gov/tamis/index.cfm?fuseaction=home.welcome). DISCOVER-AQ upper air observations were retrieved from dedicated site hosted at NASA (https://www-air.larc.nasa.gov/cgi-bin/ArcView/discover-aq.tx-2013).

In some cases, model species required unit conversion and aggregation (e.g., comparison of observed and modeled total $PM_{2.5}$ mass concentrations required summation of all $PM_{2.5}$ component species in the model output). Mapping for DISCOVER-AQ surface observations was performed with XSPCMAP (http://www.camx.com/download/support-software.aspx) by Dr.Kimura and independently reviewed and verified by Dr. Bonyoung Koo. Species mapping for surface network and aloft observations was performed by Dr. Kimura using the COMBINE IOAPI tool (https://www.airqualitymodeling.org/index.php/CMAQv5.1_Tools_and_Utilities#COMBINE_utility_program) and verified by Mr. Gary McGaughey.

Statistical performance metrics (Table 2-10) at CAMS sites were determined using AMET as described above. The calculations were replicated with Microsoft Excel for randomly selected surface monitors, confirming reproducibility.

5.2 CAMx Emission Inventory Processing

The organic gas-aerosol partitioning and oxidation schemes, 1.5-D VBS or SOAP2 (SOAP2r3), required different sets of model species for SOA precursors and IVOC, as described in Section 2.5.3. In addition, two of the mechanisms developed in this project, CB6r6d1 and CB6r6d4, required separation of APIN and TERP species, and the CB6r6d4 mechanism also required separation of PAR and PARH species (ref. Sections 3.2 and 3.3). These changes required reprocessing of emissions files. Species mappings were

performed with the XSPCMAP tool. For all cases, mapping of species was conducted by Dr. Kimura and reviewed by Dr. Koo. Tile plots of emitted species were also generated for visual confirmation.

5.3 CAMx Mechanism Development and Evaluation

Evaluation of the chemical mechanisms developed in this project, as discussed in Chapter 4, involved temporal aggregation for each model grid cell and visualization of aggregated values via tile and scatter plots. Differences in predicted concentrations between model simulations were developed using M3DIFF (https://www.cmascenter.org/ioapi/documentation/all_versions/html/M3DIFF.html) and M3TPROC https://www.cmascenter.org/ioapi/documentation/all_versions/html/M3TPROC.html) IOAPI tools, respectively. Scripts to perform the processing were written by Dr. Kimura and reviewed by Mr. McGaughey. The temporal aggregation was quality assured by independent calculation using Microsoft Excel for selected grid cells.

6. Conclusions and Recommendations

Alkyl nitrates have the potential to influence tropospheric ozone and secondary organic aerosol formation over regional to global spatial scales. Advances in analytical techniques and their applications in laboratory studies and major field campaigns have led to new insights on the atmospheric chemistry and fate of alkyl nitrates. The objectives of this study were to integrate these findings into CAMx and investigate the effects on predicted regional ozone and fine particulate mass and composition in eastern Texas. Updates to the CB6 chemical mechanism in CAMx (from a starting point of CB6r4) focused on alkyl nitrates formed from biogenic monoterpene precursors and anthropogenic alkane precursors relevant to Texas emission inventories as well as characterization of the loss of alkyl nitrates due to hydrolysis. This new mechanism version is CB6r6d4.

The most recent release of CAMx, v.6.40, with WRF v.3.6.1 meteorology and the CB6r4 gas-phase mechanism, was applied for the time period of August 18-September 30, 2013 that spanned the DISCOVER-AQ campaign in southeastern Texas. Model performance was assessed using observations from CAMs surface sites in eastern Texas and observations at the surface and aloft made during DISCOVER-AQ. Three schemes for organic gas-aerosol partitioning and oxidation in CAMx were evaluated: 1.5-D VBS, SOAP2, and a new scheme developed in this work, SOAP2r3, that included SOA loss by photolysis. The SOAP2r3 and 1.5-D VBS schemes provided generally comparable model performance for trace gases and $PM_{2.5}$ total mass and component concentrations. The SOAP2r3 scheme is expected to be more easily applied for modeling efforts that support air quality planning and management and was selected for the base case. Sensitivity studies were conducted that considered the individual and net effects of modifications to the CB6r4 gas-phase mechanism and SOA yields of the base case.

Hydrolysis of Multifunctional Organic Nitrates

Hydrolysis of multifunctional organic nitrates (i.e., the CB6 NTR2 species) was represented in the base case CB6r4 mechanism as a pseudo gas-phase reaction producing HNO_3 with lifetime of 6-hours. The lifetime against hydrolysis was reduced to 1-hour consistent with recent findings that very short lifetimes are appropriate for acidic aerosols. Regional ozone concentrations were insensitive to more rapid hydrolysis. Hourly total $PM_{2.5}$ mass concentrations increased by as much as 0.5 $\mu g/m^3$ on average due to an increase in particulate NO_3. Maximum increases in total $PM_{2.5}$ mass concentrations were approximately 6 $\mu g/m^3$ and occurred in areas where the sensitivity of multifunctional organic nitrates to BVOC emissions dominated anthropogenic emissions.

Monoterpene Chemistry

Recent studies have indicated the importance of NO_3-monoteprene chemistry to SOA formation, but that SOA yields are variable with α-pinene consistently lower than for other monoterpenes. The CB6r4 mechanism was modified to split terpenes to α-pinene (APIN) and other terpenes (TERP). Revisions were made to the gas-phase reactions of

TERP and APIN with OH, O_3, NO_3 and to SOA yields for TERP and APIN reactions with NO_3. The impacts of these modifications primarily occurred in terpene-rich areas of the modeling domain. Average decreases in hourly ozone concentrations were 0.5 ppb with a maximum of 1 to 2 ppb. Differences in hourly total $PM_{2.5}$ mass and organic aerosol were within $\pm$0.5 μg/m^3 on average with maximum differences of -2 to +5 μg/m^3.

Alkane Chemistry

Long-chain alkanes are precursors to alkyl nitrates that contribute to SOA formation and serve as a potential NO_x sink via hydrolysis. Alkanes were split into PAR and PARH, which has a high AN yield, according to chain length. Revisions were made to the gas-phase reactions for PAR and PARH as well as ketones. PAR and PARH fractions were applied by emissions source sector with, for example, lower PARH fractions were applied for the oil and gas sector (10%) than mobile sources (20%). Total $PM_{2.5}$ mass concentrations were relatively insensitive to the modifications in AN yields using the PARH scheme. Widespread increases in ozone were 1-2 ppb. Application of the PARH scheme decreased the total alkyl nitrate burden and increased ozone sensitivity to VOC emissions from the oil and gas sector and other anthropogenic sources.

We make the following recommendations:

- Faster hydrolysis of organic nitrates is recommended for use in CAMx as being more consistent with recent field study data.
- The updated SOA scheme for CAMx, SOAP2r3, is recommended for use as the primary SOA scheme in CAMx. The 1.5D VBS SOA scheme continues to provide a useful alternative but requires greater computational resources and is not compatible with PM source apportionment (PSAT).
- Additional testing and evaluation is recommended for the updated terpene and alkane chemistry developed for CB6r6d4. These mechanism changes are improvements but their impact was not large in the testing conducted here. Because these mechanism changes add reactions and species they slow down model simulations to a minor extent.
- We recommend additional study of how terpenes are represented in emission inventories, such as MEGAN version 3, and regional models, such as CAMx with the CB6r6d4. Evaluation should exploit recent field study data from the southeastern US to evaluate concentrations of terpenes, nitrate radical, and their reaction products including ANs.
- The ability of photochemical grid models to represent interaction between biogenic VOC and anthropogenic NOx in rural environments with heterogeneous landcover should be investigated as sub-grid scale interactions that have the potential to alter sensitivity of O_3 and PM to emissions and atmospheric chemistry schemes.

7. References

Atkinson, R. and Arey, J., 2003. Gas-phase tropospheric chemistry of biogenic volatile organic compounds: a review, Atmos. Environ, 37, 197-219.

Bean, J. K., Hildebrandt Ruiz, L., Gas-particle partitioning and hydrolysis of organic nitrates formed from the oxidation of α-pinene in environmental chamber experiments, 2016, Atmos. Chem. Phys. 16, 2175–2184.

Bean, J.K., Faxon, C.B., Leong, Y.J., Wallace, H.W., Cevik, B.K., Ortiz, S., Canagaratna, M.R., Usenko, S., Sheesley, R.J., Griffin, R.J., Hildebrandt Ruiz, L., 2016, Composition and sources of particulate matter measured near Houston, TX: anthropogenic-biogenic interactions. Atmosphere, 7, 73-96.

Browne, E.C., Min, K.-E., Wooldridge, P.J., Apel, E., Blake, D.R., Brune, W.H., Cantrell, C.A., Cubison, M. J., Diskin, G.S., Jimenez, J.L., Weinheimer, A.J., Wennberg, P.O., Wisthaler, A., Cohen, R.C., 2013, Observations of total RONO2 over the boreal forest: NO_x sinks and HNO_3 sources, Atmos. Chem. Phys., 13, 4543–4562, 2013.

Brown, S. S., Dubé,W. P., Bahreini, R., Middlebrook, A. M., Brock, C. A., Warneke, C., de Gouw, J. A., Washenfelder, R. A., Atlas, E., Peischl, J., Ryerson, T. B., Holloway, J. S., Schwarz, J. P., Spackman, R., Trainer, M., Parrish, D. D., Fehsenfeld, F. C., Ravishankara, A. R., Biogenic VOC oxidation and organic aerosol formation in an urban noctural boundary layer: Aircraft vertical profiles in Houston, TX, 2013, Atmos. Chem. Phys., 13, 11317–11337.

Boyd, C. M., Sanchez, J., Xu, L., Eugene, a. J., Nah, T., Tuet, W. Y., Guzman, M. I. and Ng, N. L., 2015, Secondary organic aerosol formation from the β-pinene+NO_3 system: Effect of humidity and peroxy radical fate, Atmos. Chem. Phys., 15(13), 7497–7522.

Calvert, J.G., Atkinson, R., Kerr, J.A., Madronich, S., Moortgat, G.K., Wallington, T.J. and Yarwood, G., 2000. The mechanisms of atmospheric oxidation of the alkenes, Oxford Univ. Press, New York.

Day, D.A., Dillon, M.B., Wooldridge, P.J., Thornton, J.A., Rosen, R.S., Wood, E.Z., Cohen, R.C., On alkyl nitrates, O_3, and the ''missing NO_y'', 2003, .J. Geophys. Res., 108, D16, 4501.

Day, D., Liu, S., Russell, L.M., Ziemann, P.J., Organonitrate group concentrations in submicron particles with high nitrate and organic fractions in coastal southern California, 2010, Atmos. Environ., 44, 1970-1979.

Donahue, N.M., Robinson, A. L., Stanier, C.O., Pandis, S.N., 2006, Coupled partitioning, dilution, and chemical aging of semivolatile organics, Environ. Sci. Technol., 40, 2635–43.

Donahue, N. M., Epstein, S. A., Pandis, S. N., Robinson, A. L., 2011, A two-dimensional volatility basis set: 1. organic-aerosol mixing thermodynamics, Atmos. Chem. and Phys., 11(7), 3303–3318.

Donahue, N. M., Kroll, J. H., Pandis, S. N., Robinson, A. L., 2012, A two-dimensional volatility basis set – Part 2: Diagnostics of organic-aerosol evolution, Atmos. Chem. Phys., 12, 615–634.

Emery. C., Jung, J., Koo, B., Yarwood, G., Improvements to CAMx Snow Cover Treatments and Carbon Bond Chemical Mechanism for Winter Ozone. Final Report for Utah Department of Environmental Quality, Division of Air Quality, 2015.

Emery. C., Liu, Z., Koo, B., Yarwood, G., Improved Halogen Chemistry for CAMx Modeling. Final Report for Texas Commission on Environmental Quality Work Order No. 582-16-61842-13, 2016.

Fisher, J.A., Jacob, D., Travis, K., Kim, P., Marais, E., Yu, K., Miller, C., Zhu, L., Yantosca, R., Payer Sulprizio, M., Cohen, R., Fried, A., Goldstein, A., Hanisco, T., Jimenez, J., Wennberg, P., Wisthaler, A., Organic nitrate chemistry and implications: Insights from observations in the Southeast US, Atmospheric Composition & Chemistry Observations & Modeling Conference
November 2015.

Fisher, J. A., Jacob, D.J., Travis, K.R., Kim, P.S., Marais, E.A., Miller, C.C., Yu, K. Zhu, L., Yantosca, R.M., Sulprizio, M.P., Mao, J., Wennberg, P.O., Crounse, J.D., Teng, A.P., Nguyen, T.B., St. Clair, J.M., Cohen, R.C., Romer, P., Nault, B.A., Wooldridge, R.J., Jimenez, J.L., Campuzano-Jost, P., Day, D.A., Hu, W., Shepson, P.B., Xiong, F., Blake, D.R., Goldstein, A.H., Misztal, P.K., Hanisco, T.F., Wolfe, G.M., Ryerson, T.B., Wisthaler, A., and Mikoviny, T., 2016, Organic nitrate chemistry and its implications for nitrogen budgets in an isoprene- and monoterpene-rich atmosphere: constraints from aircraft (SEAC4RS) and ground-based (SOAS) observations in the Southeast US Atmos. Chem. Phys., 16, 5969–5991.

Fry, J.L., Draper, D.C., Barsanti, K.C., Smith, J.N., Ortega, J. Winkler, P.M., Lawler, M.J., Brown, S.S., Edwards, P.M., Cohen, R.C., Lee, L., 2014, Secondary organic aerosol formation and organic nitrate yield from NO_3 oxidation of biogenic hydrocarbons, Environ. Sci. Technol., 48 (20), 11944-11953.

Fry, J.L., Draper, D.C., Zarzana, K.J., Campuzano-Jost, P., Day, D.A., Jimenez, J.L., Brown, S.S., Cohen, R.C., Kaser, L., Hansel, A., Cappellin, L., Karl, T., Hodzic Roux, A., Turnipseed,

A., Cantrell, C., Lefer, B.L., Grossberg, N., 2013, Observations of gas- and aerosol-phase organic nitrates at BEACHCON-RoMBAS 2011, Atmos. Chem. Phys., 13, 8585-8605.

Guenther, A. B., Jiang, X., Heald, C.L., Sakulyanontvittaya, T., Duhl, T., Emmons, L. K., Wang, X., 2012, The Model of Emissions of Gases and Aerosols from Nature version 2.1 (MEGAN2.1): an extended and updated framework for modeling biogenic emissions, Geosci. Model Dev., 2012, 5, 1471–1492.

Henry, K. M. and Donahue, N. M., 2012, Photochemical Aging of α-Pinene Secondary Organic Aerosol: Effects of OH Radical Sources and Photolysis, J. Phys. Chem. A, 116, 5932-5940.

Hildebrandt Ruiz, L., Yarwood, G, 2013, Interactions between Organic aerosol and NO_y : Influence on oxidant production, report submitted to the Texas Air Quality Research Program, Project # 12-012.

Hildebrandt Ruiz, L., Koo, B., Yarwood, G., 2015, Sources of organic particulate matter in Houston: Evidence from DISCOVER-AQ data - Modeling and Experiments, report submitted to the Texas Air Quality Research Program, Project # 14-024.

Hodzic, A., Kasibhatla, P. S., Jo, D. S., Cappa, C. D., Jimenez, J. L., Madronich, S., and Park, R. J., 2016, Rethinking the global secondary organic aerosol (SOA) budget: stronger production, faster removal, shorter lifetime, Atmos. Chem. Phys., 16, 7917-7941.

International Union of Pure and Applied Chemistry, Task Group on Atmospheric Chemical Kinetic Data Evaluation (2017). Available at http://iupac.pole-ether.fr/index.html, accessed 31 March 2017.Johnson, J., Karamchandani, P., Wilson, G. and Yarwood, G., TCEQ Ozone Forecasting System, Prepared for Mark Estes., 2013.

Karamchandani, P., Vijayaraghavan, K., Yarwood, G., 2011, Sub-grid scale plume modeling, Atmosphere, 2, 389-406.

Koo, B., Knipping, E., Yarwood, G., 2014, 1.5-Dimensional volatility basis set approach for modeling organic aerosol in CAMx and CMAQ, Atmos. Environ., 95, 158-164.

Lee, B. H., Mohr, C., Lopez-Hilfiker, F. D., Lutz, A., Hallquist, M., Lee, L., Romer, P., Cohen, R. C., Iyer, S., Kurtén, T., Hu, W., Day, D. A., Campuzano-Jost, P., Jimenez, J. L., Xu, L., Ng, N. L., Guo, H., Weber, R. J., Wild, R. J., Brown, S. S., Koss, A., de Gouw, J., Olson, K., Goldstein, A. H., Seco, R., Kim, S., McAvey, K., Shepson, P. B., Starn, T., Baumann, K., Edgerton, E. S., Liu, J., Shilling, J. E., Miller, D. O., Brune, W., Schobesberger, S., D'Ambro, E. L. and Thornton, J. A., 2016, Highly functionalized organic nitrates in the southeast United States: Contribution to secondary organic aerosol and reactive nitrogen budgets, Proc. Natl. Acad. Sci., 113(6), 1516-1521.

Leong Y.J., Sanchez, N.P., Wallace, H.W., Karakurt Cevik, B., Hernandez, C.S., Han, Y., Flynn J.H., Massoli, P., Floerchinger, C., Fortner, E.C., Herndon, S., Bean, J.K., Hildebrandt Ruiz, L., Jeon, W., Choi, Y., Lefer, B., Griffin, R.J., 2017, Overview of surface measurements and spatial characterization of submicrometer particulate matter during the DISCOVER-AQ 2013 campaign in Houston, TX, J. Air Waste Manag. Assoc., 67(8), 854-872.

Liu, S., Shilling, J.E., Song, C., Hiranuma, N., Zaveri, R. A., Russell, L.M., Hydrolysis of organonitrate functional groups in aerosol particles, 2012, Aerosol Sci. Technol., 46, 1359–1369.

Mao, J., Carlton, A., Cohen, R.C., Brune, W.H., Jimenez, J.L., Pye, H.O.T., Ng, N.L., McDonald, R., Warneke, C., de Gouw, J., Mickley, L.J., Leibensperger, E.M., Mathur, R., Horowitz, L., 2016, Southeast Atmosphere Studies: learning from model-observation syntheses, Atmos. Chem. Phys. Discuss., in review.

McGaughey, G., Kimura, Y., McDonald-Buller, E., 2017. Replication of the TCEQ Photochemical Modeling Episode for May – September 2012 including a Performance Evaluation for Ozone in the Victoria Area, submitted to the City of Victoria, Grant No. 582-16-60188, July 2017.

Nenes, A, C. Pilinis, and S.N. Pandis. 1998. ISORROPIA: A New Thermodynamic Model for Multiphase Multicomponent Inorganic Aerosols. Aquatic Geochemistry, 4, 123-152.

Nenes, A., Pilinis, C., Pandis, S.N., 1999. Continued Development and Testing of a NewThermodynamic Aerosol Module for Urban and Regional Air Quality Models. Atmos. Environ. 33, 1553-1560.

Ng, L.N., Brown, S.S., Archibald, A. T., Atlas, E., Cohen, R. C., et al. , 2017, Nitrate radicals and biogenic volatile organic compounds: oxidation, mechanisms, and organic aerosol, Atmos. Chem. Phys., 17, 2103-2162.

Nguyen, T.B., Crounsea, J.D., Tenga, A.P., St. Clair, J.M., Paulot, F., Wolfe,G.M., Wennberg, P.O., 2015, Rapid deposition of oxidized biogenic compounds to a temperate forest, PNAS, 112, E392–E401.

Nopmongcol, U., Liu, Z., Johnson, J., Rassmusen, D.J., Wentland, A., Yarwood, G., 2015, Three-dimensional performance comparison of CAMx and CMAQ using the DISCOVER-AQ field study data base, Final Report, TCEQ Work Order No. 582-15-54264-010, Contract N#582=15-50417.

Nah, T., Sanchez, J., Boyd, C.M., Ng, N.L., 2016, Photochemical aging of α-pinene and β-pinene secondary organic aerosol formed from nitrate radical oxidation, 50(1), 222-231.

Perring, A. E., Pusede, S. E. and Cohen, R. C.: An observational perspective on the atmospheric impacts of alkyl and multifunctional nitrates on ozone and secondary organic aerosol, Chem. Rev., 2013, 113(8), 5848–5870, doi:10.1021/cr300520x.

Pye, Havala O. T., Luecken, D. J., Xu, L., Boyd, C. M., Ng, N. L., Baker, K. R., Ayres, B. R., Bash, J. O., Baumann, K., Carter, W.P.L., Edgerton, E., Fry, J. L., Hutzell, W. T., Schwede, D. B., Shepson, P.B., 2015, Modeling the current and future roles of particulate organic nitrates in the Southeastern United States, Environ. Sci. Tech., 49, 14195−14203.

Ramboll Environ. 2016. User's Guide: Comprehensive Air Quality Model with extensions, Version 6.40. Available at http://www.camx.com.

Rindelaub, J.D., McAvey, K.M., Shepson, P.B., 2015. The photochemical production of organic nitrates from α-pinene and loss via acid-dependent particle phase hydrolysis. Atmos. Environ., 100, 193–201.

Rindelaub, J.D., Borca, C.H., Hostetler, M.A., Lipton, M.A., Slipchenko, L.V., 2016, The acid-catalyzed hydrolysis of an α-pinene-derived organic nitrate: kinetics, products, reaction mechanisms, and atmospheric impact, Atmos. Chem. Phys. Discuss., 16, 15425–15432.

Rosen, R. S., Wood, E.C., Wooldridge, P.J., Thornton, J.A., Day, D.A., Kuster, W., Williams, E.J., Jobson, B.T., Cohen, R.C., 2004, Observations of total alkyl nitrates during Texas Air Quality Study 2000: Implications for O_3 and alkyl nitrate photochemistry, J. Geophys. Res., 109, D07303.

Ryerson, T.B., Trainer, M., Angevine, W.M., Brock, C.A., Dissly, R.W., Fehsenfeld, F.C., Frost, G.J., Goldan, P.D., Holloway, J.S., Hubler, G. et al., 2003, Effect of petrochemical industrial emissions of reactive alkenes and NO_x on tropospheric ozone formation in Houston, Texas. J. Geophys. Res. Atmos. 108(D8):24.

Simon, H., Baker, K., Phillips, S., 2012, Compilation and interpretation of photochemical model performance statistics published between 2006 and 2012, Atmos Environ, 61,124-139.

Strader, R., F. Lurmann, and S.N. Pandis. 1999. Evaluation of secondary organic aerosol formation in winter. Atmos. Environ., 33, 4849-4863.

Stutz, J., Weng Wong, K., Lawrence, L., Ziemba, L., Flynn, J.H., 2010, Noctural NO3 radical chemistry in Houston, TX, Atmos. Environ. 44, 4099-4106.

Teng, A.P., Crounse, J.D., Lee, L. , St. Clair, J. M., Cohen, R.C., Wennberg, P.O., 2015, Hydroxy nitrate production in the OH-initiated oxidation of alkenes, Atmos. Chem. Phys., 15, 4297–4316.

Xu, L., Suresh, S., Guo, H., Weber, R. J., Ng, N. L., 2015, Aerosol characterization over the southeastern United States using high-resolution aerosol mass spectrometry: spatial and seasonal variation of aerosol composition and sources with a focus on organic nitrates, Atmos. Chem. Phys., 15, 7307-7336.